International Journal of Scientific Research in Engineering and Management (IJSREM)
Volume: 10 Issue: 01 | Jan - 2026 SJIF Rating: 8.586 ISSN: 2582-3930

Simulation-Based Performance Analysis of Ventilation and Fire Protection System in Road Tunnel Fires

[a]Rohan Jaiswal, [b]Nakul Mahalle, [a]Aayush Dubey, [a]Ravi Shankar Kumar, [a]Anuj Goswami, [a]Nirmalya Shukla, [a]Piyush Chaudhary

[a]Undergraduate Student, Department of Fire Engineering, National Fire Service College, Nagpur, India
[b]Assistant Professor, Department of Fire Engineering, National Fire Service College, Nagpur, India

Abstract

This paper evaluates the performance of ventilation and fire-protection system in a 200 metre road tunnel using PyroSim/FDS. Three design fires were modelled — heavy goods vehicle (100 MW), bus/truck (25 MW) and passenger car vehicle (10 MW)— under two configurations: natural ventilation (baseline) and an integrated system combining longitudinal mechanical ventilation with sprinklers. Under baseline conditions, simulations show rapid smoke back-layering, rising thermal loads and loss of tenability within minutes. The integrated configuration preserved upstream tenability and directed smoke downstream, moderating—but not entirely eliminating—severe local heating; in the integrated runs the fire growth was constrained, with HRR behaviour capped at values comparable to those observed under the natural-ventilation cases. The discussion interprets thermal fields, smoke and CO distribution, visibility and sensor/sprinkler response, and draws implications for evacuation routing, control strategy for jet fans, and performance-based design. Simulation fidelity was corroborated using an Artificial Neural Network (ANN) regression (R = 0.97–0.99), supporting the reliability of the numerical findings. The results underline the limitations of natural ventilation alone and the practical benefits of coordinated ventilation–suppression strategies for tunnel fire safety.

Keywords: Tunnel fire, Ventilation, Sprinkler suppression, PyroSim, Back-layering

1. Introduction

Road tunnels are an essential part of modern transportation infrastructure, offering efficient routes through urban centers, mountainous terrain, and waterways. Their increasing use is accompanied by heightened fire safety concerns due to their enclosed geometry, limited ventilation, restricted access for firefighting, and constrained evacuation options. [1][2] Fires in such environments are particularly hazardous because toxic smoke and heat accumulate rapidly, reducing visibility and creating untenable conditions within minutes (Beard & Carvel,2005).[3][4]

Over the past decades, a number of catastrophic tunnel fire incidents have demonstrated the severity of these risks. Most casualties in such events are not caused by direct flame contact but by smoke inhalation and toxic gas exposure (Carvel & Marlair, 2005).[2][5] Table 1 highlights some of the most notable cases, where inadequate smoke control and delayed response contributed to high fatality rates.[4][6]

These events have shifted global attention toward improving tunnel fire safety. Prescriptive-based design approaches, which rely on fixed assumptions about fire size and single-system reliance (usually ventilation), have been shown to be inadequate for modern tunnels with higher traffic density and larger fire loads (Ingason et al., 2015).[7] International guidelines such as NFPA 502 and recommendations from PIARC now encourage performance-based design using computational fluid dynamics (CFD) and the integration of suppression with ventilation systems (Fera & Macchiaroli, 2010; Sarvari & Mazinani, 2019).[8][9]

Table 1. Notable Tunnel Fire Incidents [10] and Key Lessons

Incident	Year	Location	Cause	Casualities	Key Lessons Learned
Mont Blanc Tunnel [11]	1999	France–Italy	Truck fire (flour & margarine)	39 deaths	Importance of smoke control & evacuation routes
Gotthard Tunnel [12]	2001	Switzerland	HGV collision & fire	11 deaths	Need for effective longitudinal ventilation
Fréjus Tunnel	2005	Italy	HGV fire	2 deaths	Rapid smoke propagation despite firefighting efforts
Burnley Tunnel	2007	Australia	Multi-vehicle HGV fire	3 deaths	HRR exceeded 100 MW; design fire underestimated
Yanhou Tunnel	2014	China	Tanker fire (methanol)	31 deaths	Toxic smoke spread as main cause of fatalities
Wyoming Green River Tunnel (I-80) [12]	2025	Wyoming, USA	Multi-vehicle pile-up involving 26 vehicles.	3 deaths	Underscores need for fire resistant lining, rapid suppression, and traffic control
KPE Tunnel [13]	2024	Singapore	Car engine fire	0	Automatic sprinklers activated promptly; fire suppressed quickly, ventilation cleared smoke, no injuries reported

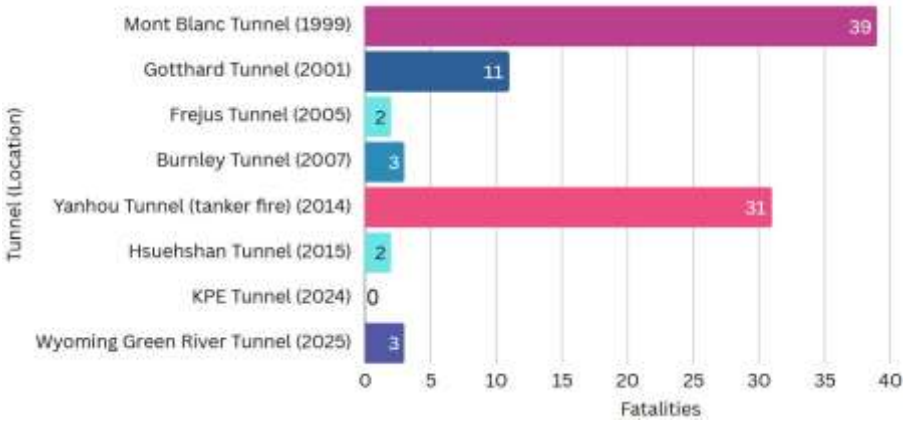

Fig. 1. Fatality Distribution in Major Tunnel Fire Incidents

While many past tunnel fires highlight the devastating consequences of inadequate safety measures, recent incidents also demonstrate the effectiveness of integrated protection strategies. For example, in the 2024 KPE Tunnel car fire in

Singapore, the prompt activation of sprinklers in combination with tunnel ventilation systems successfully contained the flames and cleared smoke, preventing injuries and minimizing disruption. This outcome shows that when detection, suppression, and ventilation work in synergy, the impact of tunnel fires can be greatly reduced. Such cases underscore the importance of installing and maintaining integrated systems, as they not only mitigate risk but also provide critical time for evacuation and emergency response.

Simulation tools like PyroSim and FDS provide a powerful means to replicate tunnel fire scenarios, enabling safe and cost-effective testing of different safety strategies.[14] They allow researchers to analyze smoke propagation, temperature development, visibility, and toxic gas concentrations under various fire intensities and system configurations (Zhou et al., 2019). Recent research has shown that while ventilation can improve smoke control, it can also intensify fire growth by supplying oxygen;[15][10] suppression systems, on the other hand, reduce heat release rates but may interfere with airflow if not properly integrated (Ingason et al., 2015). This indicates that neither system alone is sufficient, and their combined effect must be assessed.

The present study addresses this need by conducting a simulation-based performance analysis of road tunnel fires using PyroSim. Three fire scenarios of varying heat release rates (light, moderate, and severe) are modeled under two system configurations:

1. Without active safety measures (baseline),

2. With integrated longitudinal ventilation and sprinkler suppression.

The study aims to provide a comparative analysis supported by temperature, visibility, gas concentration, and activation-time curves from simulation outputs. The overarching objective is to demonstrate how integrated ventilation and suppression systems significantly enhance tunnel tenability and occupant survivability compared to conventional single-system approaches.

This work contributes to ongoing discussions in tunnel fire safety by filling a research gap: while past studies have investigated ventilation or suppression individually, fewer have comprehensively analyzed their synergistic performance under different HRR fire scenarios.

2. Methodology

2.1 Simulation framework

2.1.1. PyroSim and fire dynamics simulation (FDS)

PyroSim is an advanced fire modelling software that serves as a graphical interface for the Fire Dynamics Simulator (FDS), allowing detailed analysis of fire behaviour and fluid dynamics.[1] It assists researchers and engineers in designing fire scenarios, predicting smoke movement, evaluating heat transfer, and studying variations in gas concentrations within enclosed environments. In this study, PyroSim (version 2024.2), developed by Thunderhead Engineering, was used as the main platform for developing and configuring the simulation model. The preprocessor of the software generates the necessary input data files, which are then executed by FDS to perform the fire dynamics calculations in confined spaces.[16]

FDS applies a large-eddy simulation (LES) approach, which focuses on modelling low-speed fluid flow while accurately capturing heat and mass transfer generated by fire . During the simulation, physical properties such as temperature, pressure, air density, and velocity are continuously updated at every computational cell of the model. As the fire evolves, FDS calculates combustion rates, heat release rates, surface temperature rise, and other outcomes until the termination point is reached.[17]

The computational framework of FDS is based on the fundamental governing equations of Newtonian fluid mechanics:

1. Conservation of Mass (Continuity): Ensures that fluid mass is preserved across the entire domain.

$$\frac{\partial \rho}{\partial t} + \nabla \cdot (\rho u) = m_b'' \quad (1)$$

Where, ρ: Density (kg/m3), u: Velocity vector (m/s), m_b": Mass production rate per unit volume Typically from the evaporation of liquid droplets or the pyrolysis of solid materials (kg/m³/s).

2. Conservation of Momentum (Newton's Second Law): Accounts for fluid motion influenced by pressure, gravity, and external forces.

$$\frac{\partial(\rho u)}{\partial t} + \nabla \cdot (\rho u u) + \nabla p = \rho g + f_b + \nabla \cdot \tau_{ij} \quad (2)$$

Where, p: Pressure (Pa), g: gravitational acceleration vector (m/s²), fb: External body force per unit volume, such as from a fan or sprinkler spray (N/m^2), τ_{ij}: Viscous stress tensor, representing the frictional forces within the fluid(N/m^2).

3. Conservation of Energy (First Law of Thermodynamics): Describes the transport of energy within the domain, considering heat release from combustion and other transfers.

$$\frac{\partial(\rho h)}{\partial t} + \nabla \cdot (\rho u h) = \frac{Dp}{Dt} + q''_m - q''_r - \nabla \cdot q'' + \varepsilon \quad (3)$$

Where , h: Specific enthalpy(J/kg), Dp/Dt: Material derivative of pressure, representing work done by pressure changes., q_m": Heat release rate per unit volume from chemical reactions (W/m³), q_r'': Energy transferred away from the gas phase, for example, to evaporate droplets (W/m³), q": Heat flux vector, representing heat transfer via thermal conduction and radiation (W/m²), ε: Dissipation rate, where kinetic energy is converted to thermal energy by viscosity (W/m³).

2.1.2. Mesh

In CFD-based fire simulations, the computational mesh plays a decisive role in determining both the precision of the results and the overall runtime of the analysis.[6] In this study, the scenario was developed in PyroSim using a single, uniform mesh designed to adequately represent the fire dynamics while maintaining computational efficiency. The simulation was carried out within a computational domain representing the physical region of interest. The domain covers a total volume of 200 m × 8 m × 9 m (Fig. 4), with coordinate limits defined as follows:

• **X-axis:** 0 m to 200 m

• **Y-axis:** 0 m to 8 m

• **Z-axis:** 0 m to 9 m

This domain was discretized into a structured mesh of 100 cells along the x-axis, 16 cells along the y-axis, and 18 cells along the z-axis, giving a total of 115,200 grid cells. Each cell measures approximately 0.5 m × 0.5 m × 0.5 m, resulting in a uniform aspect ratio of 1:1:1. Maintaining nearly cubic cell proportions helps to improve numerical stability and enhances the reliability of solutions obtained in the Fire Dynamics Simulator (FDS). Figure 2 illustrates the mesh configuration applied for the tunnel case.

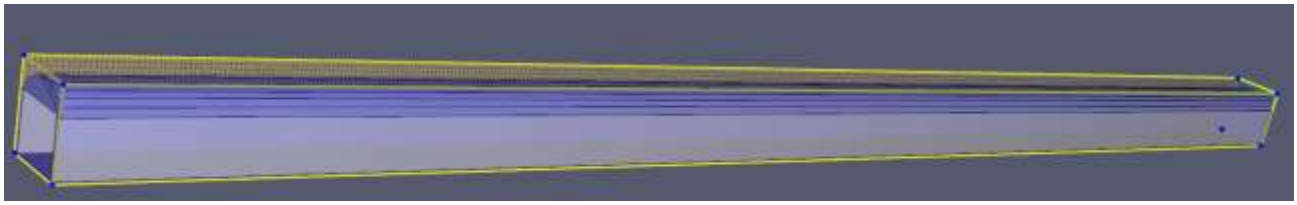

Fig. 2. The meshes of the analyzed case study are shown, highlighted in yellow

2.1.3. Mesh Resolution Rationale

The selection of the grid size is fundamental to the fidelity of a fire simulation. A finer grid generally produces more accurate results but at a significantly higher computational cost. Therefore, the resolution must be sufficient to capture the essential physics of the fire without being excessively demanding. Mesh resolution is determined based on the characteristic fire diameter, a key scaling parameter for plume resolution in fire simulations .

It can be described as:

$$D^* = \left(\frac{Q}{\rho\infty cpT\infty\sqrt{g}} \right)^{2/5} \quad (4)$$

Where, (Q) is the maximum heat release rate (kW), ($\rho\infty$) is the air density (1.204 kg/m³), ($T\infty$) is the ambient temperature (293.15 K), (Cp) is the specific heat capacity of air (1.005 kJ/kg·K), and (g) is the acceleration due to gravity (9.81 m/s²). The heat release rate is expressed in relation to the ambient density, the specific heat at constant pressure, the surrounding temperature, and the gravitational acceleration.[17]

To sufficiently capture the fire plume, the recommended range for the ratio is 4–16, where Δx represents the nominal cell size .[18] In this study, the chosen nominal cell size of ≈ 0.5 m ensures compliance with this criterion, thereby resolving key gradients in velocity and temperature near the flame without imposing excessive computational cost. The FDS pressure solver is based on a Poisson algorithm with Fast Fourier Transform (FFT). For optimal efficiency, the number of cells along each axis should be divisible into products of small primes, typically of the form.[19] The chosen grid satisfies this condition, ensuring both solver performance and computational efficiency without compromising resolution.

2.2. Tunnel Geometry and Model Setup

The following tunnel configuration was developed using PyroSim software for the purpose of fire and ventilation performance analysis. The tunnel has a total length of 200 meters, with a rectangular cross-sectional profile of 6 meters in height and an internal width of 7 meters, enclosed by concrete walls of 0.5 meters thickness on both sides. The structural elements of the tunnel, including the floor, walls, and ceiling, were constructed using the obstruction tools in PyroSim, with the material properties defined as concrete to ensure realistic representation of thermal and structural behaviour during fire simulations.[3]

The floor of the tunnel was created using the slab obstruction tool to cover the entire 200-meter length. The side walls were generated using the wall obstruction tool, each with a thickness of 0.5 meters, extending the full length of the tunnel. For the ceiling, a hemispherical slab obstruction was constructed with a thickness of 3m radius, providing a realistic overhead geometry while maintaining structural integrity.

Ventilation conditions were established using the vent tool, with vents placed at both ends of the tunnel, acting as the inlet and outlet openings. These tunnel portals were also opened in the computational meshes to allow proper airflow simulation. At the inlet side, a longitudinal air velocity of 0.5 m/s was defined, ensuring natural ventilation conditions representative of real-world tunnel environments.

Tenability criteria are commonly used to define safe evacuation conditions during a fire. The concentration of carbon monoxide (CO) should not exceed 0.0012 mol/L (1200 ppm), visibility in the smoke layer should remain above 10 m, and the ambient temperature should be kept below 60 °C.[20] Smoke concentration is often expressed in terms of the extinction coefficient, where values greater than 0.1–0.15 m^{-1} (equivalent to 3–5% obscuration per meter) are regarded as unsafe due to their impact on visibility and evacuation.[1]

Fig. 5 illustrates the distribution of vehicles along the tunnel, with each vehicle labeled by number and equipped with a thermocouple attached to its hood. The fire vehicle is located at the center (THCP 18). Vehicles positioned to the right of the fire vehicle (Vehicles 4, 5, 6, 7, 11, 12, and 13) represent the downstream area, while those to the left (Vehicles 1, 2, 3, 8 and 9) represent the upstream area. The temperature conditions recorded by these thermocouples are plotted for each vehicle and analyzed for each scenario.

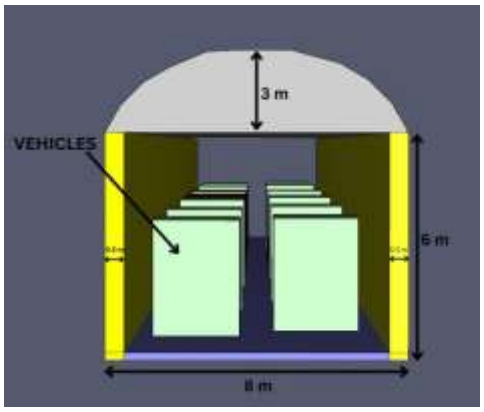

Fig. 3. Front view of tunnel geometry

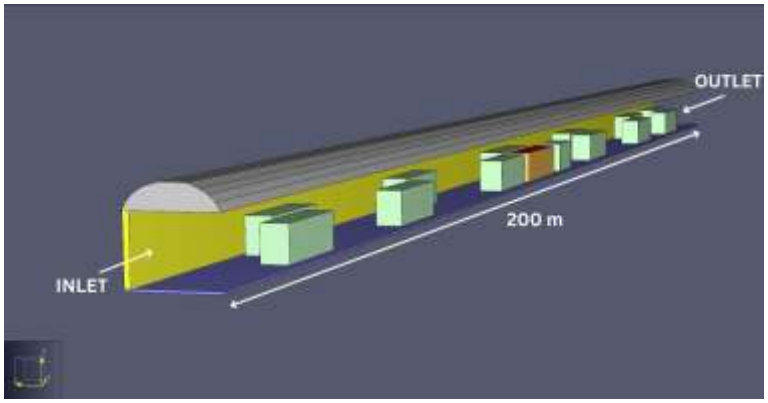

Fig. 4. Side view of tunnel geometry

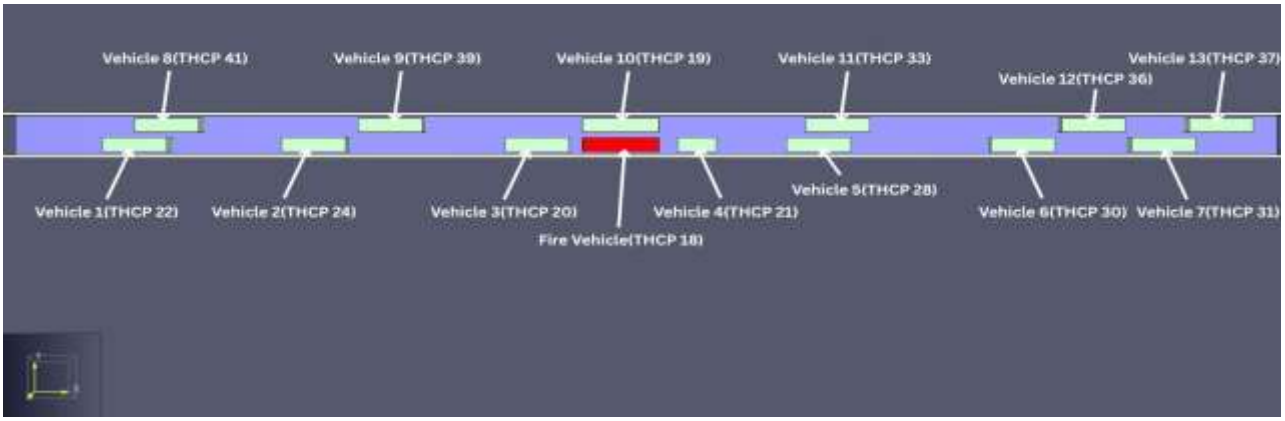

Fig. 5. Vehicles location in tunnel

2.3. Instrumentation and data collections

Thermocouple Instrumentation and Thermal Field Mapping

Temperature measurement is a key tool for describing fire dynamics, and bare-bead thermocouples are commonly used due to their low cost, durability, and suitability for large-scale fire testing.[21] In the tunnel study, thermocouples were placed both on vehicle surfaces and along the tunnel walls to capture the evolving thermal field. Fourteen hood-mounted thermocouples (one on each vehicle) monitored surface heating directly at the fire source, while 18 wall-mounted thermocouples were installed at 2.5 m height along the tunnel—9 on the left wall and 9 on the right, spaced at 20 m intervals across the 200 m tunnel length. This arrangement provided dense spatial coverage of both surface and gas-phase conditions.

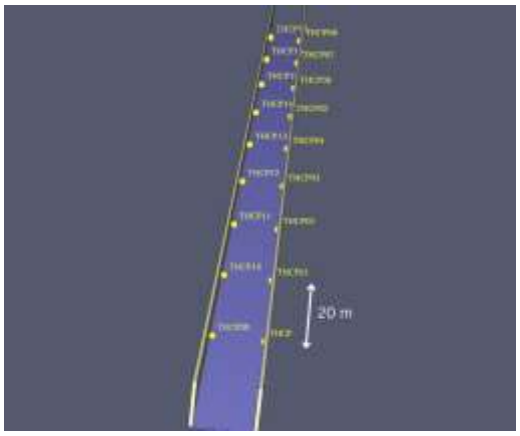

Fig. 6. Thermocouple Layout on wall and Spacing for Temperature Monitoring

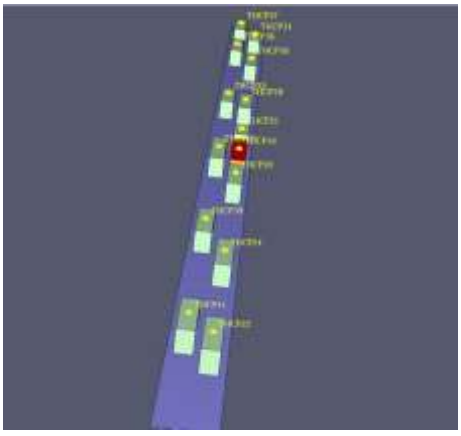

Fig. 7. Thermocouple placement on vehicles

The vehicle sensors measured how each car ignited and transferred heat to its neighbours, while the wall-mounted sensors tracked the hot smoke layer moving along the tunnel at near breathing height. Together, they produced time–temperature histories under three simulated fire scenarios of 100 MW, 25 MW, and 10 MW, with and without ventilation or sprinklers. These datasets revealed longitudinal temperature gradients, smoke front movement, and stratification, as well as the impact of suppression. By combining profiles along the tunnel with individual time-series curves, the measurements clearly highlighted hot spots, growth rates, and control effectiveness across the different fire loads.

2.4. System configuration

2.4.1. Mechanical longitudinal ventilation system

Longitudinal ventilation is one of the most widely implemented engineering controls in tunnel fire safety, as it directly governs smoke movement, heat stratification, and the availability of tenable conditions for firefighting intervention. In this study, a longitudinal ventilation system was modelled using two jet fans installed near the tunnel inlet, located at 25m from the entrance. The fans were modelled with rectangular dimensions of 1 m × 1 m having the capability of delivering variable flow rates but are fixed to a velocity of 2 m/s according to the fire intensity and smoke concentration. This approach reflects modern ventilation systems that regulates air velocity in response to the fire conditions.[22]

The primary objective of the jet fan system was to control smoke propagation along the 200 m tunnel, thereby limiting smoke back-layering and assisting in directing hot gases downstream. The application of variables speed control jet fans may provide more adaptive representation of tunnel operation compared with fixed velocity system. But this paper delves into the traditional fixed velocity system due to the outline of this paper which deals with constant scenarios with fixed systems.

In each case, smoke distribution, density, and visibility were monitored at multiple longitudinal sections of the tunnel. The comparative results demonstrated the influence of the jet fans on reducing smoke accumulation near the ignition source and on stabilizing hot gas movement under varying fire intensities. the model can capture both the aerodynamic influence of forced ventilation and its combined performance with suppression systems.

2.4.2. Smoke detector and visibility measurement

Photoelectric smoke detectors were employed due to their superior sensitivity to dense smoke particles, which are characteristic of tunnel fire scenarios. The detectors were installed at a height of 5 m, centrally positioned across the tunnel width to ensure uniform coverage. A spacing of 10 m was maintained between detectors along the tunnel length, providing adequate resolution for tracking smoke propagation and detection response under different fire conditions.

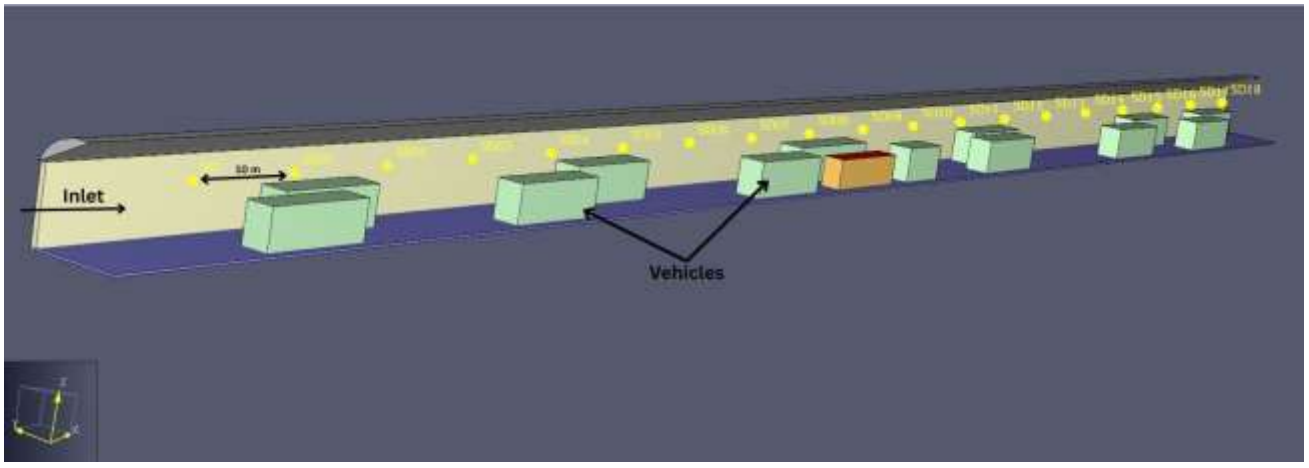

Fig. 8. Smoke detector configuration

2.4.3. Fire Suppression System (Sprinkler)

To evaluate the impact of an active fire suppression system, a wet-pipe sprinkler system was added to the tunnel model. The system aimed to cover the entire 200-meter length of the tunnel. Individual sprinkler heads were placed every 5 meters. Each sprinkler head was set up as a thermally activated device. It would only release water when the

temperature around it reached a specific level. For this simulation, the activation temperature was set to 93°C. This ensured that the system would respond right near the fire once the ceiling jet generated enough heat.[23]

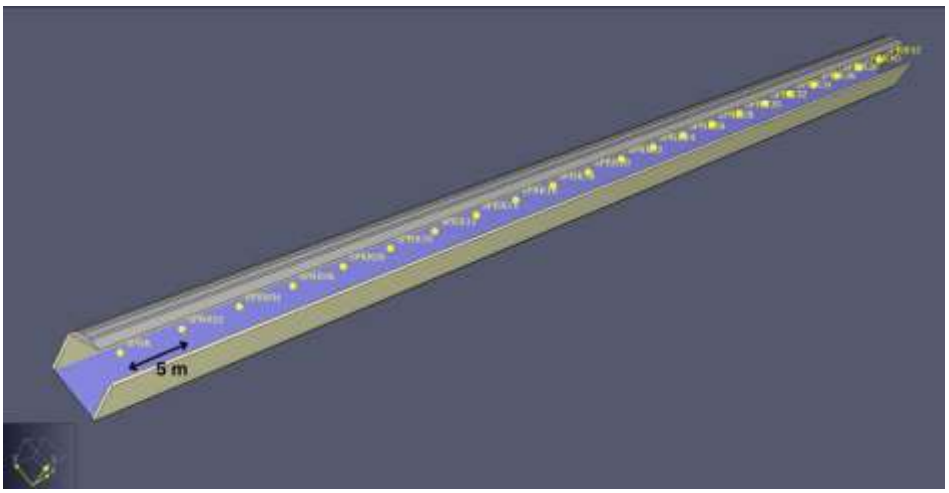

Fig. 9. Sprinklers nozzle configuration

The hydraulic performance of each sprinkler was defined by a nominal pressure of 0.5 bar and a K-factor of 360 LPM/ √bar.[24] Upon activation, each individual sprinkler head was configured to discharge water droplets at a rate of 5,000 particles per second, with a spray cone defined by an angle between 60 and 75 degrees. This setup ensures that water is applied directly to the fire and the surrounding superheated gas layer, maximizing the cooling and smoke-suppression effects in the critical area without needlessly discharging water in unaffected sections of the tunnel

2.5 Fire Scenario and Heat Release Rate (HRR)

To investigate the influence of different fire sizes on tunnel dynamics, three representative fire scenarios were developed, each corresponding to a specific vehicle category.[25] The fires were modelled using a t^2 growth curve until the designated peak heat release rate (HRR) was reached, after which a steady-state burning phase was maintained. The selected HRR values are consistent with full-scale vehicle fire test data reported in the literature and NFPA 502.

Table 2: Measured peak HRR value based on NFPA 502 standard.[25]

Vehicle	Peak HRR (MW)
Passenger car	5-10
Multiple passenger car	10-20
Bus	25-34
Heavy truck	20-200

Scenario 1- Heavy good vehicle (HGV) fire (100 MW)

The first and most severe scenario considers a heavy goods vehicle fire, modelled with a peak HRR of 100 MW.[15][26] The HGV was modelled with dimensions of 12 m length, 2.5 m width, and 3.5 m height. The fuel bed was assumed to be polyurethane, representing highly combustible transported goods. Although such fires are less frequent, they are the most dangerous due to the high fuel load and presence of combustible cargo. Past tunnel fire disasters, such as Mont Blanc and Gotthard, have demonstrated the catastrophic consequences of HGV fires, with HRR values sometimes exceeding 100 MW. In this study, 100 MW was selected as a representative severe case. Fires of this scale generate extreme temperatures, dense smoke, and widespread tenability loss, while also posing a risk of structural damage to the tunnel lining and ceiling. Immediate intervention with active suppression systems and mechanical ventilation becomes essential to prevent escalation and support safe evacuation.

Scenario 2 – Bus/Truck Fire (25 MW)

This case represents a fire involving a bus or medium-sized truck, modelled with a peak HRR of 25 MW.[27][28] The vehicle was modelled with dimensions of 10 m length, 2 m width, and 3 m height. The fuel bed for this case was also assumed to be polyurethane, representing seating and cargo materials with high combustibility. Such vehicles carry larger fuel tanks and a greater combustible load than passenger cars, which contributes to faster fire growth and higher energy release. Fires of this size produce significant smoke and heat, causing rapid reduction in visibility and posing a serious challenge to tenability within the tunnel. Smoke back-layering is more likely under natural ventilation, complicating both evacuation and firefighting operations, and making mechanical ventilation a critical factor for controlling smoke propagation.

Scenario 3 – Passenger Vehicle Fire (10 MW)

This scenario represents a fire originating from a passenger car, modelled with a peak HRR of 10 MW.[28] The passenger vehicle was assumed to have dimensions of 4 m length, 2 m width, and 1.5 m height. The combustible fuel bed for this scenario was taken to be polyurethane, representing upholstery and interior materials commonly present in passenger cars. Passenger vehicles are the most common category of tunnel traffic, and their fire sizes typically range between 5 MW and 15 MW depending on fuel load and materials. A 10 MW case reflects a realistic but moderate severity fire, producing localized heating and smoke accumulation. While thermal stress on the tunnel lining remains limited, visibility near the source can deteriorate quickly, and natural ventilation alone may not be sufficient to ensure safe evacuation conditions.

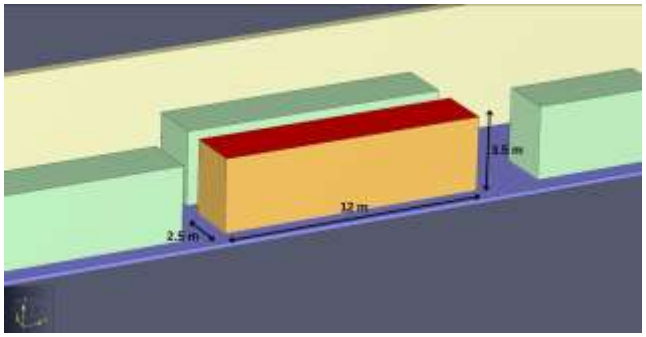

(a)

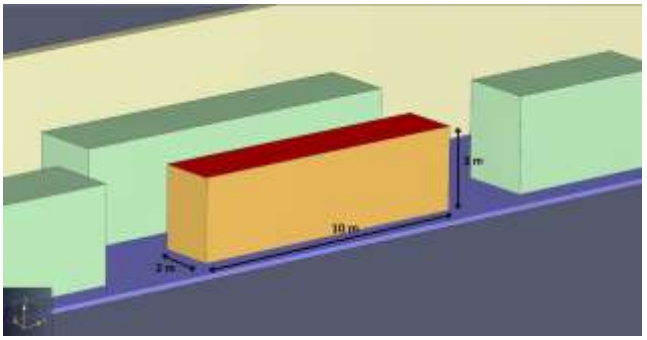

(b)

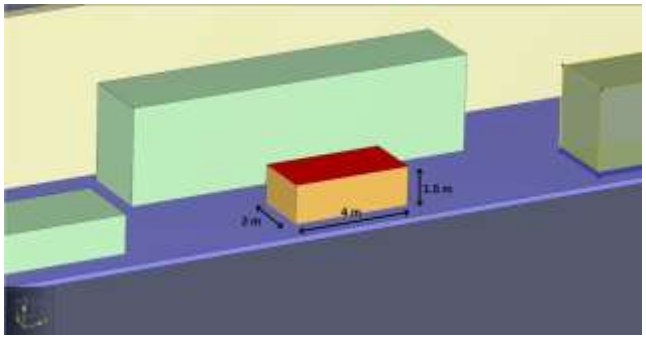

(C)

Fig. 10. fire vehicle dimensions for different design fire scenarios: (a) 100 MW fire (12 × 2.5 × 3m), (b) 25 MW fire (10 × 2 × 3 m), and (c) 10 MW fire (4 × 2 × 1.5 m).

For a comprehensive analysis of tunnel fire behaviour, two distinct cases were developed for each of the three fire scenarios defined earlier. These cases were designed to replicate conditions ranging from minimal safety infrastructure to a fully equipped modern tunnel environment.

Case 1: Natural Ventilation Only

In the first case, the tunnel was assumed to operate under natural ventilation only, with no mechanical longitudinal ventilation system or active fire protection measures. The airflow inside the tunnel was maintained at a low velocity of 0.5 m/s, corresponding to natural wind and buoyancy-driven flow entering through the tunnel portals. This setup was intended to simulate a baseline condition where smoke propagation is largely uncontrolled, and its movement is governed primarily by buoyant forces and limited natural air exchange. The absence of suppression mechanisms allows the fire to develop unhindered until it reaches its peak heat release rate, resulting in elevated temperatures, dense smoke accumulation, and potential back-layering along the ceiling. This case reflects situations in older tunnels or during failure of critical safety systems, thereby providing a worst-case scenario for fire and smoke development.

Case 2: Mechanical Ventilation and Fire Protection System Present

In the second case, the tunnel was modeled with both mechanical longitudinal ventilation and an active fire protection system. The mechanical ventilation system was applied to induce a controlled airflow along the tunnel axis, thereby directing smoke movement and reducing the likelihood of back-layering. In parallel, an active fire protection system, modeled in the form of sprinklers, was introduced to suppress the fire by limiting its growth rate and reducing the peak heat release rate. The combined effect of mechanical ventilation and fire suppression was expected to improve tenability conditions, lower ceiling gas temperatures, and maintain a manageable smoke layer height for evacuation and firefighting activities. This case was designed to replicate the conditions of modern tunnels constructed in compliance with contemporary fire safety standards.

Table 3. Tabular representation of cases and scenarios

Scenario	Vehicle type	Peak HRR	Case 1: natural ventilation only	Case 2: ventilation + fire protection system (Integrated system)
Scenario 1	Heavy goods vehicle	100 MW	Natural ventilation at 0.5 m/s; extreme smoke and temperature; extended back-layering; untenable conditions	Mechanical ventilation and sprinklers present; reduced fire growth; directional smoke flow; conditions remain critical but improved compared to Case 1
Scenario 2	Bus/truck	25 MW	Natural ventilation at 0.5 m/s; severe smoke spread; higher ceiling temperatures; visibility hazard	Mechanical ventilation and sprinklers present; reduced HRR; controlled smoke flow; improved safety
Scenario 3	Passenger vehicle	10 MW	Natural ventilation at 0.5 m/s; no suppression; moderate smoke accumulation and back-layering	Mechanical ventilation and sprinklers present; effective smoke clearance; reduced thermal load

Note: ventilation + fire protection system case is regarded as integrated system from hereafter.

2.6 Application Across Fire Scenarios

2.6.1. Heavy Goods Vehicle Fire (100 MW HRR)

The first scenario, representing a heavy goods vehicle (HGV) fire with a peak HRR of 100 MW, was considered the most severe case. Under Case 1 conditions, this scenario produced extremely high thermal energy, leading to rapid smoke accumulation, extended back-layering along the tunnel ceiling, and untenable conditions throughout a large section of the tunnel. The natural ventilation velocity of 0.5 m/s proved grossly insufficient to manage smoke movement, resulting in a highly hazardous environment for both occupants and emergency responders. In contrast, Case 2 demonstrated the effectiveness of mechanical ventilation and fire protection systems in controlling such a severe fire. Although the scale of the fire was considerably greater than in the previous scenarios, the sprinklers were expected to reduce the fire's effective HRR, while the mechanical ventilation provided directional airflow that limited smoke recirculation. Even in this case, however, the conditions remained critical, highlighting the need for robust design of tunnel safety systems when dealing with high fire loads such as those associated with heavy goods vehicles.

2.6.2. Bus/Truck Fire (25 MW HRR)

In the second scenario, which modeled a bus or truck fire with a peak HRR of 25 MW, the impact of the two cases became more distinct. In Case 1, the absence of active control measures was expected to result in severe smoke propagation along the tunnel length, with higher ceiling temperatures and lower visibility posing significant hazards for evacuation. The buoyancy-driven smoke movement, coupled with insufficient natural airflow, created conditions for intense back-layering, making this a highly challenging fire scenario under minimal safety conditions. In Case 2, however, the presence of mechanical ventilation and fire suppression significantly altered the fire dynamics. The sprinklers reduced the growth and peak intensity of the fire, while the longitudinal ventilation system helped maintain a unidirectional smoke flow, thereby mitigating back-layering and improving evacuation safety.

2.6.3. Passenger Vehicle Fire (10 MW HRR)

In the third scenario, representing a passenger vehicle fire, the fire source was modeled to reach a peak HRR of 10 MW. Under Case 1 conditions, the relatively low intensity fire combined with natural ventilation of 0.5 m/s was expected to cause significant localized smoke accumulation and moderate back-layering, though the severity remained somewhat limited due to the smaller fire size. Under Case 2, the activation of mechanical ventilation and sprinklers was expected to rapidly improve smoke clearance and reduce thermal loads, ensuring safer conditions within the tunnel.

3. Result and analysis

3.1. Heavy good vehicle fire (100 MW)

3.1.1. Heat release rate characterisation of the fire vehicle

Case-1: With natural ventilation only

The Heat Release Rate (HRR) for the fire under natural ventilation conditions is shown in Figure 11(a). The fire exhibits a characteristic t-squared growth curve, beginning a slow development phase before accelerating into a period of rapid and sustained growth. The HRR reaches approximately 7,500 kW (7.5 MW) by 100 seconds, increases to over 25,000 kW (25 MW) by 175 seconds, and continues to climb to a turbulent peak of approximately 37,500 kW (37.5 MW) by the end of the 250-second simulation.

This unchecked fire growth is a direct consequence of the absence of an active fire suppression system. This fire is allowed to develop based primarily on its fuel load and the available air from natural ventilation. This substantial and uncontrolled energy output is the primary driver for the catastrophic conditions observed in this scenario. It directly causes the severe temperatures and dense smoke that propagate throughout the tunnel, leading to the rapid and widespread loss of tenable conditions in both upstream and downstream condition confirming that natural ventilation alone is incapable of mitigating the hazard.

Case-2: Integrated system

The total Heat Release Rate (HRR) of the fire over the 250-second simulation is presented in Figure 9. The fire exhibits a growth phase consistent with a t-squared model, showing a slow initial development followed by a rapid and steady increase in energy output. The HRR reaches approximately 10,000 kW (10 MW) at 110 seconds, climbs to 25,000 kW (25 MW) by 190 seconds, and continues to grow to a peak of approximately 45,000 kW (45 MW) at the end of the simulation period.

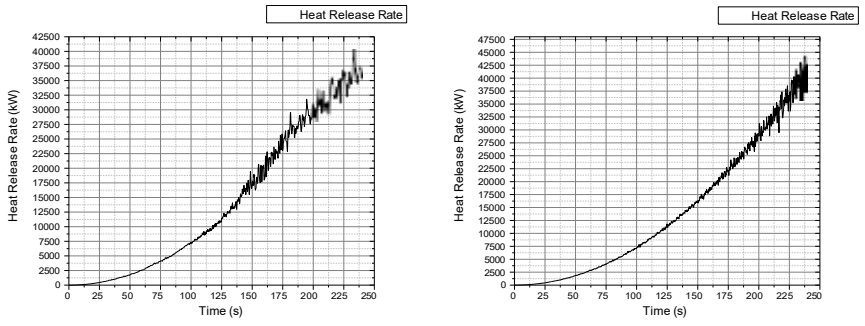

(a) (b)

Fig. 11. Heat Release Rate (HRR) for 100 MW design fire: (a) natural ventilation only, (b) integrated system

3.1.2. Thermal response of tunnel boundaries

Left wall

Case-1: With natural ventilation only

The temperature profiles along the left tunnel wall in the absence of mechanical ventilation demonstrate a drastically different and more hazardous environment. The data shows that the heat from the fire, located at the 100 m mark, propagates in both the upstream and downstream directions simultaneously. A significant temperature rise is recorded at all thermocouple locations. Upstream of the fire, the temperature at 80 m begins to rise after 75 seconds, eventually exceeding 60°C. Even as far upstream as 40 m, the temperature starts to climb after 125 seconds and surpasses the 60°C tenability limit by 210 seconds. Similarly, all downstream locations (120 m, 140 m, 160 m, and 180 m) also show a steady increase in temperature over time.

This bidirectional spread of heat is definitive evidence of back-layering, which occurs when the natural buoyancy of the hot smoke overpowers the weak natural airflow.[22] This is a critical finding as it illustrates a catastrophic failure of the tunnel's life safety system. The contamination of the upstream section with high temperatures and, by extension, toxic smoke, eliminates what would otherwise be the primary escape route for occupants. Under these conditions, the entire tunnel becomes untenable in a short period, severely limiting the potential for self-rescue and creating extremely dangerous conditions that would prevent any safe access for emergency responders. This result starkly contrasts with the mechanically ventilated scenarios and highlights the essential role of forced ventilation in controlling the fire environment.

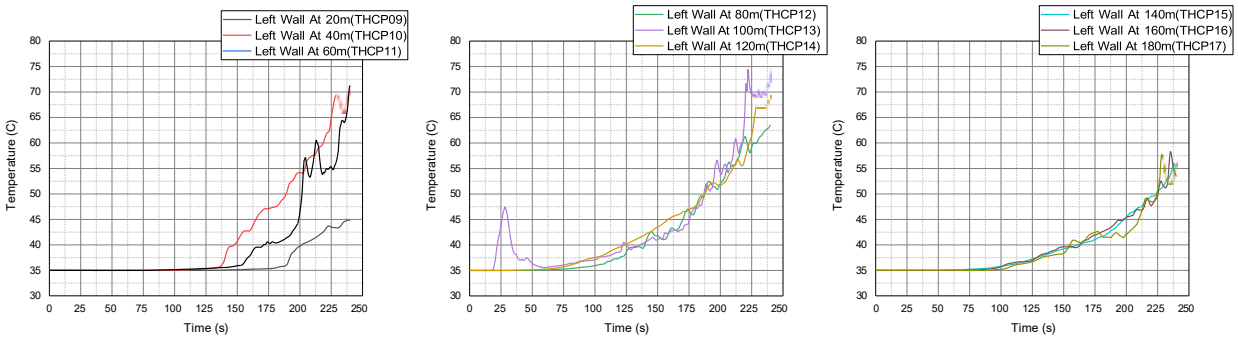

Fig. 12. Temperature vs. time profile from left-wall thermocouples for 100 MW fire under natural ventilation at upstream and downstream locations.

Case-2: Integrated system

The simulation results for air temperature, recorded from thermocouples along the tunnel wall, reveal a clear distinction between the thermal conditions upstream and downstream of the fire. At locations upstream of the fire (20 m, 40 m, 60 m, 80 m, and 100 m), the temperature remains stable at the ambient level of approximately 35°C throughout the 250-second simulation. This stability confirms the effectiveness of the longitudinal ventilation system in preventing smoke and heat back-layering, thereby maintaining a tenable environment for evacuation and emergency access in the entire section upstream of the fire.

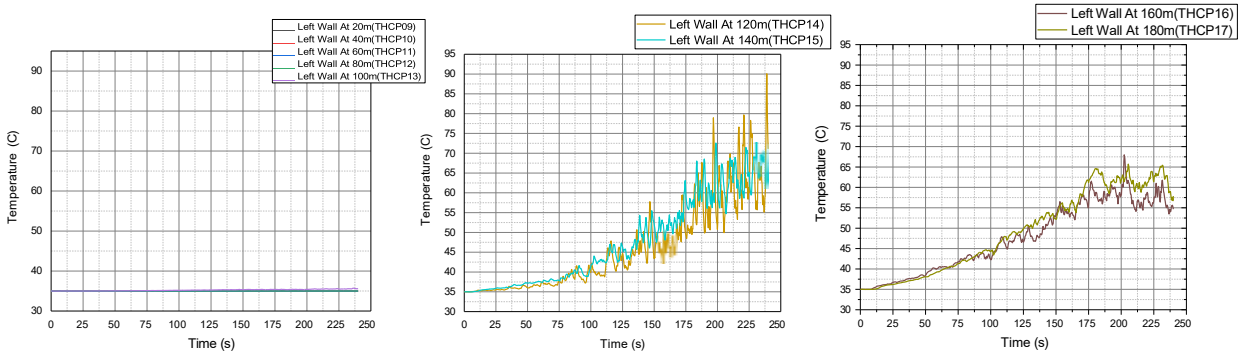

Fig. 13. Temperature vs. time profile from left-wall thermocouples for 100 MW fire under integrated system, showing near-ambient conditions with no significant rise at upstream.

In contrast, a significant temperature rise is observed at all locations downstream of the fire. At the 120 m and 140 m marks, the temperature begins to increase at approximately 100 seconds, eventually reaching fluctuating peaks above 75°C and 70°C, respectively. Further downstream at 160 m and 180 m, temperatures also rise steadily, surpassing the 60°C tenability limit for human safety. The highly turbulent fluctuations in the downstream temperature curves are characteristic of the mixing of hot fire gases with the ventilating air. Although the fire protection systems have likely reduced the overall heat release rate, the downstream portion of the tunnel still becomes thermally hazardous, underscoring the critical importance of rapid evacuation from this area.

Right wall (Fire side wall)

Case-1: With natural ventilation only

The temperature data from the right wall, the same side as the fire, confirms the catastrophic failure of the environment under natural ventilation conditions. The results are broadly consistent with those observed on the left wall, showing a significant and hazardous temperature rise in both the upstream and downstream directions from the fire source at 100 m. The thermocouples located upstream at 80 m, 60 m, and 40 m all record a substantial increase in temperature, with several locations exceeding the 60°C tenability limit. The downstream locations at 120 m and 140 m also show a rapid temperature increase, similarly breaching the life safety threshold.

This bidirectional heat spread provides further definitive evidence of back-layering. The analysis confirms that without mechanical intervention, the fire's buoyant plume moves unimpeded in all directions, rendering the entire tunnel environment thermally untenable. While the temperatures on the fire side are marginally higher than on the left wall, the overall conclusion remains the same: the lack of forced ventilation leads to the complete loss of a safe egress path. This finding illustrates that under such conditions, the primary hazard is the uncontrolled movement of the smoke layer itself, which creates life-threatening conditions throughout the entire length of the affected tunnel area.

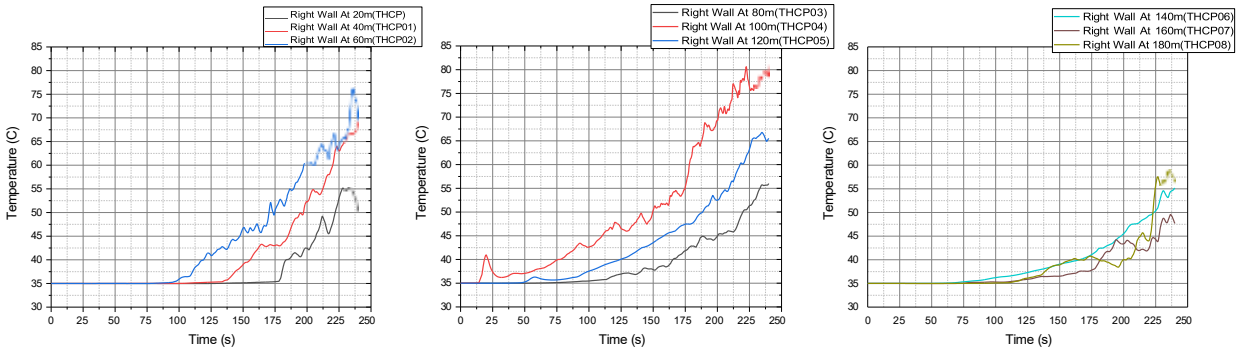

Fig.14. Temperature vs. time profile from right-wall thermocouples for 100 MW fire under natural ventilation

Case-2: Integrated system

The temperature readings from thermocouples on the right wall, which is on the same side as the fire, show a more severe thermal environment compared to the left wall, particularly in the immediate vicinity of the fire. Consistent with previous findings, the upstream locations at 20 m, 40 m, 60 m, and 80 m remained at an ambient temperature of approximately 35°C, reinforcing the conclusion that the ventilation system successfully prevented any upstream heat propagation. However, the thermocouples at the 100 m and 120 m marks—located adjacent to and just downstream of the fire—recorded a rapid and intense temperature rise. The temperature at the 100 m mark began to climb sharply after just 75 seconds, reaching a highly turbulent peak of over 120°C. Similarly, the 120 m location saw temperatures exceed 110°C. Further downstream, at 140 m, 160 m, and 180 m, temperatures also rose significantly, exceeding the 60°C tenability limit well before 150 seconds. These results highlight the asymmetric nature of the thermal environment, with conditions on the fire side of the tunnel becoming life-threatening much more rapidly and severely. This intense, localized heating underscores the extreme danger for any occupants in the immediate vicinity of the fire and demonstrates that while ventilation contains the direction of the hazard, it does not eliminate the severe thermal threat close to the fire source.

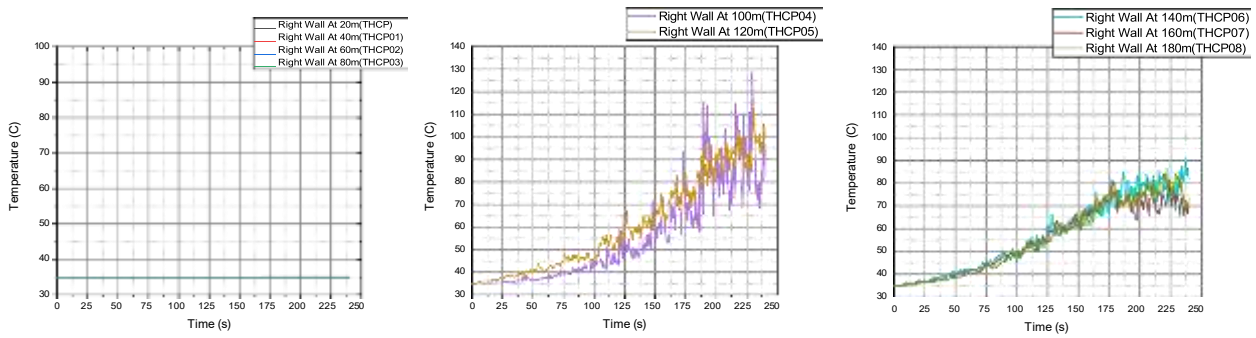

Fig. 15. Temperature vs. time from right-wall thermocouples for 100 MW fire integrated system, showing significant rise at 100 m due to fire origin at right side of the tunnel, unlike the left-wall case.

3.1.3. In-vehicle thermocouple temperature evaluation

Case-1: With natural ventilation only

The thermal conditions at evacuation height, measured by thermocouples above each vehicle, demonstrate a catastrophic and widespread loss of tenability in the natural ventilation scenario. The data reveals that vehicles both upstream and downstream of the fire are exposed to hazardous temperatures due to the uncontrolled bidirectional spread of heat. The temperature above the fire vehicle itself rises to a peak of over 850°C, creating instantly lethal conditions. The vehicles immediately adjacent to the fire are also subjected to unsurvivable temperatures; the thermocouple above Vehicle 10 (upstream) shows a rapid increase to over 700°C, while Vehicle 4 (downstream) experiences temperatures exceeding 250°C. Critically, vehicles located far upstream, such as Vehicle 9 and Vehicle 2, also show a significant temperature rise, eventually exceeding the 60°C tenability limit.

This comprehensive data set provides a stark illustration of the failure of natural ventilation. The high temperatures recorded above vehicles in both directions is a direct result of back-layering, which contaminates the entire tunnel and eliminates any safe escape route. Unlike the mechanically ventilated cases where the upstream path was preserved, this scenario creates a "no-escape" situation where all occupants are eventually exposed to untenable thermal conditions, regardless of their location relative to the fire. This finding unequivocally highlights the critical role of mechanical ventilation in maintaining at least one viable path to safety for evacuees.

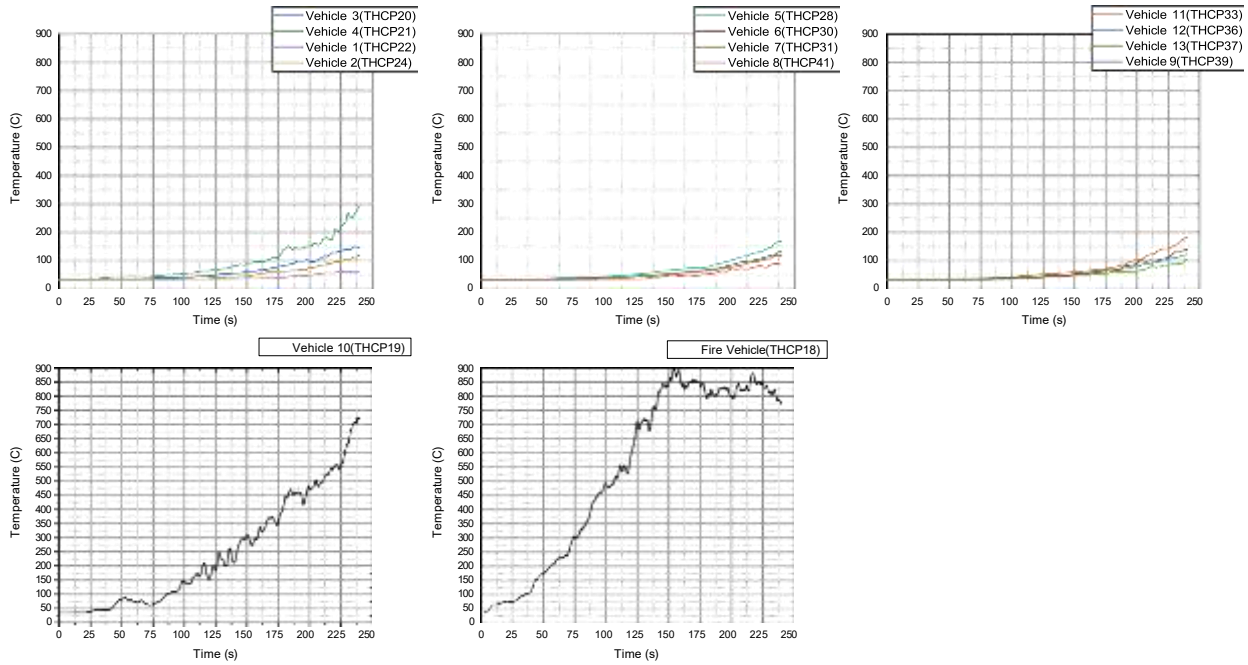

Fig. 16. Temperature vs. time profile from thermocouples placed above vehicles inside the tunnel for 100 MW fire under natural ventilation condition.

Case-2: Integrated system

An analysis of the thermal conditions at evacuation height, measured by thermocouples placed above the midpoint of each vehicle, reveals the localized and extreme nature of the hazard. The data shows that the temperature directly above the fire vehicle itself increased dramatically throughout the simulation, peaking at over 800°C. The vehicle immediately downstream of the fire (Vehicle 4) was also subjected to extremely severe conditions, with temperatures rising rapidly to over 550°C. The subsequent downstream vehicles (Vehicles 5, 6, 7, 10, 11, 12, and 13) experienced a less severe but still significant increase in temperature, with peaks generally remaining below 100°C. In stark contrast, all vehicles located upstream of the fire (Vehicles 1, 2, 3, 8, and 9) remained entirely unaffected, with temperatures holding steady at the ambient level of ~35-40°C.

These findings are critical for assessing occupant tenability. The temperatures above the fire vehicle and its immediate neighbour are instantly lethal and far exceed any survivability thresholds. This highlights that the area of greatest risk is highly concentrated around the fire's origin. For the vehicles further downstream, the temperatures, while lower, still breach the 60°C tenability limit, indicating that this area becomes unsafe for evacuation over time, though less immediately than the fire zone. The safe conditions maintained above all upstream vehicles once again provide definitive proof of the ventilation system's success in preventing back-layering and preserving a viable escape route in the upstream direction.

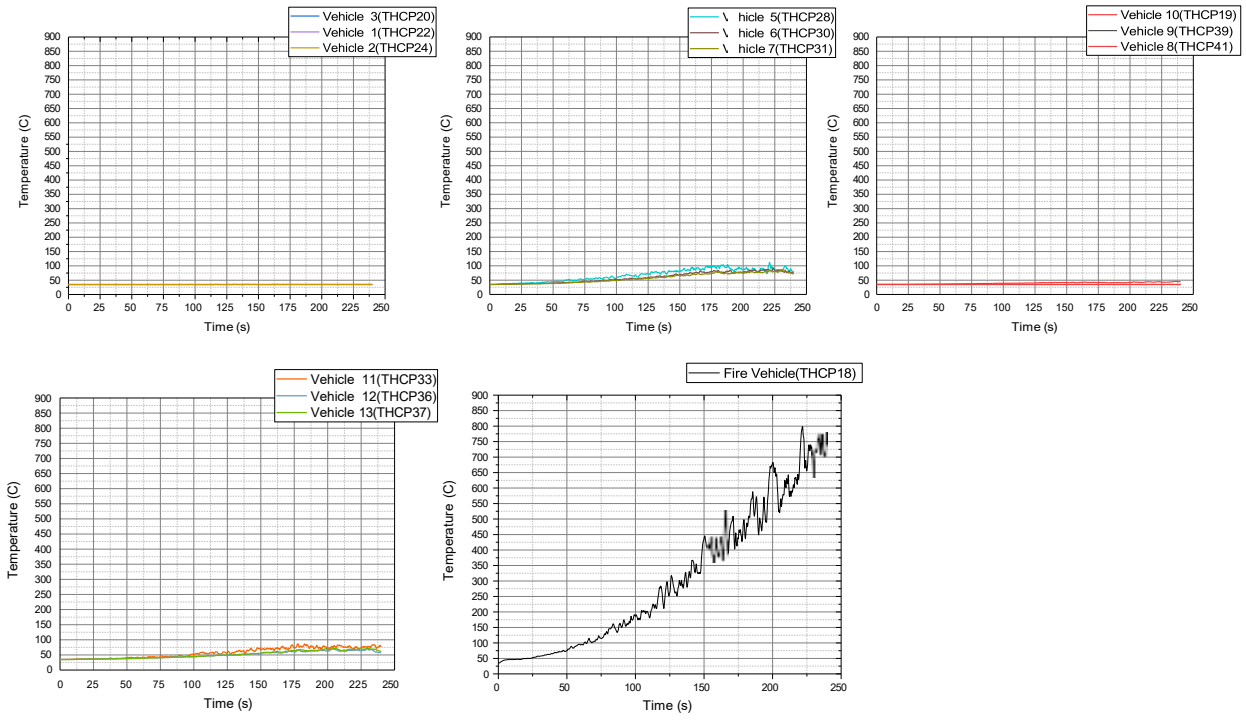

Fig. 17. Temperature vs. time profile from thermocouples placed above vehicles inside the tunnel for 100 MW fire under integrated system.

3.1.4. Temperature profile

Case-1: With natural ventilation only

The temperature distribution for the 100 MW fire under natural ventilation at 240 seconds reveals a marked difference between ceiling-level conditions and thermocouple measurements at lower elevations. While the thermocouples placed along the tunnel walls at 2.5 m height recorded elevated but comparatively moderate temperatures, the ceiling layer shows significantly higher values reaching peak of 700 °C above fire vehicle and 400 near to the fire seat, both upstream and downstream of the fire vehicle due to the stratification of hot smoke and gases at the tunnel crown. This highlights the limitation of point measurements at mid-height, which may underestimate the extreme ceiling temperatures visible in the contour plots. In addition, the thermocouples mounted on the engine hoods of vehicles (≈3.5 m height) registered sharp rises in temperature near the fire vehicle, capturing localized heating effects more faithfully than the wall-

mounted sensors. Together, these observations confirm that ceiling-level conditions are considerably harsher than indicated by standard thermocouple placements, with smoke accumulation driving elevated thermal loads across the tunnel roof.

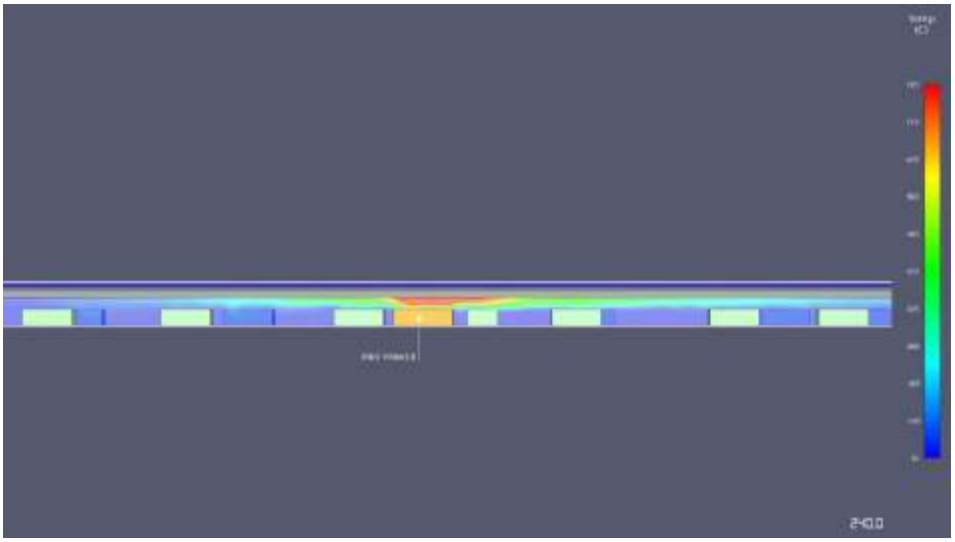

Fig. 18. Temperature profile along tunnel length under natural ventilation for 100 MW fire, showing longitudinal heat build-up

Case-2: Integrated system

At 240 seconds into the 100 MW tunnel fire scenario with longitudinal mechanical ventilation and sprinkler protection, the temperature profile demonstrates clear spatial variations along the tunnel length. On the inlet side of the fire, temperatures remain low, in the range of 35–55 °C, due to the continuous supply of fresh air by the ventilation system, which effectively prevents back-layering of smoke. In the vicinity of the fire vehicle, thermocouples positioned at 2.5 m height on both tunnel walls register significantly higher temperatures, rising to approximately 195–235 °C, indicating direct exposure to the fire plume and convective heat. Moving downstream from the fire, a stratified hot gas layer develops along the ceiling, with temperatures between 155–195 °C, while thermocouple readings at 2.5 m height in this zone show moderate levels in the range of 95–155 °C.

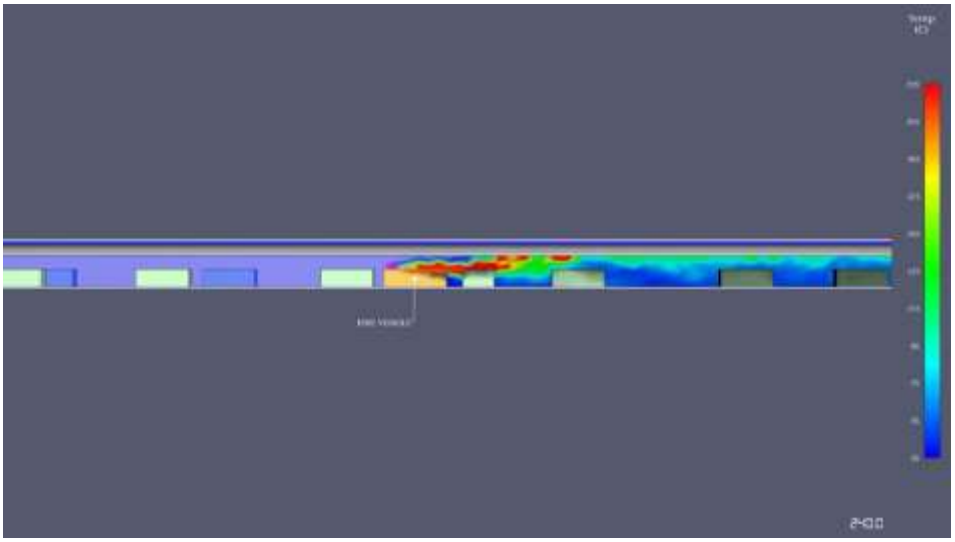

Fig. 19. Temperature profile along tunnel length under integrated system for 100 MW fire, illustrating controlled temperature rise

Further downstream, the temperature gradually reduces, stabilizing between 75–135 °C, as the hot gases are transported and diluted by the ventilation system. The sprinklers contribute to reducing peak fire temperatures and slowing down heat spread, although high temperatures persist in the immediate fire zone. Overall, the combined effect of the ventilation and sprinkler systems maintains upstream tenability while controlling downstream thermal conditions to manageable levels.

3.1.5. Smoke dynamics and concentration profile

Case-1: With natural ventilation only

The initial buoyant plume creates a ceiling jet that propagates at a similar velocity and volume both upstream and downstream. From the onset of the event through the first 60 seconds, the smoke layer spreads longitudinally along the ceiling in both directions. As the fire develops towards 240 seconds, the smoke layer deepens uniformly on both sides of the fire source. The final state shows a thick, stable smoke layer that is equally extensive and hazardous upstream and downstream, completely eliminating any directional advantage for evacuation within the upper part of the tunnel.

The simulation results for the 100 MW tunnel fire with only natural ventilation show a rapid and complete saturation of the tunnel with smoke. The time it took to reach a 100% smoke concentration generally decreased as the distance from the fire decreased, demonstrating the fast spread of smoke from the fire source. The detector at 10m reached full saturation at approximately 145 seconds , while the detector at 50m reached it at around 85 seconds . Further down the tunnel, the detectors at 60m and 70m saw a more rapid increase, reaching 100% concentration at approximately 70 and 60 seconds respectively. The detectors at 80m and 90m reached the maximum concentration even faster, at around 50 and 45 seconds respectively.

The detector at 100m showed an early rise in concentration around 15 seconds, reaching a peak of approximately 55% before dropping and then stabilizing at 100% by 30 seconds. The detectors in the downstream sections of the tunnel, from 110m to 190m, followed a similar trend, with all of them reaching and stabilizing at 100% concentration between 50 and 90 seconds. The data confirms that with a 100 MW fire and only natural ventilation, the tunnel quickly becomes completely saturated with smoke.

(a)

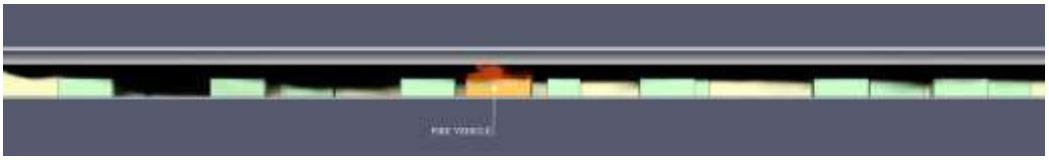

(b)

(c)

Fig. 20. Smoke distribution along tunnel length for 100 MW fire under natural at (a) 60s, (b) 150s, and (c) 240s.

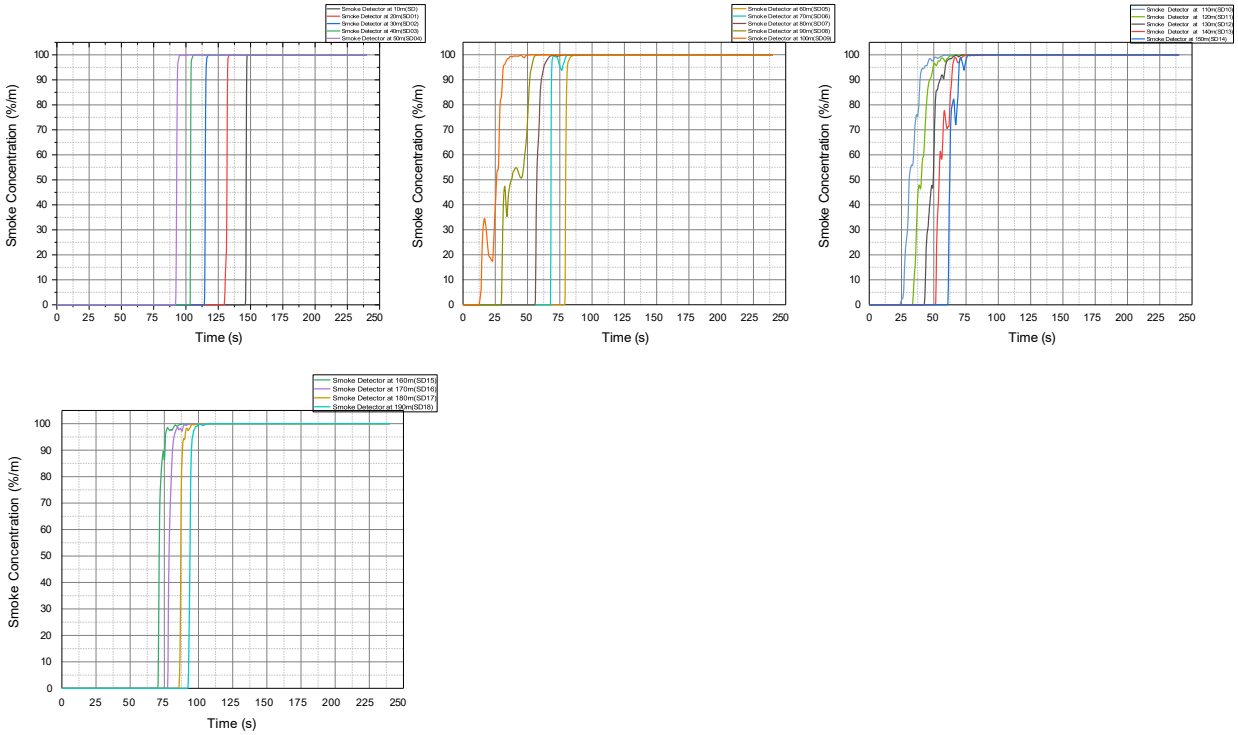

Fig. 21. Smoke concentration vs time from smoke detectors placed across tunnel length for 100 MW fire under natural ventilation

Case-2: Integrated system

This section details the results of a tunnel fire simulation conducted to assess the performance of fire protection and ventilation systems against a 100 MW heavy goods vehicle fire. The simulation was run for 240 seconds, with data collected from smoke detectors positioned at various distances from the fire's source. The analysis covers the smoke concentration trends over a 240-second period. the smoke concentration data revealed distinct patterns based on location relative to the fire's origin. On the upstream side of the tunnel (10m to 90m), the smoke detectors registered a consistent 0% smoke concentration over the entire 240-second measurement period, indicating that the ventilation system was highly effective in this region.

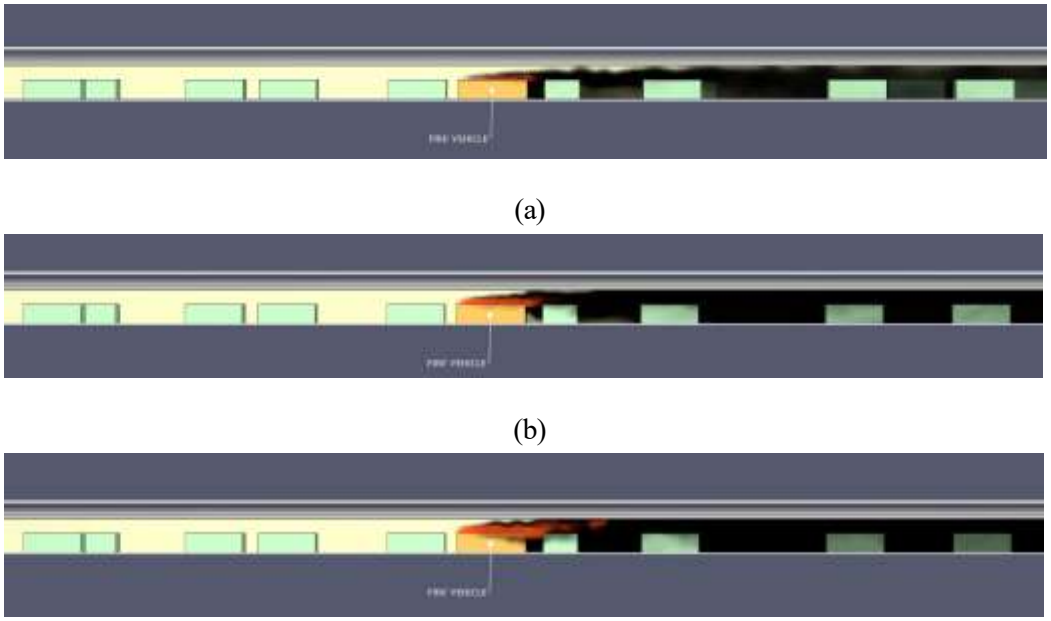

(a)

(b)

(c)

Fig. 22. Smoke distribution along tunnel length for 100 MW fire under integrated system at (a) 60s, (b) 15s, and (c) 240s.

Moving to the midstream area, specifically close to the seat of fire (100m to 120m), smoke concentration began to rise after approximately 25 seconds. At 100m, intermittent spikes of over 80% concentration were observed, while at 110m and 120m, the concentration frequently spiked to 100% between 75 and 125 seconds. Further into the tunnel, the downstream side (130m to 190m) showed an even more rapid and severe increase in smoke concentration, with detectors registering a rise from 25 seconds onward. At these distances, smoke concentration reached and stabilized at a constant 100% by approximately 80 to 150 seconds, indicating that the smoke had fully filled the tunnel in this section despite the ventilation efforts.

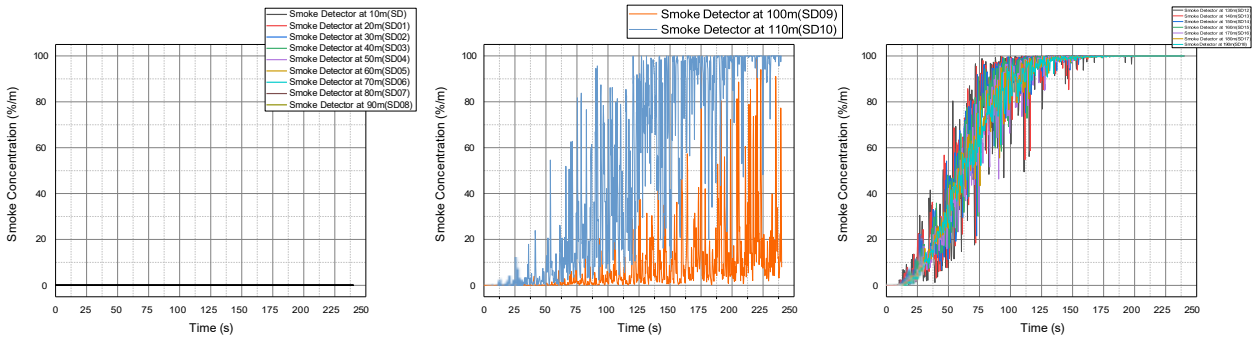

Fig. 23. Smoke concentration vs time from smoke detectors placed across tunnel length for 100 MW fire under integrated system

3.1.6. Visibility assessment

Case-1: With natural ventilation only

The evolution of visibility within the tunnel under natural ventilation conditions demonstrates a rapid and severe degradation over the 240-second period. Initially, at 60 seconds, a clear stratification is evident, with a tenable layer near the floor offering visibility of up to 30 meters, particularly on the upstream side of the fire. However, as buoyant smoke spreads bi-directionally, conditions worsen significantly. By 120 seconds, the descending smoke layer reduces visibility to below 15 meters in the fire's immediate vicinity and downstream. Critically, by 180 seconds, the smoke layer reaches the floor, completely eliminating the initial 30-meter clear zone. In the final stages, at 240 seconds, visibility drops to less than 5 meters along the majority of the tunnel's length, rendering conditions untenable for occupant egress.

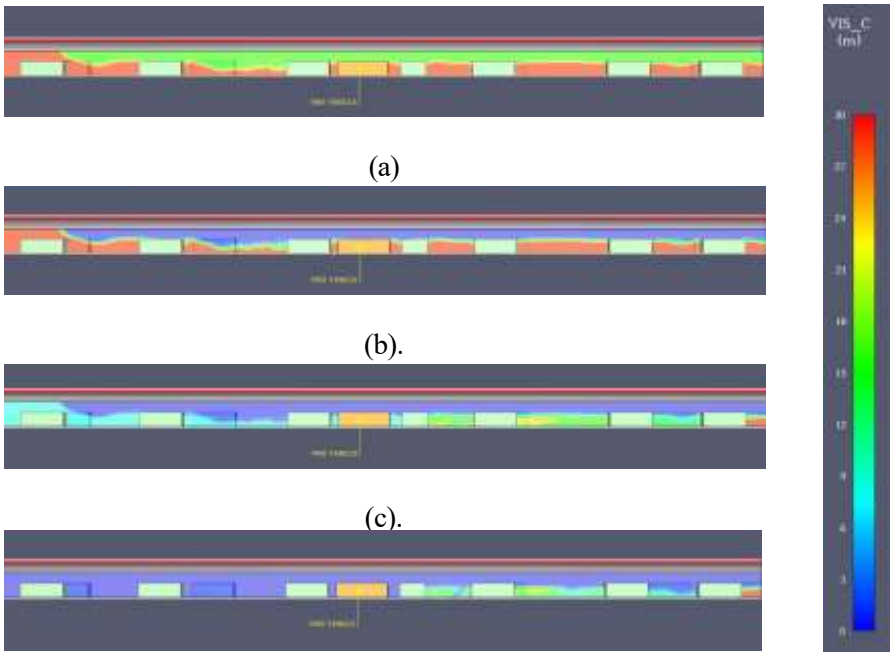

Fig. 24. Visibility distribution along tunnel length for natural ventilation in 100 MW fire at (a) 60s, (b) 120s, and (c) 210 s and (d) 240s

Case-2: Integrated system

The time-lapsed visibility slices illustrate the development and spread of smoke at evacuation height within the tunnel. At the start of the simulation (t=0s), conditions are clear with unlimited visibility throughout the tunnel. As the fire develops, smoke is generated and is immediately transported downstream by the longitudinal ventilation system. By 60 seconds, a plume of smoke has formed, and the visibility in the area immediately downstream of the fire vehicle has already begun to degrade. The progression from 90 seconds to 240 seconds shows this zone of reduced visibility extending further downstream and becoming more severe. The colour map indicates that from 120 seconds onwards, a significant portion of the downstream tunnel experiences visibility levels below 15 meters near to vehicle 4 (cyan) and even below 10 meters further downstream (blue), which is the critical threshold for safe evacuation.

The analysis of these images confirms two critical aspects of the simulation. First, the ventilation system is highly effective at controlling the direction of smoke flow. The entire tunnel upstream of the fire remains completely clear (red, indicating >30 m visibility) for the full duration, preserving a safe and tenable escape route for occupants in that section. Second, the downstream environment rapidly becomes untenable due to smoke obscuration. The degradation of visibility below the 5-meter safety threshold would severely impede or halt self-rescue efforts for any occupants located downstream, as they would be unable to locate emergency exits. This highlights a fundamental principle of tunnel fire safety: in a longitudinally ventilated fire, the upstream direction is the primary and most viable path to safety.

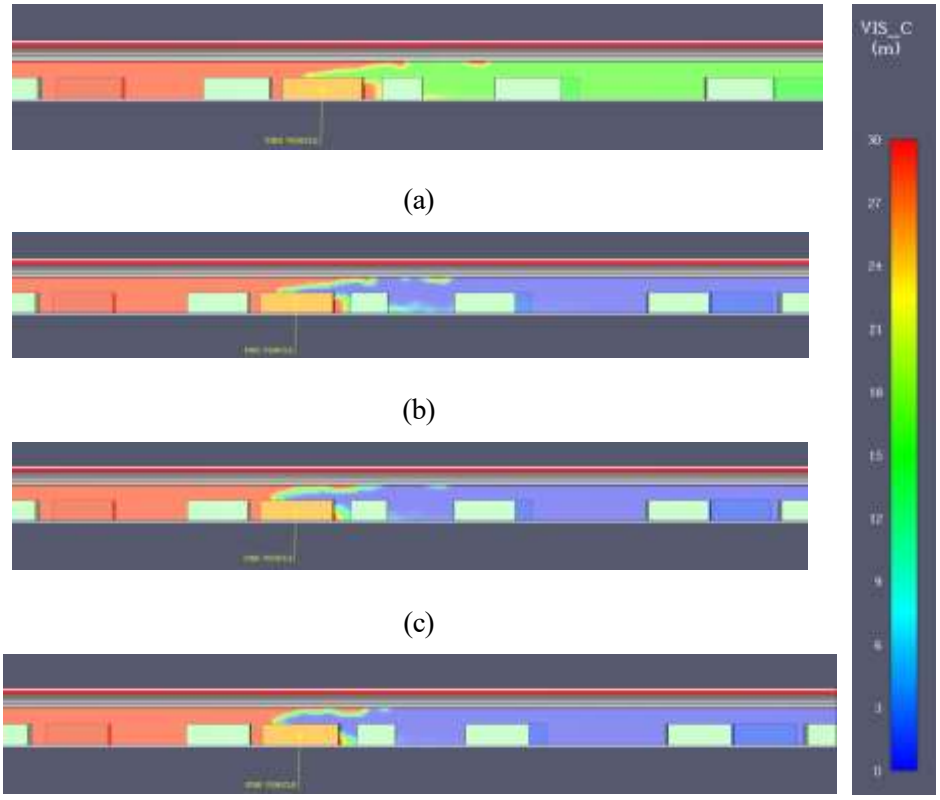

(a)

(b)

(c)

(d)

Fig. 25. Visibility distribution along tunnel length for integrated system in 100 MW fire at (a) 60s, (b) 120s, and (c) 210s and (d) 240s

3.1.7. Carbon monoxide distribution and evaluation

Case-1: With natural ventilation only

Under the 100 MW natural ventilation scenario, a hazardous accumulation of carbon monoxide is observed. By 180 seconds, a concentrated CO mass flux reaching approximately 0.001 kg/s/m² is established at the ceiling directly above the fire. By 240 seconds, while the peak flux value remains similar, the simulation shows this high-flux region spreading extensively along the ceiling, particularly downstream.

Although this hazardous layer is initially confined to the ceiling, its significant longitudinal spread indicates that subsequent smoke descent and mixing would cause CO concentrations at the breathing height (1.5 m) to surpass the tenability limit of ~1200 ppm over a large portion of the tunnel. This quantitative progression confirms the failure of natural ventilation to contain toxic gases and maintain a safe environment.

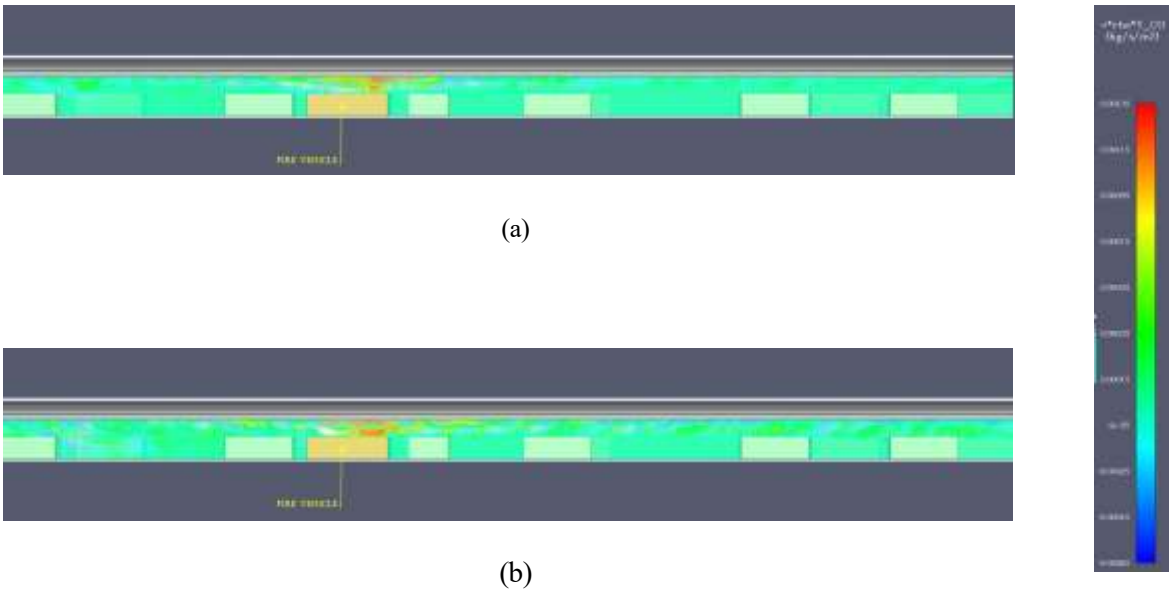

(a)

(b)

Fig. 26. CO concentration distribution along tunnel length for 100 MW fire (natural condition) at 180s and 240s

Case-2: Integrated system

the CO concentration in the tunnel simulation for a 100 MW heavy goods vehicle fire shows a clear progression over time. The analysis focuses on the colour-coded visualizations, where warmer colours (yellow, orange, red) represent higher CO concentrations.

At the beginning of the simulation (0 seconds), the entire tunnel shows a uniform green colour, indicating a negligible CO concentration. This state remains consistent up to the 60-second mark. Around 90 seconds, a small area of elevated CO concentration (indicated by yellow and light orange colours) begins to form directly above the fire vehicle.

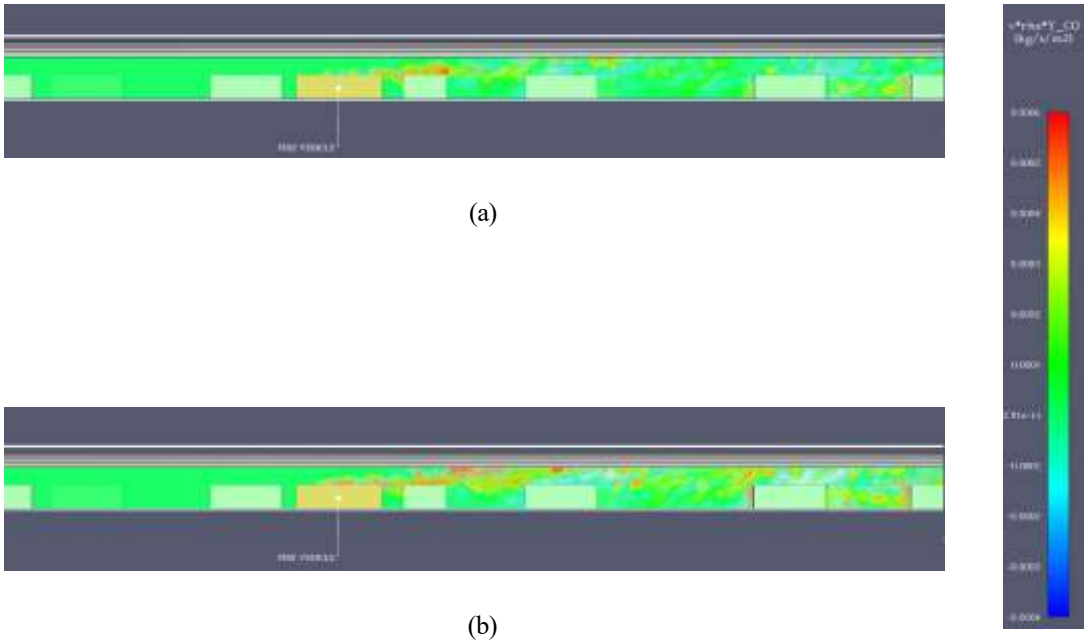

(a)

(b)

Fig. 27. CO concentration distribution along tunnel length for 100 MW fire (integrated system) at 180s and 240s

This elevated CO zone expands and intensifies over time. By 120 seconds, the concentration directly above the fire vehicle appears to have increased. At 150 seconds, a larger area of orange and red indicates a significant rise in CO concentration. The maximum CO concentration is reached at 240 seconds, where large sections of the tunnel ceiling are dark red and orange, indicating the highest levels of CO. This high concentration zone appears to extend down the tunnel from the fire source, showing that CO is spreading to the downstream side of the tunnel only because of the presence of the mechanical ventilation system which is after the vehicle fire

3.1.8 Sprinkler system response

The performance of the automatic sprinkler system was evaluated by monitoring the temperature at each sprinkler head along the tunnel ceiling. The data reveals a clear and sequential activation pattern, beginning with the sprinklers closest to the fire and propagating downstream.[29]

The sprinklers located upstream of the fire (from 4.5 m to 99 m) did not activate, as the ceiling gas temperatures in this region remained near ambient levels of ~35-40°C. The first activations occurred just downstream of the 100 m fire source. The temperature at the sprinkler located at 108 m showed a rapid increase, followed by the sprinklers at 112.5 m and 117 m.

In these plots, the temperature rises steadily until it reaches approximately 80-85°C, at which point a sharp drop occurs. This drop signifies the activation of the sprinkler and the cooling effect of the water spray on the device. Following the initial discharge, the temperature often begins to rise again before being suppressed by subsequent cycles of water spray, resulting in a sawtooth pattern. Sprinklers located further downstream (157.5 m to 198 m) show a steady temperature increase but do not reach a high enough activation temperature within the 250-second simulation time.[30]

The sprinkler activation data demonstrates the system is performing as designed. The lack of activation upstream of the 100 m mark is a positive result, confirming that the ventilation system effectively prevents the hot ceiling jet from flowing upstream (back-layering). The sequential activation of sprinklers downstream of the fire provides a clear picture of the fire's progression and the sprinkler system's response.

The sharp temperature drop preventing the actuation of sprinklers, particularly visible at the 135 m and 139.5 m locations, is a critical finding. It demonstrates the immediate cooling effect of the water spray on the surrounding atmosphere, which is essential for reducing the fire's heat release rate and preventing further fire spread. This cooling also slows the activation of sprinklers further downstream, concentrating the water application where it is most needed. This targeted response is a key advantage of an automatic sprinkler system, as it helps to control the fire efficiently without expending unnecessary water resources far from the fire's origin. The results collectively show a well-coordinated interaction between the ventilation and suppression systems.

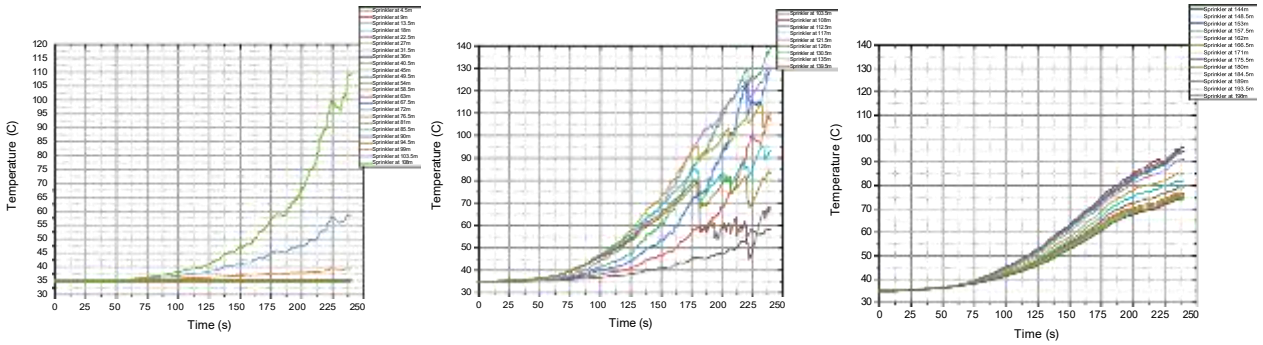

Fig. 28. Temperature–time profiles of sprinklers along tunnel length for 100 MW fire; activation occurs at 93 °C.

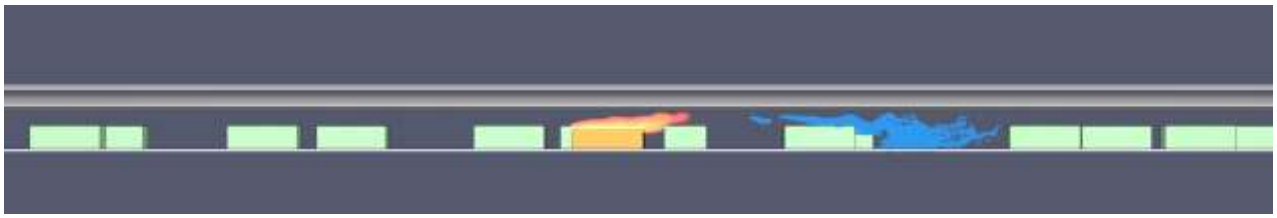

Fig. 29. First sprinkler activation at 136 s, illustrating tunnel conditions at initiation.

3.2. Bus/Truck Fire (25 MW)

3.2.1. Heat release rate characterisation of the fire vehicle

Case-1: With natural ventilation only

The heat release rate for 25 MW with natural ventilation shows a steady rise after ignition, reaching a peak of about 25,000 kW near 150 s. After this point, it gradually declines with small fluctuations, stabilizing near 10,000 kW at about 250 s. This time history captures a clear growth phase, a dominant peak, and a sustained post-peak decay without secondary surges, which is typical of a large, naturally ventilated fire. The decline is influenced by both fuel and ventilation limitations: as easily combustible fractions are consumed, the burning surface and pyrolysis rate reduce; oxygen availability around the fire core also decreases due to intense consumption and turbulent mixing at peak, slowing down reactions. The relatively low natural airflow of 0.5 m/s allows stratification of hot gases and carries heat away, reducing the feedback to the fuel surface. With flame height also decreasing after peak, surface impingement and entrainment lessen, further lowering the HRR.

Case-2: Integrated system

The Heat Release Rate (HRR) curve for the scenario with forced ventilation and sprinklers tells a compelling story of intervention and control, standing in stark contrast to a free-burning fire. Initially, the fire exhibits a natural growth phase, following a characteristic curve that accelerates significantly after 75 seconds as the fire spreads across the vehicle. The most critical event on the graph is captured at approximately 135 seconds, where the exponential growth is abruptly arrested. This sharp "knee" in the curve is the signature of the sprinkler system activating and successfully suppressing the fire's further development. Instead of reaching a natural peak and then entering a decay phase, the fire is forced into a controlled, steady-state plateau. For the remainder of the simulation, the HRR fluctuates intensely around a constant 25,000 kW (25 MW), representing a sustained and powerful thermal challenge to the tunnel environment. This demonstrates that while the suppression system did not extinguish the fire, it effectively capped its output, transforming the event from a transient, growing threat into a constant, high-intensity fire that the tunnel's ventilation system must continuously manage.

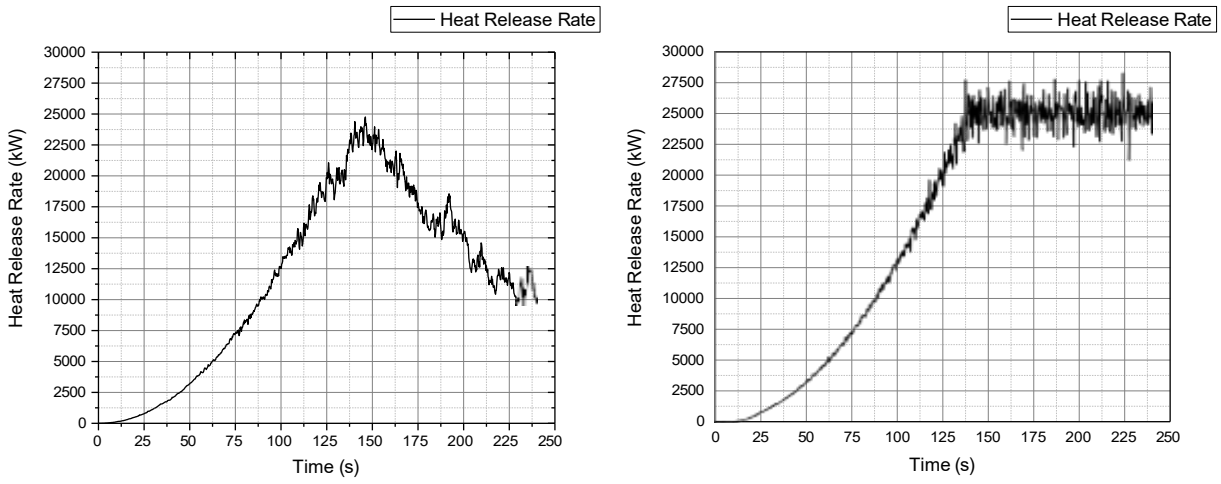

(a) (b)

Fig. 30. Heat Release Rate (HRR) for 25 MW design fire: (a) natural ventilation only, (b) integrated system

3.2.2. Thermal response of tunnel boundaries

Left wall

Case-1: With natural ventilation only

The thermal data for the 25 MW fire under natural ventilation reveals a widespread and untenable environment, characterized by significant bidirectional heat spread. The thermocouple at the 100 m mark, opposite the fire, recorded the most severe conditions, with a turbulent temperature increase to a peak of nearly 250 °C after 212 seconds. This thermal hazard propagated extensively in both directions, demonstrating a catastrophic failure of smoke and heat

control. Upstream locations, such as 80 m, and downstream locations, such as 120 m, both experienced temperatures that rose to and exceeded the 60 °C tenability limit, confirming the presence of extensive back-layering. However, at positions further upstream (<80 m) and further downstream (>140 m), the temperatures did not reach catastrophic levels within the 240-second period, indicating that pockets of tenable conditions remain in these outer regions and that evacuation may still be feasible if initiated promptly. Overall, this progression confirms that a fire of this magnitude overwhelms natural ventilation near and around the fire core, while leaving only limited escape potential at the far ends of the tunnel.

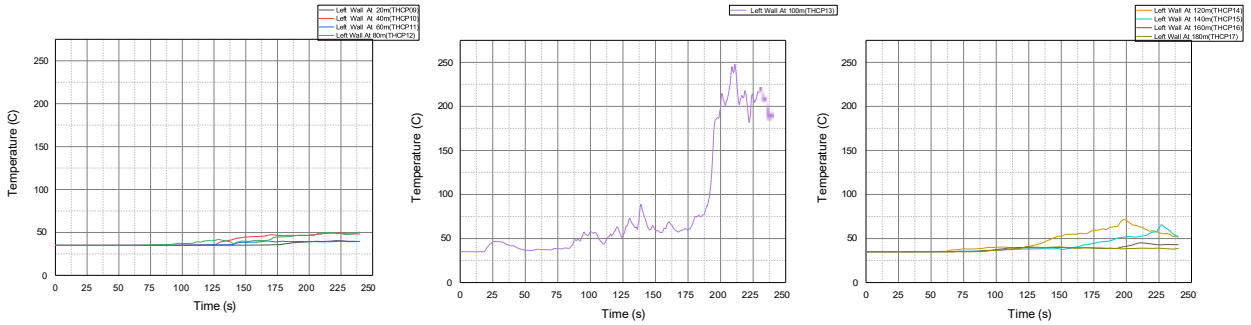

Fig. 31. Temperature vs. time profile from left-wall thermocouples for 25 MW fire under natural ventilation at upstream and downstream locations.

Case-2: Integrated system

The thermocouple data from the left tunnel wall reveals a distinct spatial distribution of heat from the fire located on the right side. A clear thermal boundary is evident: the wall section from 20m to 100m shows no increase from the ambient temperature of 35°C. In sharp contrast, the wall sections from 120m to 180m experience a significant temperature rise, which begins approximately 50 seconds after ignition and reaches fluctuating peaks of about 65-70°C. This localized heating confirms that the fire is situated in the central region of the tunnel. The data also demonstrates that while hot gases may be spreading along the ceiling, their significant thermal impact on the wall structures is concentrated in the immediate vicinity of the fire.

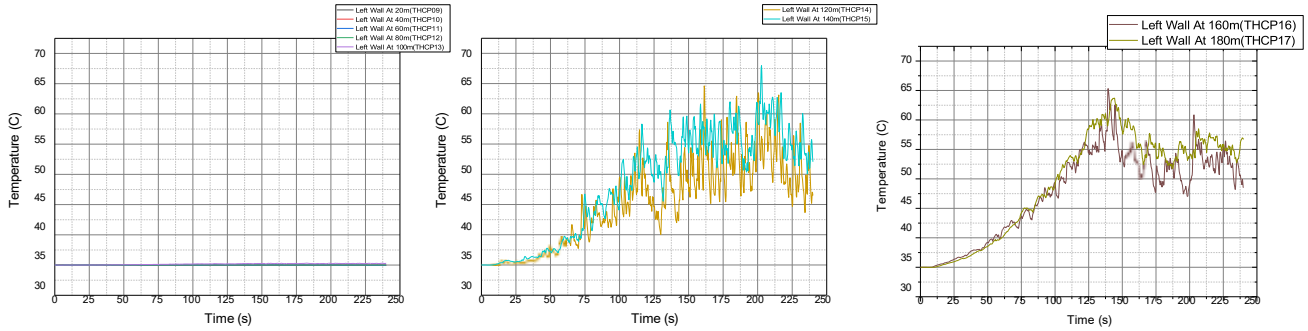

Fig. 32. Temperature vs. time profile from left-wall thermocouples for 25 MW fire under integrated system, showing near-ambient conditions with no significant rise at upstream.

Right wall (Fire side wall)

Case-1: With natural ventilation only

The thermal data from the right wall, adjacent to the fire, reveals an extremely hazardous and widespread thermal environment under the 25 MW natural ventilation scenario. The thermocouple at the 100 m mark recorded the most severe conditions, with a turbulent temperature increase peaking at over 350°C at about 210 second mark, a level that would cause rapid structural damage and is instantly lethal. The data confirms a significant bidirectional heat spread,

with the downstream thermocouple at 120 m showing temperatures rising to and exceeding the 60°C tenability limit. Critically, all upstream locations also recorded a temperature rise, confirming extensive back-layering, although the temperatures remained below the 60°C threshold. This quantitative progression proves that the 25 MW fire completely overwhelms the natural ventilation, creating a thermally untenable downstream environment while contaminating the upstream escape route with a hazardous smoke layer, rendering safe egress impossible from any direction.

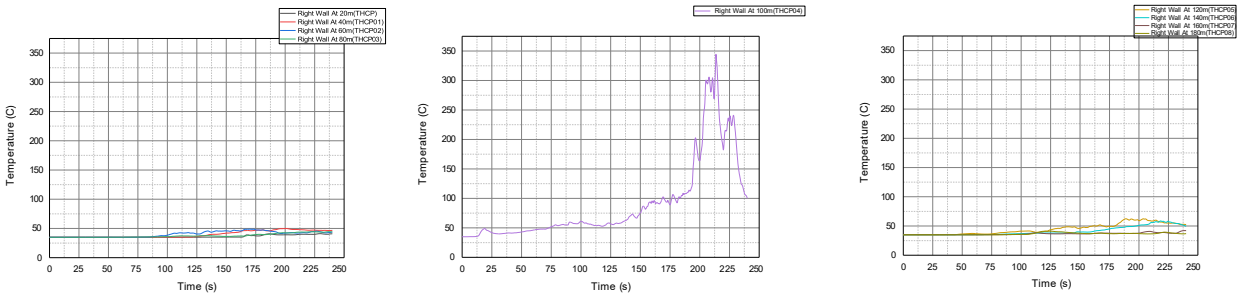

Fig.33. Temperature vs. time profile from right-wall thermocouples for 25 MW fire under natural ventilation

Case-2: Integrated system

The temperature data from the right tunnel wall, the side of the fire's origin, pinpoints the fire's exact location and its thermal impact . The wall section from 20m to 80m remains completely unaffected, holding a steady ambient temperature of about 35°C. In stark contrast, the thermocouple at 100m shows a dramatic temperature rise starting around 50 seconds, with intense fluctuations peaking at nearly 190°C, clearly identifying the fire's center . Further along, the downstream wall sections from 120m to 180m are heated more gradually by the moving hot gas layer, reaching peak temperatures of about 110°C. This creates a clear thermal map: no impact upstream, a highly intense and localized impact at the fire, and moderate heating downstream.

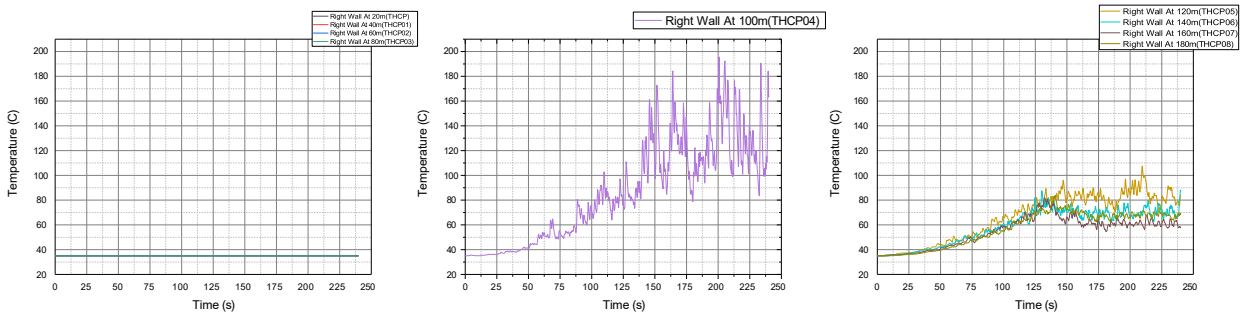

Fig. 34. Temperature vs. time from right-wall thermocouples for 25 MW fire integrated system, showing significant rise at 25 m due to fire origin at right side of the tunnel, unlike the left-wall case.

3.2.3. In-vehicle thermocouple temperature evaluation

Case-1: With natural ventilation only

The thermocouple data quantifies the fire's thermal impact and heat distribution, revealing a peak temperature of approximately 600°C around 90 seconds on the fire vehicle. The results show a steep thermal gradient with distance from the source; a nearby vehicle (Vehicle 10) recorded a peak temperature of nearly 300°C , whereas more distant vehicles experienced significantly less heat, with temperatures generally remaining below 125°C. This analysis confirms that while the most severe temperatures were highly localized to the fire's origin, the moderately elevated temperatures recorded across the wider vehicle array corroborate the widespread propagation of the hot gas layer observed in the visual profiles.

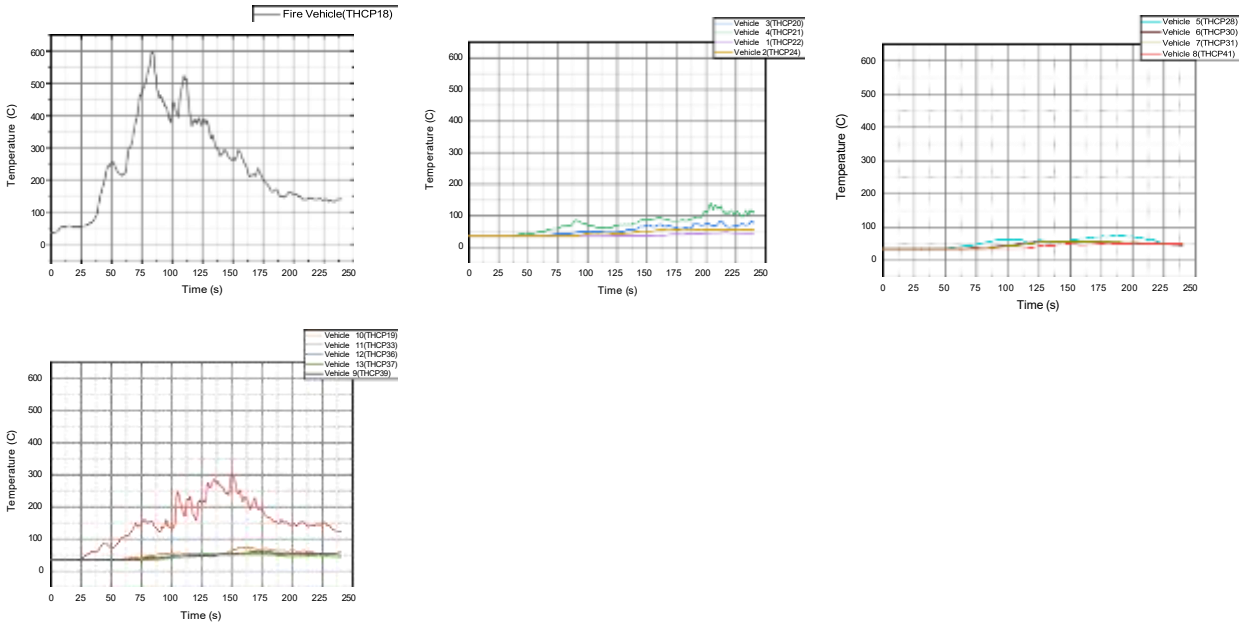

Fig. 35. Temperature vs. time profile from thermocouples placed above vehicles inside the tunnel for 25 MW fire under natural ventilation condition

Case-2: Integrated system

The thermocouple data reveals how forced ventilation and sprinklers create distinct thermal zones in the tunnel . The sprinkler's cooling effect is clear on the fire vehicle, which peaked at approximately 450°C, significantly lower than in the scenario without suppression. The 2 m/s forced ventilation creates a safe upstream zone, where Vehicles 1 and 2 remained at ambient temperature. In sharp contrast, it also directs the hazard downstream, immediately engulfing Vehicles 3 and 4 in gases over 400°C. This heat then decays with distance, as vehicles located further downstream recorded much lower peak temperatures between 75°C and 100°C. This analysis shows how the systems successfully contain the hazard but create an extremely dangerous environment just downstream of the fire.

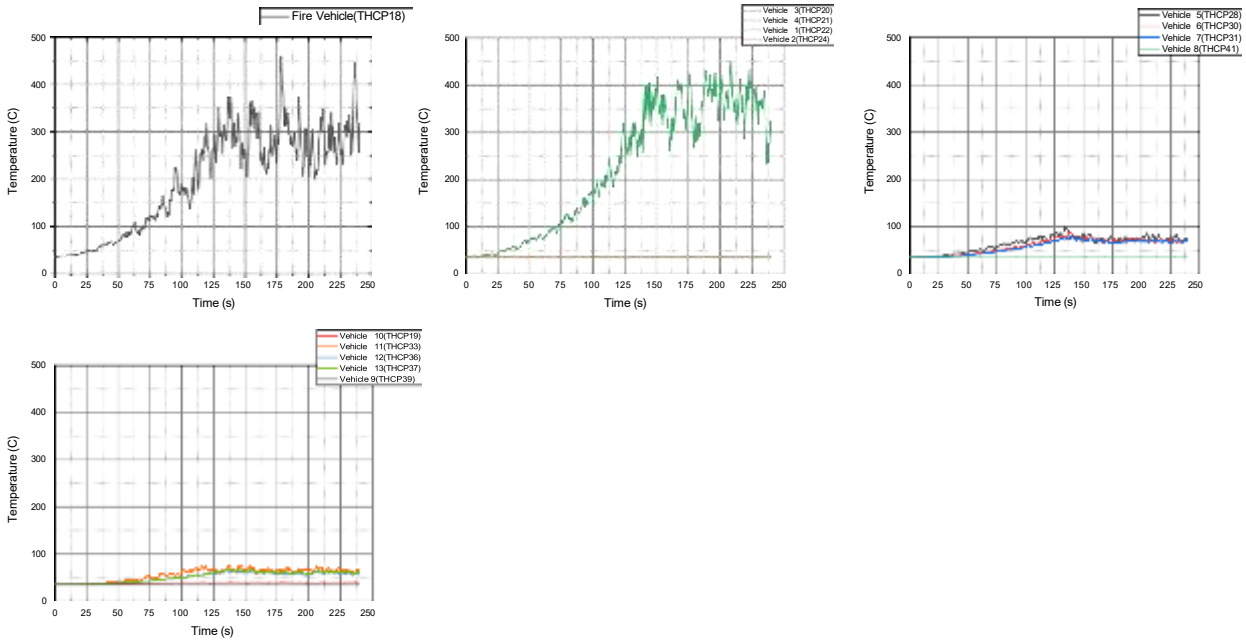

Fig. 36. Temperature vs. time profile from thermocouples placed above vehicles inside the tunnel for 25 MW fire under integrated system

3.2.4. Temperature profile

Case-1: With natural ventilation only

The time-series temperature profiles from 0 to 240 seconds reveal the rapid development of a hot, stratified gas layer from the 25 MW fire. Critically, the simulation shows a nearly symmetrical, bidirectional smoke spread along the ceiling, indicating that the fire's powerful buoyancy forces overwhelm the weak 0.5 m/s natural ventilation, causing significant backlayering. With temperatures exceeding 335°C above the fire, this uncontrolled spread contaminates both upstream and downstream escape routes almost simultaneously. This result highlights a severe life safety hazard and demonstrates the ineffectiveness of low-velocity ventilation in managing smoke for a fire of this magnitude.

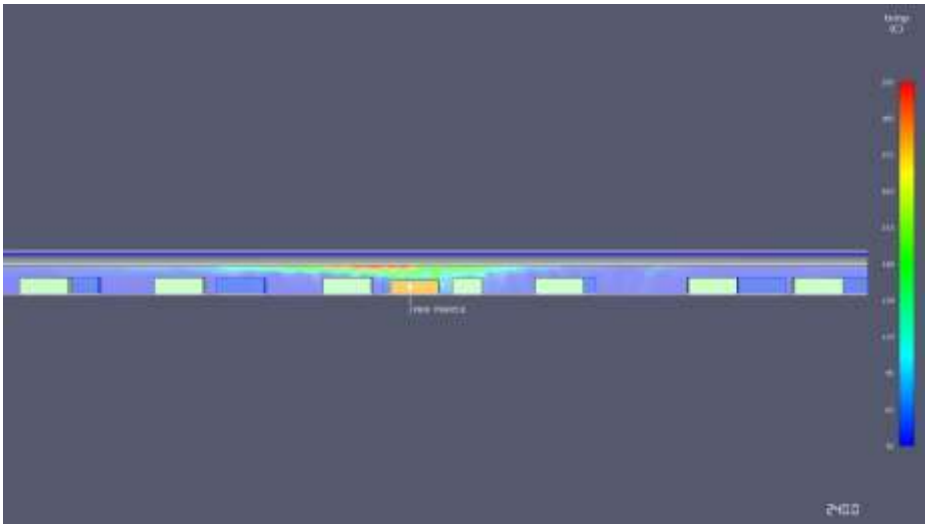

Fig. 37. Temperature profile along tunnel length under natural ventilation for 25 MW fire, showing longitudinal heat build-up

Case-2: Integrated system

This temperature profile shows the powerful impact of combining forced ventilation and a sprinkler system . The 2 m/s forced ventilation is highly effective, completely preventing backlayering by pushing all hot gases and smoke exclusively downstream (to the right of the fire vehicle). This keeps the entire upstream section clear and tenable. The cooling from the sprinkler system is also evident, as the peak temperatures are significantly reduced, only reaching about 185°C. This cooling causes the smoke to lose buoyancy and de-stratify, mixing throughout the downstream area instead of staying at the ceiling. While these systems successfully control the fire's spread, they create a turbulent, smoke-logged environment downstream.

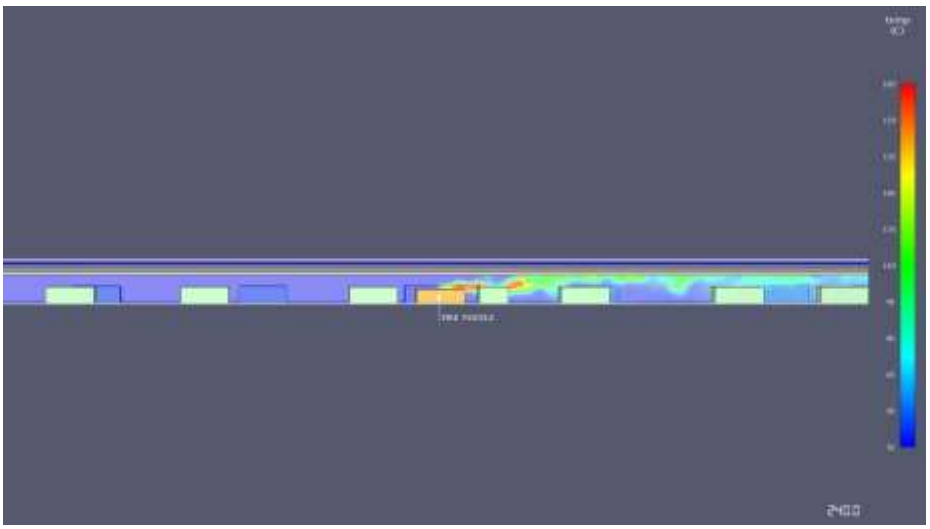

Fig. 38. Temperature profile along tunnel length under integrated system for 25 MW fire, illustrating controlled temperature rise

3.2.5. Smoke dynamics and concentration profile

Case-1: With natural ventilation only

In the 25 MW tunnel fire simulation with natural ventilation, the smoke concentration, measured at the ceiling, demonstrates a rapid and complete saturation of the tunnel. The time taken for the smoke to reach the detectors and stabilize at 100% concentration generally decreased as the distance from the fire decreased. At 10m, the concentration remained at 0% for approximately 125 seconds before a near-instantaneous jump to 100% . Similarly, the detectors at 20m, 30m, 40m, and 50m all showed a sharp rise to 100% at 115, 105, 95, and 85 seconds, respectively . Moving closer to the fire, the detectors at 60m and 70m reached maximum concentration at approximately 70 and 60 seconds, respectively . At 80m, the smoke rose rapidly to 100% around 50 seconds, while at 90m, it spiked to 100% at approximately 45 seconds . The detector at 100m showed an early rise in concentration around 15 seconds, reaching a peak of approximately 55% before dropping and then stabilizing at 100% by 30 seconds . Further down the tunnel, the detectors from 110m to 190m all reached and stabilized at 100% smoke concentration between approximately 40 seconds and 75 seconds . This data confirms that with a 25 MW fire and only natural ventilation, the tunnel quickly becomes completely saturated with smoke

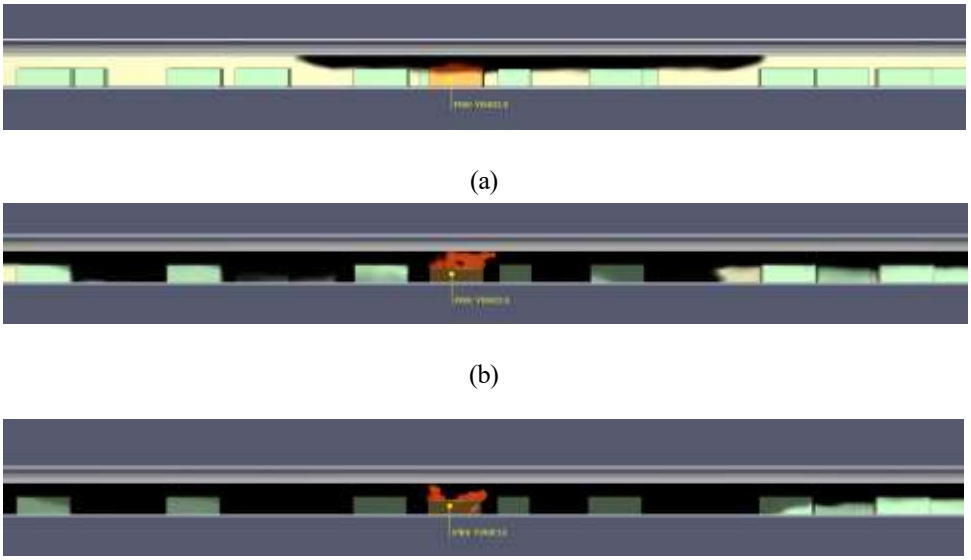

(a)

(b)

(c)

Fig. 39. Smoke distribution along tunnel length for 25 MW fire under natural at (a) 60s, (b) 150s, and (c) 240s.

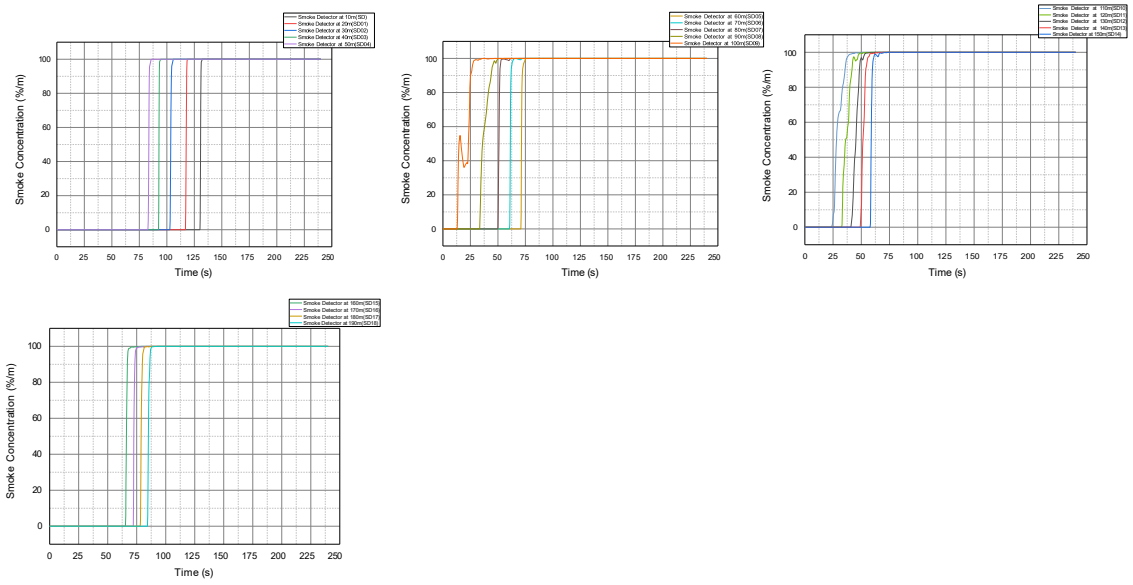

Fig. 40. Smoke concentration vs time from smoke detectors placed across tunnel length for 25 MW fire under natural ventilation

Case-2: Integrated system

In the 25 MW tunnel fire simulation with both longitudinal mechanical ventilation and a sprinkler system, the smoke concentration, measured at the ceiling, shows a varying level of control depending on the distance from the fire. From 10m to 90m from the fire source, all detectors registered a consistent 0% smoke concentration for the entire 250-second simulation period, demonstrating the effective performance of the combined systems in preventing smoke from spreading to this section of the tunnel . At 100m, the concentration remained low, with small spikes that never exceeded 20% . However, at 110m and 120m, the concentration became highly volatile, fluctuating rapidly between 0% and 100%. the downstream detectors from 130m to 190m showed a clear trend of rising and stabilizing at 100% concentration . The smoke concentration at 130m stabilized at 100% by approximately 75 seconds, while at 190m, it reached full saturation around 105 seconds . This indicates that the higher heat release rate of the 25 MW fire overwhelmed the system's ability to prevent smoke from completely filling the downstream portion of the tunnel.

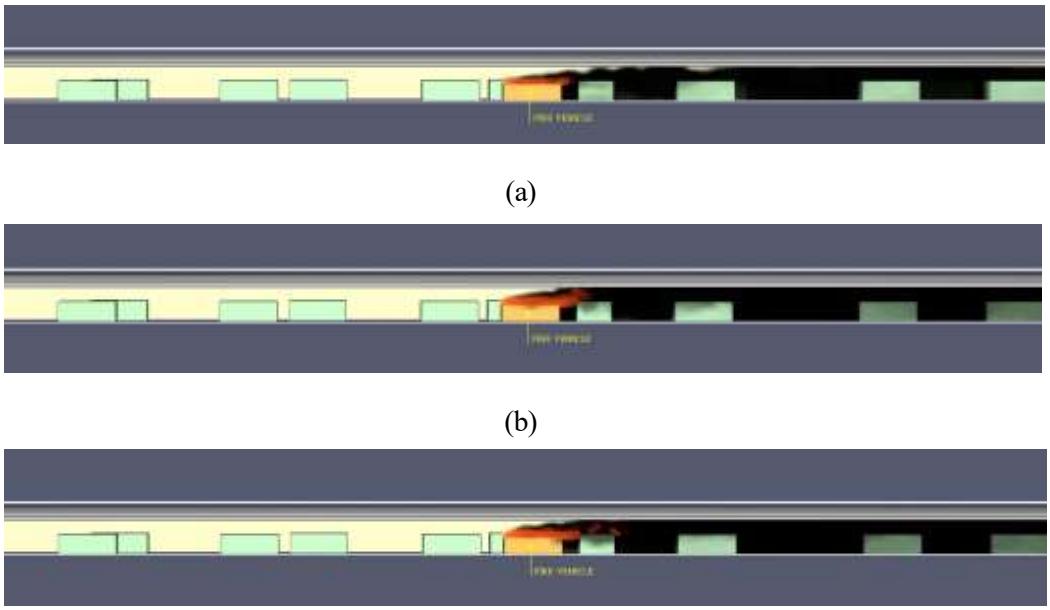

(a)

(b)

(c)

Fig. 41. Smoke distribution along tunnel length for 25 MW fire under integrated system at (a) 60s, (b) 15s, and (c) 240s.

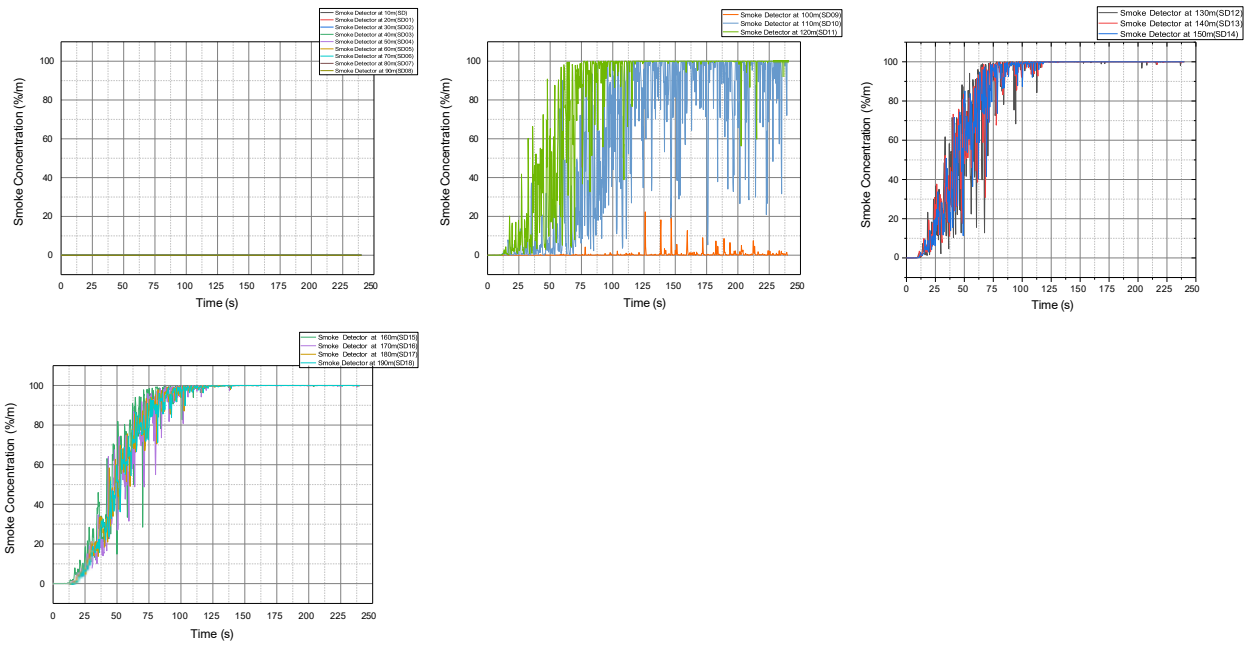

Fig. 42. Smoke concentration vs time from smoke detectors placed across tunnel length for 25 MW fire under integrated system

3.2.6. Visibility and Smoke Propagation (25 MW with Protection and Ventilation)

Case-1: With natural ventilation only

The visibility simulation shows a rapid degradation of tenability due to the bidirectional spread of a stratified smoke layer. In the initial stage, up to about 90 seconds, visibility between vehicles and at lower heights around them is relatively maintained, as the vehicles themselves obstruct and delay the downward propagation of smoke. Within 60 seconds, however, the ceiling layer already shows a reduction in visibility to approximately 15–20 meters. By 120 seconds, as the smoke layer deepens and extends beyond vehicle shielding, visibility drops below the 10-meter threshold necessary for safe evacuation. By 240 seconds, near-zero visibility engulfs the tunnel's upper volume, completely obscuring escape routes. This rapid and symmetrical deterioration confirms that, without active smoke control, opportunities for self-rescue from both upstream and downstream directions are severely compromised

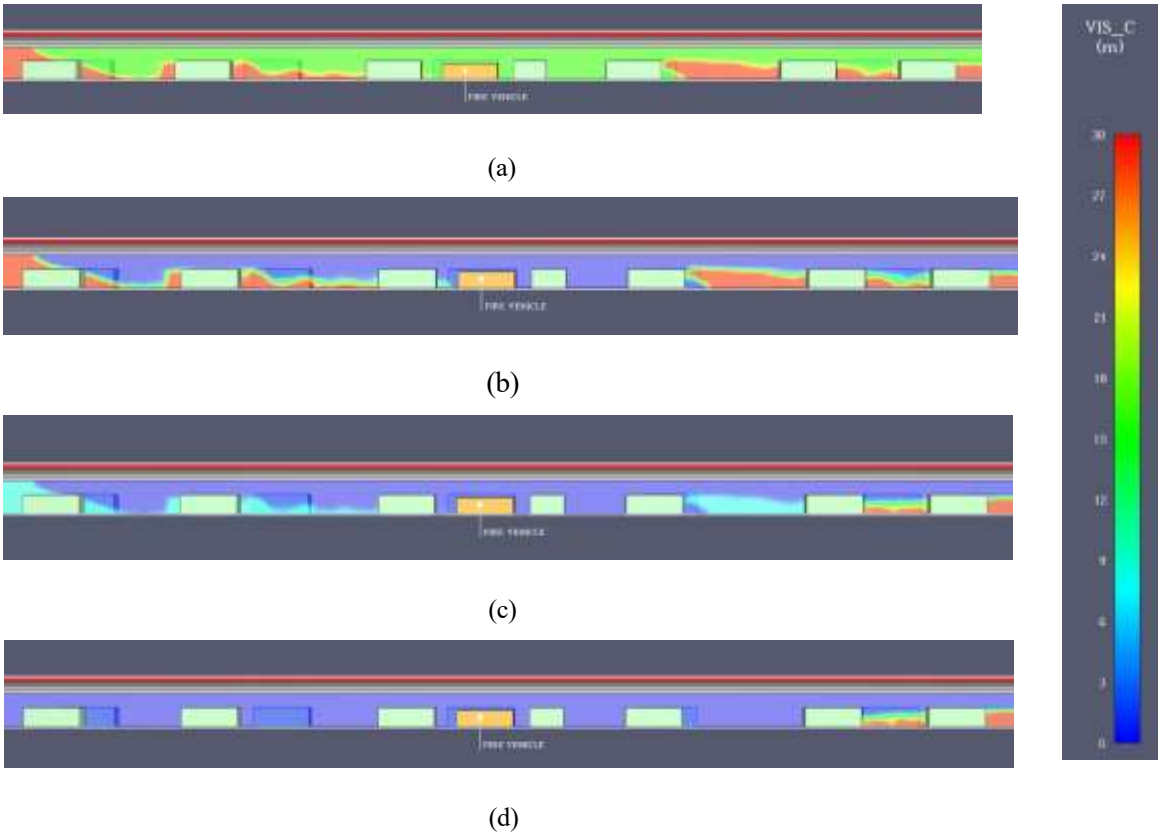

(a)

(b)

(c)

(d)

Fig. 43. Visibility distribution along tunnel length for natural ventilation in 25 MW fire at (a) 60s, (b) 120s, and (c) 210s and (d) 240s

Case-2: Integrated system

The visibility profiles clearly show the complex interaction between forced ventilation and sprinklers. The forced ventilation is highly successful in preventing back layering, maintaining clear visibility (>30m) in the entire upstream section throughout the simulation. However, the cooling effect of the sprinklers causes the smoke downstream to de-stratify, lose buoyancy, and mix down to the road level. This process completely fills the downstream cross-section with smoke, and by 240 seconds, visibility in this extensive area drops well below the critical 10-meter threshold for safe evacuation. While the systems protect the upstream route, they create a widespread, low-visibility, and untenable environment for anyone located downstream of the fire.

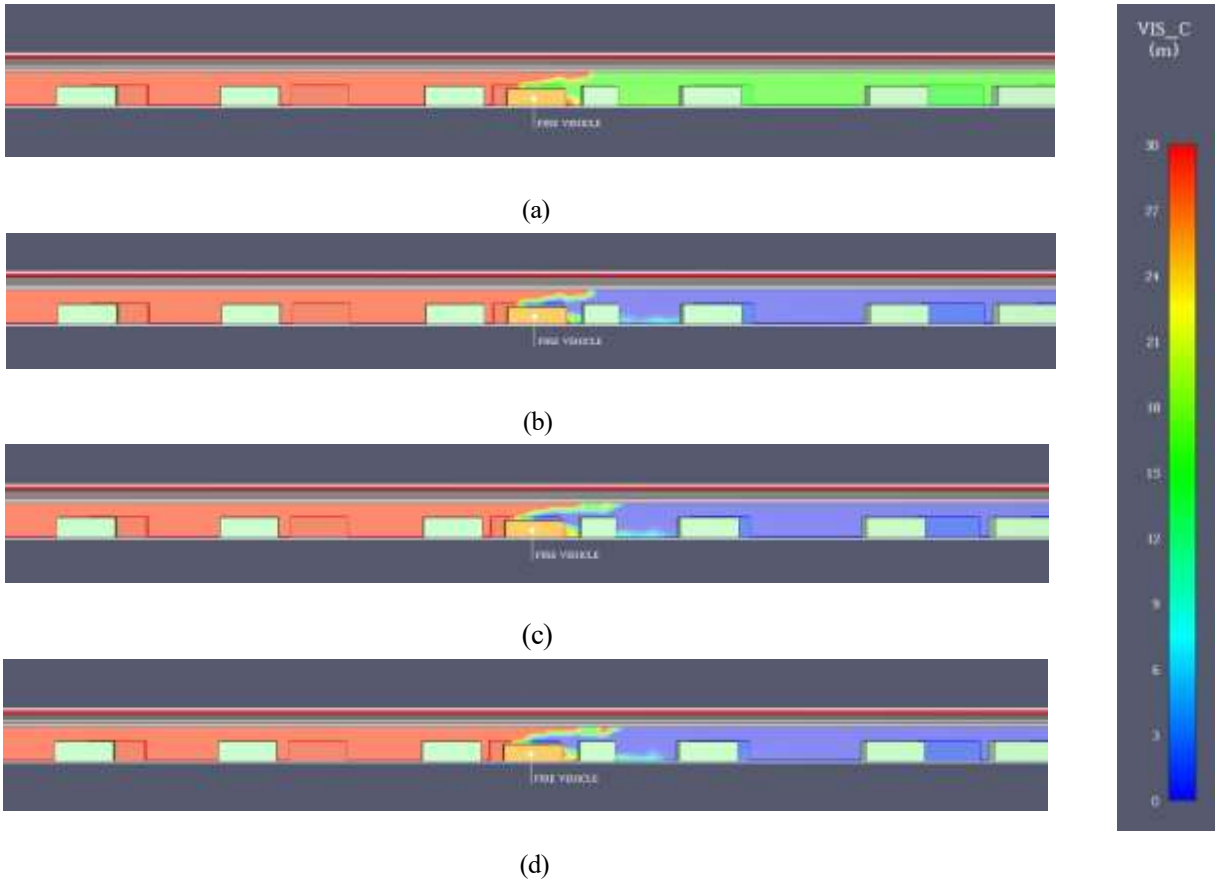

(a)

(b)

(c)

(d)

Fig. 44. Visibility distribution along tunnel length for integrated system in 25 MW fire at (a) 60s, (b) 120s, and (c) 210s and (d) 240s

3.2.7. Carbon monoxide distribution and evaluation

Case-1: With natural ventilation only

In the 25 MW fire with natural ventilation, the accumulation of carbon monoxide is gradual. A localized CO mass flux first appears at 90 seconds, peaking at approximately 0.0008 kg/s/m² at the ceiling above the fire. By 180 seconds, this zone expands bi-directionally, and the flux begins to intensify in pockets, with peak values reaching approximately 0.0010 kg/s/m² (orange). This trend continues to 240 seconds, where the CO flux is at its maximum near the fire seat and diminishes with distance. At this final stage, the weak 0.5 m/s ventilation causes a slightly more pronounced downstream spread, creating inconsistent pockets of elevated flux at the ceiling level.

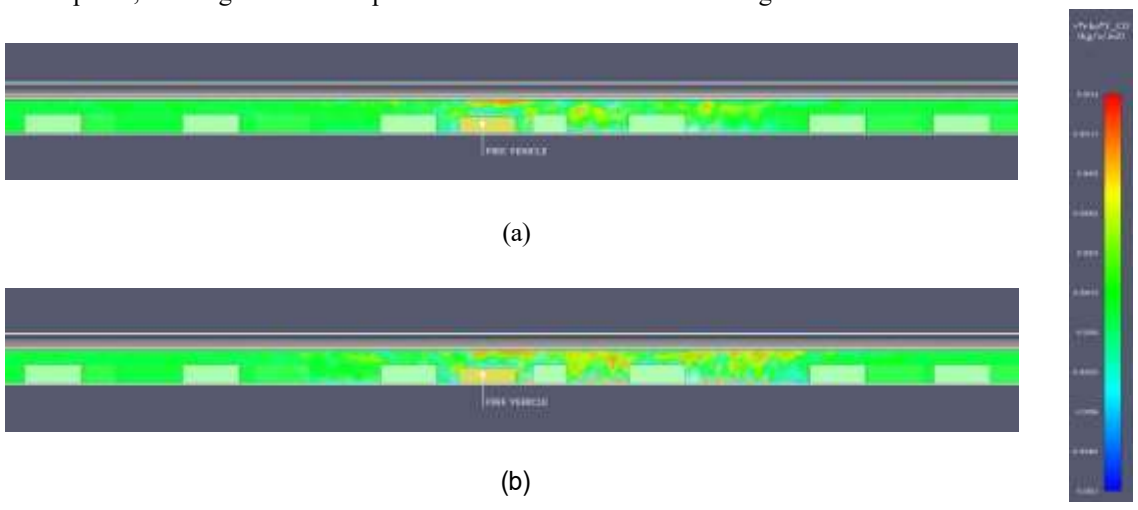

(a)

(b)

Fig. 45. CO concentration distribution along tunnel length for 25 MW fire (natural condition) at 180s and 240s

This mass flux represents the rate of toxic gas transport; as the smoke layer cools and mixes downwards, it increases the CO concentration (ppm) at the breathing height (1.5 m) especially between the vechile space where the CO concentration flux is distributed throughout the tunnel height, eventually posing a risk to occupants by approaching hazardous thresholds (~1200 ppm)

Case-2: Integrated system

The simulation results for Carbon Monoxide (CO) distribution demonstrate the powerful, though incomplete, effect of the 0.5 m/s natural ventilation. The flow is overwhelmingly unidirectional, with the vast majority of the toxic CO gas being pushed downstream (to the right of the fire). This creates a highly concentrated, rapidly expanding hazardous zone in the direction of the ventilation. However, a minimal amount of back layering is still observable, as a small, low-concentration layer of CO extends approximately one vehicle length upstream against the flow. This shows that while the ventilation successfully directs the bulk of the hazard

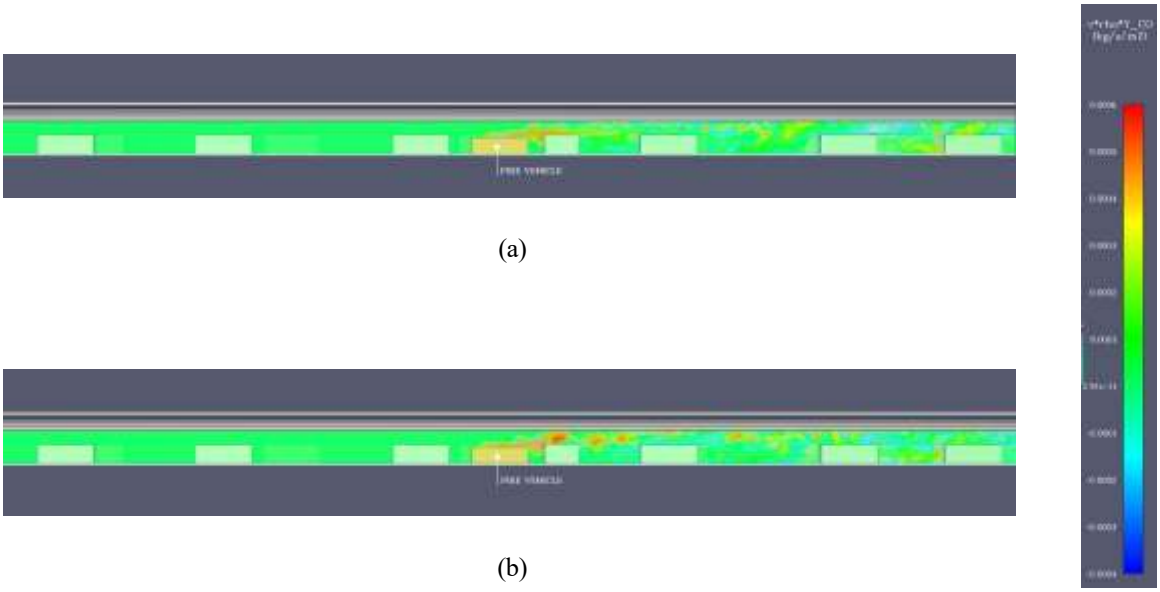

(a)

(b)

Fig. 46. CO concentration distribution along tunnel length for 25 MW fire (integrated system) at 180s and 240s

3.2.8. Sprinkler system response

In the 25 MW tunnel fire simulation with a fire protection system, the temperature data, measured at the ceiling, reveals that the heat generated was sufficient to actuate sprinklers in a specific section of the tunnel. Sprinklers located from 4.5m to 99m from the fire did not actuate, as the temperature in this section remained at a stable 35°C throughout the simulation, well below the 93°C actuation threshold. The temperatures at the sprinklers from 103.5m to 108m gradually increased to a peak of approximately 75°C after 150 seconds, still failing to trigger the system. However, sprinklers located from 112.5m to 135m showed a more significant rise in temperature, with several locations exceeding the actuation threshold. Specifically, the temperature at 112.5m and 117m peaked at approximately 120°C to 125°C, which would have triggered the sprinklers.

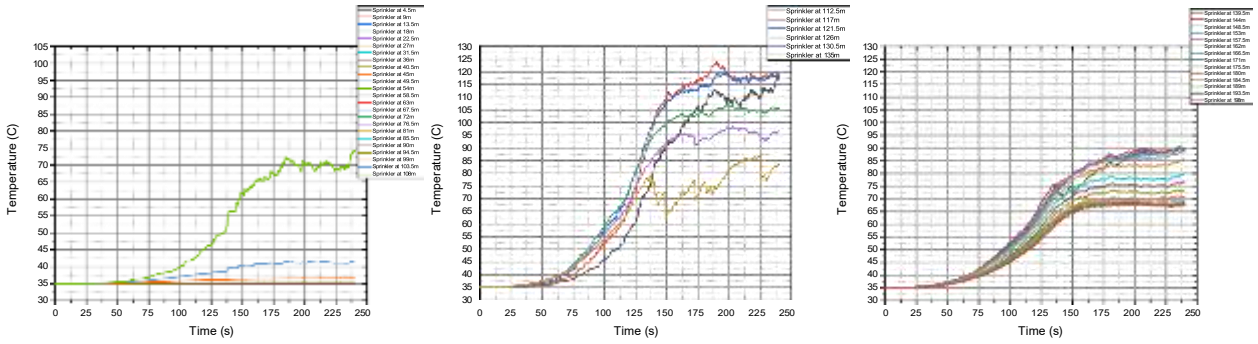

Fig. 47. Temperature–time profiles of sprinklers along tunnel length for 25 MW fire; activation occurs at 93 °C.

Further down the tunnel, the temperatures at sprinklers from 139.5m to 198m rose to a maximum of 70°C to 90°C, but did not reach the necessary temperature for actuation. This demonstrates that the 25 MW fire generated enough heat to successfully actuate the sprinkler system in a specific zone.

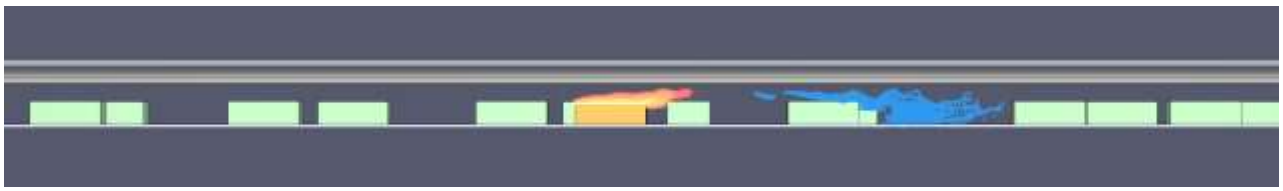

Fig. 48. First sprinkler activation at 136 s, illustrating tunnel conditions at initiation.

3.3. Passenger Vehicle Fire (10 MW)

3.3.1. Heat release rate characterisation of the fire vehicle

Case-1: With natural ventilation only

The Heat Release Rate (HRR) for the 10 MW fire under natural ventilation is presented in Figure 49(a). The fire exhibits a distinct growth phase consistent with a t-squared model, followed by a fully developed, steady-state phase. The HRR grows rapidly from ignition, reaching its peak of approximately 7,500 kW (7.5 MW) at around 100 seconds into the simulation. After reaching this peak, the fire maintains a relatively steady, albeit turbulent, energy output for the remainder of the 250-second period.

This HRR profile is characteristic of an unsuppressed fire, where the growth is limited only by the fuel and available oxygen. The sustained, high-energy output of approximately 7.5 MW is the fundamental driver of the hazardous conditions observed throughout this scenario. This continuous release of thermal energy is directly responsible for the rapid temperature rise and the generation of dense, toxic smoke that propagates bidirectionally through the tunnel. The analysis confirms that without any fire suppression to control the HRR, the fire is allowed to reach its full potential, leading to the swift and widespread loss of tenable conditions.

Case-2: Integrated system

The Heat Release Rate (HRR) for the 10 MW fire under the influence of the integrated safety systems is presented in Figure 49(b). The fire exhibits an initial t-squared growth phase, reaching a peak of approximately 7,500 kW (7.5 MW) at around 100 seconds into the simulation. Following this, the HRR transitions into a controlled, steady-state phase, where it is maintained at this level for the remainder of the 250-second period, with minor fluctuations characteristic of the interaction between the fire and the sprinkler spray.

This HRR profile provides a quantitative measure of the fire suppression system's effectiveness. The analysis shows that the sprinkler system successfully controls the fire capping it at around 7.5 MW. The integrated system also allows for the highly tenable condition observed upstream of the tunnel in this scenario. By limiting the HRR, the sprinkler system directly reduces the amount of heat and smoke being produced, which in turn allows the ventilation system to manage the hazard more effectively. This result demonstrates a successful synergy between the suppression and ventilation systems, leading to a well-controlled fire and a high level of life safety.

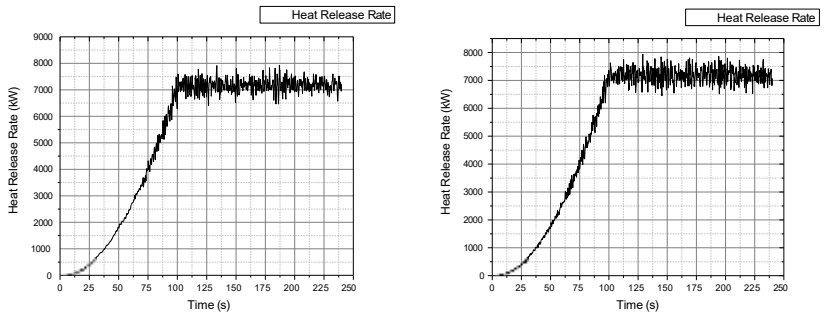

(a) (b)

Fig. 49. Heat Release Rate (HRR) for 10 MW design fire: (a) natural ventilation only, (b) integrated system

3.3.2. Thermal response of tunnel boundaries

Left wall

Case-1: With natural ventilation only

The temperature profiles along the left wall for the 10 MW fire with only natural ventilation demonstrate a hazardous bidirectional spread of heat. The thermocouple at 100 m, located opposite the fire, shows a highly turbulent temperature rise starting around 25 seconds and peaking above 100°C. Critically, this thermal hazard is not confined to the downstream section. A significant temperature increase is also recorded at upstream locations; the sensor at 80 m shows temperatures beginning to rise after 90 seconds, and even the sensor at 40 m shows a distinct temperature increase after 130 seconds, eventually exceeding 50°C. The downstream thermocouples at 120 m and 140 m similarly show a steady rise in temperature, with the 120 m location exceeding the 60°C tenability limit.

This bidirectional heat propagation is clear evidence of back-layering. The analysis confirms that even a smaller, 10 MW fire generates enough buoyant energy to overcome the weak natural airflow, causing the hot, toxic smoke layer to spread in both directions. The contamination of the upstream section renders the primary escape route untenable, effectively trapping occupants between two advancing fronts of heat and smoke. This finding is significant because it proves that the failure of natural ventilation is not limited to large-scale fires; even a common passenger vehicle fire can create life-threatening conditions throughout the tunnel, underscoring the necessity of mechanical systems for maintaining a safe egress path.

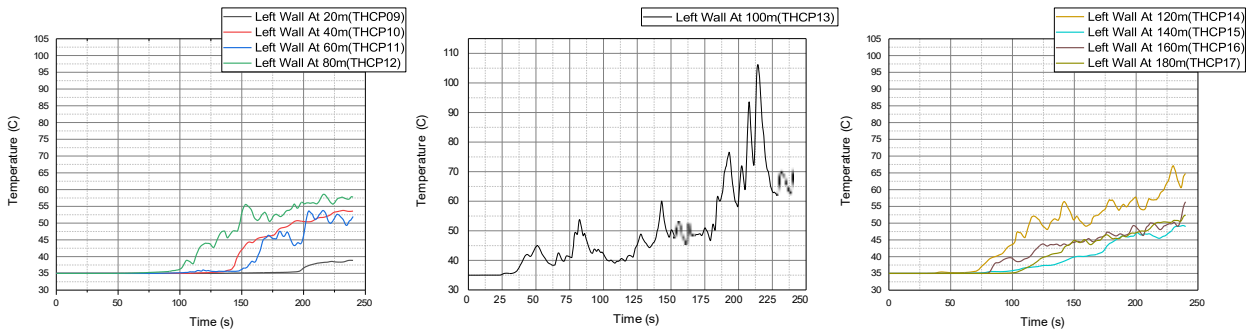

Fig. 50. Temperature vs. time profile from left-wall thermocouples for 10 MW fire under natural ventilation at upstream and downstream locations.

Case-2: Integrated system

The thermal conditions along the left wall, as measured by thermocouples, demonstrate a highly controlled and tenable environment throughout the simulation. All thermocouples located upstream of the fire (at 20 m, 40 m, 60 m, 80 m, and 100 m) show that the temperature remains stable at the initial ambient level of approximately 35°C for the entire 250-second duration. Downstream of the fire, a moderate and controlled temperature rise is observed. At the 120 m and 140 m locations, temperatures become turbulent but generally fluctuate below 50°C. Further downstream at 160 m and 180 m, the temperatures rise smoothly before stabilizing in a similar range, peaking at approximately 50°C.

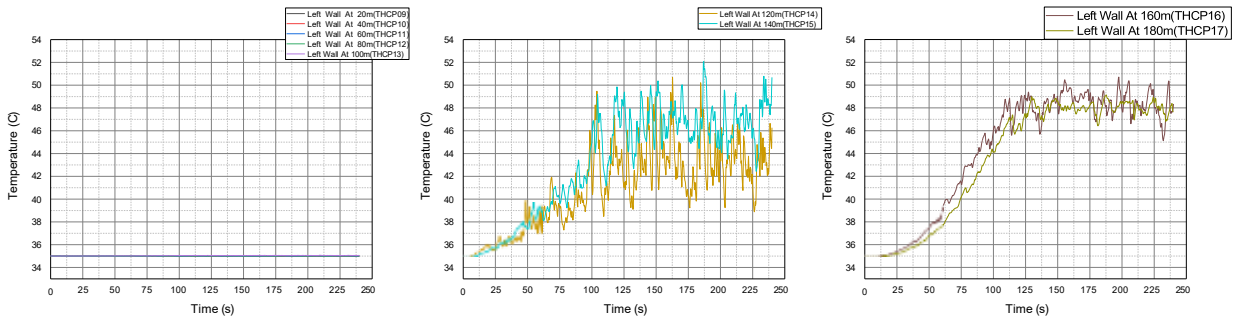

Fig. 51. Temperature vs. time profile from left-wall thermocouples for 10 MW fire under integrated system, showing near-ambient conditions with no significant rise at upstream.

This comprehensive data set provides definitive proof of the success of the integrated fire safety systems. The complete absence of any temperature rise in the upstream section confirms that the longitudinal ventilation is highly effective at preventing back-layering, thus preserving a safe escape route. Critically, the temperatures in the downstream section remain well below the 60°C tenability limit for human safety. This is a direct result of the combined effect of the sprinkler system cooling the fire and the ventilation system providing a steady supply of cool air. This analysis demonstrates that for a 10 MW fire, the integrated systems work in concert to successfully maintain survivable thermal conditions throughout the entire tunnel.

Right wall (Fire side wall)

Case-1: With natural ventilation only

The temperature data from the right wall, the same side as the fire, further confirms the hazardous conditions created by the 10 MW fire under natural ventilation. The results show a clear bidirectional spread of heat, with significant temperature increases occurring both upstream and downstream of the fire source. The thermocouple at 100 m, directly adjacent to the fire, recorded a rapid temperature rise beginning around 25 seconds, with turbulent peaks exceeding 70°C. Critically, the upstream location at 60 m also shows a rapid increase after 90 seconds, with temperatures quickly surpassing the 60°C tenability limit. Downstream locations, such as 120 m and 180 m, also breached this safety threshold, confirming a widespread thermal hazard.

This analysis reinforces the conclusion that the tunnel environment becomes entirely untenable. The data from the fire-side wall shows a slightly faster and more severe temperature rise compared to the left wall, but the fundamental finding of back-layering remains the same. The heat and smoke are not contained, and they contaminate the entire tunnel cross-section, eliminating any safe path for egress. This result underscores the comprehensive failure of natural ventilation to control the thermal environment, proving that even a 10 MW fire creates life-threatening conditions throughout the tunnel, irrespective of an occupant's proximity to the fire source.

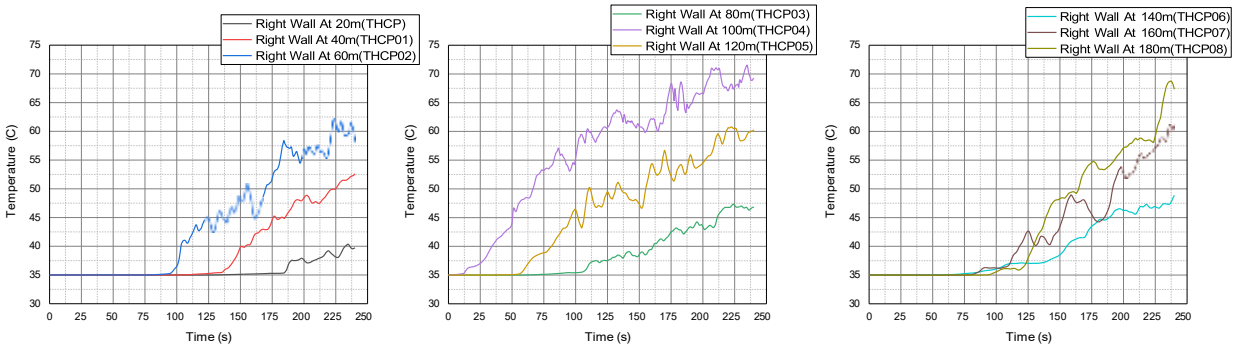

Fig. 52. Temperature vs. time profile from right-wall thermocouples for 10 MW fire under natural ventilation

Case-2: Integrated system

The temperature data from the right wall, the same side as the fire, provides a detailed view of the thermal hazard and the efficiency of the safety systems. The thermocouples located upstream of the fire at 20 m, 40 m, 60 m, and 80 m all recorded a stable ambient temperature of approximately 35°C throughout the simulation, confirming that no upstream heat propagation occurred. The most severe conditions were observed at the 100 m mark, directly adjacent to the fire, where temperatures rose rapidly after 25 seconds and exhibited highly turbulent fluctuations with peaks exceeding 200°C. In the downstream section, the thermocouples at 120 m, 140 m, 160 m, and 180 m showed a controlled temperature rise, with values generally fluctuating between 50°C and 70°C, near the 60°C tenability limit.

This analysis confirms the successful performance of the integrated safety systems. The complete prevention of back-layering, evidenced by the stable upstream temperatures, is a critical success, preserving a safe escape route. While the temperatures directly adjacent to the fire were intense, they were effectively controlled by the sprinkler system, preventing a much larger thermal impact. The downstream temperatures, hovering near the tenability threshold but not escalating uncontrollably, demonstrate that the combination of sprinkler cooling and ventilation airflow successfully

mitigates the thermal hazard. This result indicates that for a 10 MW fire, the systems work in concert to contain the primary hazard and maintain largely survivable conditions throughout the rest of the tunnel.

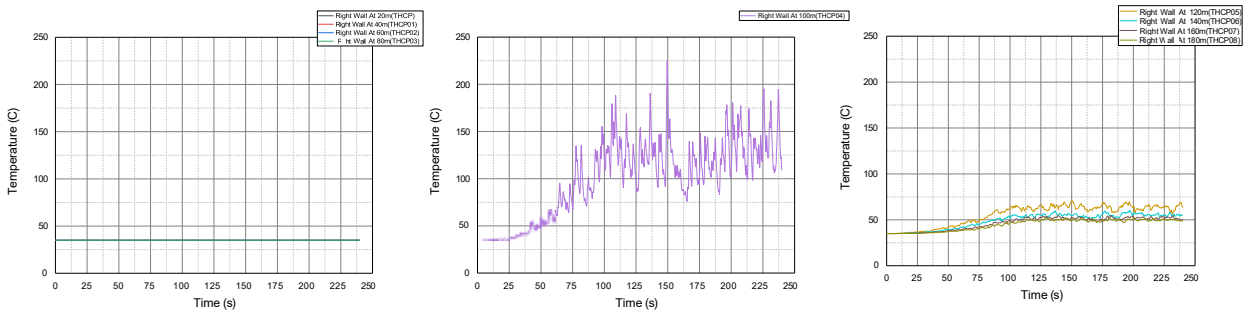

Fig. 53. Temperature vs. time from right-wall thermocouples for 10 MW fire integrated system, showing significant rise at 100 m due to fire origin at right side of the tunnel, unlike the left-wall case.

3.3.3. In-vehicle thermocouple temperature evaluation

Case-1: With natural ventilation only

The thermal conditions at evacuation height, measured by thermocouples placed above each vehicle, reveal a widespread and hazardous environment under the 10 MW fire with natural ventilation. The temperature directly above the fire vehicle shows a rapid and severe increase, reaching a turbulent peak of approximately 850°C, a condition that is instantly lethal. Critically, the data demonstrates a clear bidirectional spread of heat, with vehicles both upstream and downstream of the fire experiencing a significant rise in temperature. All vehicles, regardless of their location, show an increase in temperature over time, with those closer to the fire, such as Vehicle 4 and Vehicle 10, showing a more pronounced and rapid rise that surpasses the 60°C tenability limit. Even vehicles located further away, both upstream and downstream, show a steady temperature increase, indicating the entire tunnel section is becoming thermally contaminated.

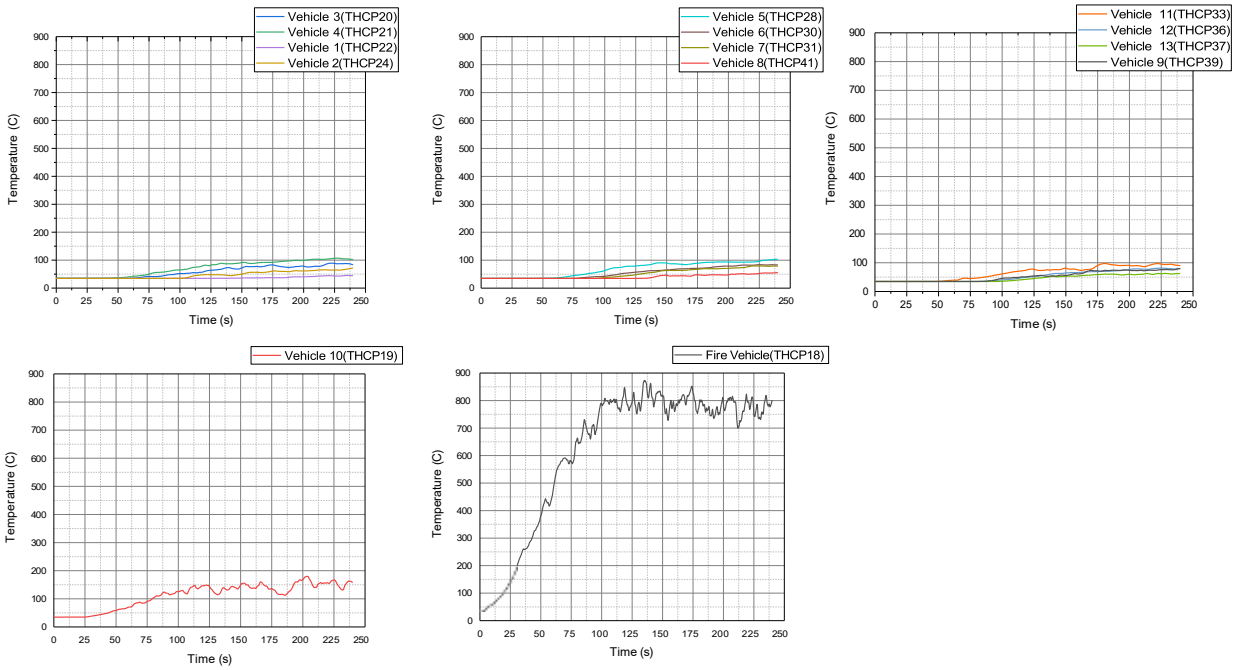

Fig. 54. Temperature vs. time profile from thermocouples placed above vehicles inside the tunnel for 10 MW fire under natural ventilation condition.

This comprehensive data set confirms the catastrophic failure of natural ventilation to manage the thermal hazard. The significant temperature rise above vehicles in both directions is definitive proof of **back-layering**, which eliminates any potential for a safe escape route. Unlike scenarios with effective smoke control where the upstream path is preserved, these results illustrate a "no-escape" situation where the entire tunnel becomes untenable at evacuation height. This finding underscores that even a 10 MW fire, without the intervention of mechanical ventilation or suppression, creates life-threatening thermal conditions that make safe egress impossible

Case-2: Integrated system

The thermocouple data reveals how forced ventilation and sprinklers create distinct thermal zones in the tunnel . The sprinkler's cooling effect is clear on the fire vehicle, which peaked at approximately 600°C, significantly lower than in the scenario without suppression. The 2 m/s forced ventilation creates a safe upstream zone, where Vehicles 1, 2, 3 remained at ambient temperature. In sharp contrast, it also directs the hazard downstream, immediately engulfing Vehicle 4 in gases below 100°C. This heat then dissipates with distance, as vehicles located further downstream recorded lower peak temperatures between 75°C and 100°C. This analysis shows how the systems successfully contain the hazard but create an heated environment just downstream of the fire.

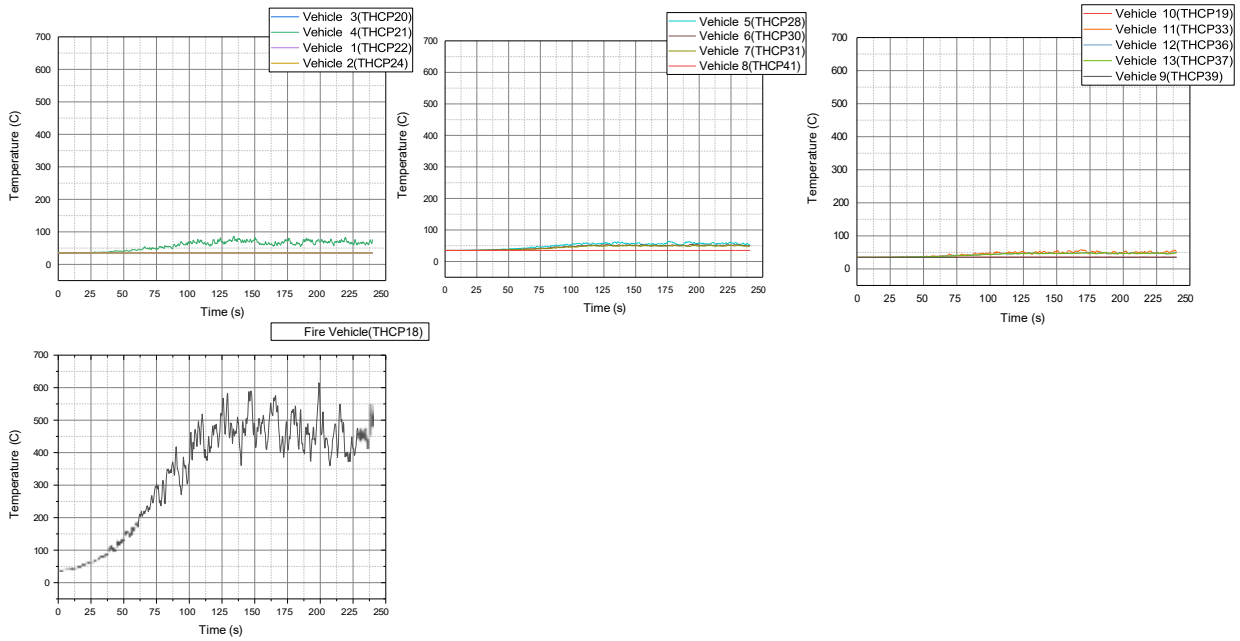

Fig. 55. Temperature vs. time profile from thermocouples placed above vehicles inside the tunnel for 10 MW fire under integrated system.

3.3.4. Temperature profile

Case-1: With natural ventilation only

The time-lapsed temperature slices for the 10 MW fire with only natural ventilation illustrate the rapid development of a hazardous thermal environment throughout the tunnel. After ignition, a plume of hot gas forms and rises to the ceiling, where it immediately begins to spread in both the upstream and downstream directions. As the simulation progresses, this hot gas layer, with temperatures in its core exceeding 150°C, propagates extensively along the ceiling in both directions. By 240 seconds, a significant portion of the tunnel is affected by this thermal layer, which shows clear evidence of back-layering, or the upstream movement of smoke and heat against the natural airflow.

This bidirectional heat spread is a critical finding, as it demonstrates the failure of natural ventilation to control the fire environment, even for a smaller 10 MW fire. The contamination of the upstream section with a hot gas layer effectively eliminates the primary escape route for occupants, trapping them between two advancing fronts of heat and smoke. The analysis confirms that without the intervention of mechanical ventilation or a fire suppression system, even a common passenger vehicle fire can quickly render the entire tunnel untenable, posing a severe threat to life safety and preventing safe access for emergency responders.

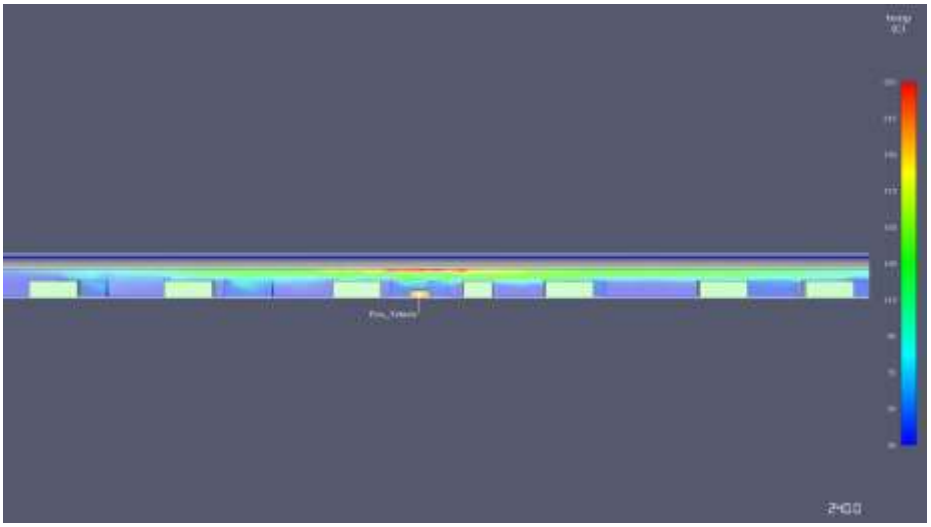

Fig. 56. Temperature profile along tunnel length under natural ventilation for 10 MW fire, showing longitudinal heat build-up

Case-2: Integrated system

The time-lapsed temperature slices for the 10 MW fire with active fire protection and ventilation systems show a highly controlled and stable thermal environment. Following ignition, a small plume of hot gas rises to the ceiling and is immediately transported in the downstream direction by the longitudinal ventilation. The images clearly show that the thermal layer is confined to a thin, stratified layer at the ceiling and does not propagate upstream, ensuring the upstream section remains at a safe ambient temperature. The temperature within this ceiling jet is remarkably low, with the color map indicating that peak temperatures rarely exceed 85°C throughout the 240-second simulation.

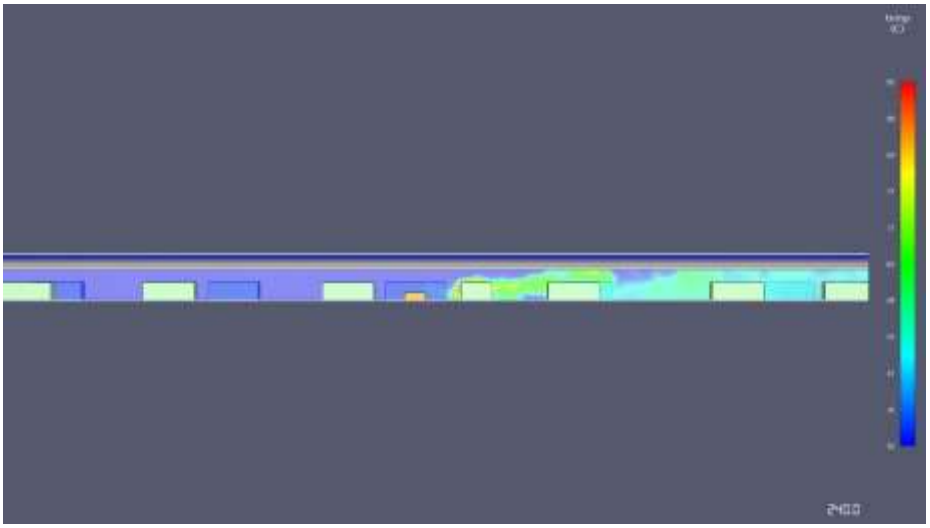

Fig. 57. Temperature profile along tunnel length under integrated system for 10 MW fire, illustrating controlled temperature rise

This visual analysis provides powerful evidence of the success of the integrated safety systems. The complete prevention of back-layering confirms that the ventilation preserves a safe upstream escape route. Critically, the sprinkler system's cooling effect is so effective on the 10 MW fire that it keeps the downstream ceiling jet temperatures well below the levels that would pose an immediate threat to the tunnel structure or to evacuating occupants. This result demonstrates that for a 10 MW fire, the combination of fire suppression and ventilation does not just mitigate the hazard but almost completely controls it, maintaining a tenable environment throughout the vast majority of the tunnel and ensuring a very high level of life safety.

3.3.5. Smoke dynamics and concentration profile

Case-1: With natural ventilation only

scenario with only natural ventilation, the simulation results show a rapid and complete saturation of the tunnel with smoke. The time it took to reach a 100% smoke concentration decreased as the distance to the fire decreased, showing the rapid spread of smoke from the fire source. The detector at 10m reached full saturation at approximately 150 seconds, while the detector at 50m reached it at around 100 seconds. Further down the tunnel, the detectors at 80m, 90m, and 100m saw a more rapid increase, reaching 100% concentration at approximately 60, 55, and 50 seconds respectively. The detectors in the downstream sections of the tunnel, from 110m to 190m, followed a similar trend, with all of them reaching and stabilizing at 100% concentration between 50 and 100 seconds. This data demonstrates that while natural ventilation may slightly alter the spread pattern and timing of the smoke, it is ultimately ineffective in preventing the tunnel from becoming completely saturated with smoke.

(a)

(b)

(c)

Fig. 58. Smoke distribution along tunnel length for 10 MW fire under natural at (a) 60s, (b) 150s, and (c) 240s.

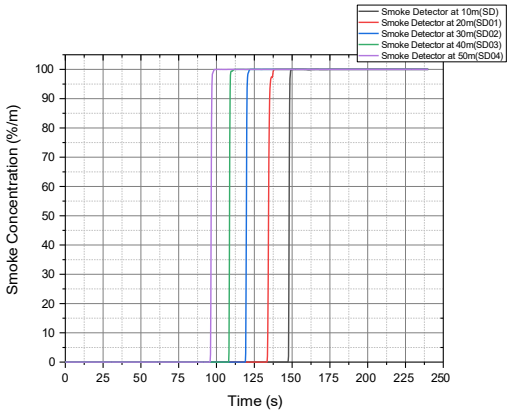

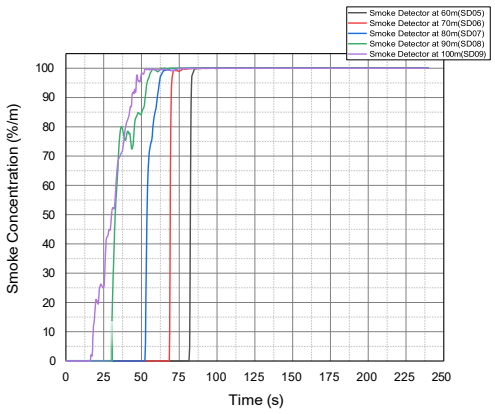

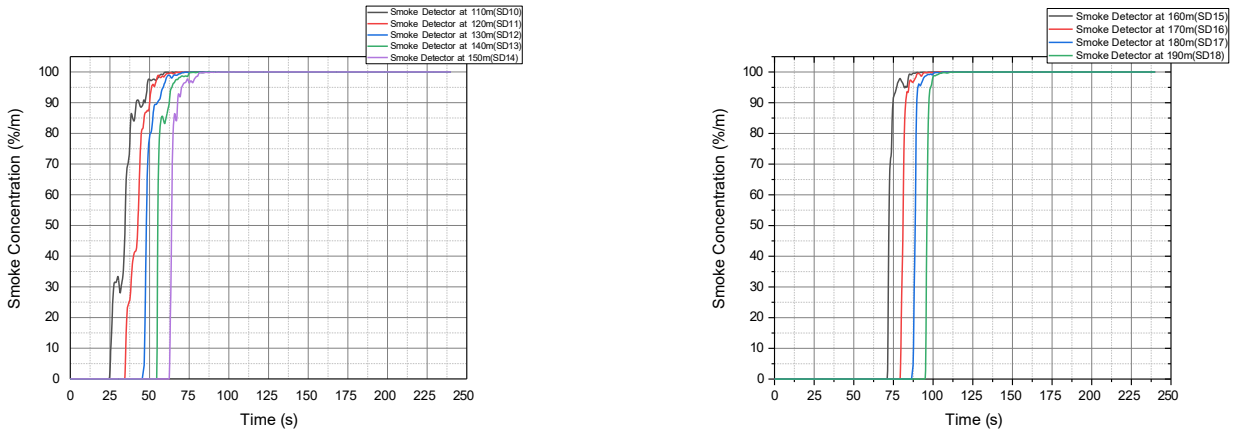

Fig. 59. Smoke concentration vs time from smoke detectors placed across tunnel length for 10 MW fire under natural ventilation

Case-2: Integrated system

In the 10 MW tunnel fire simulation with both longitudinal mechanical ventilation and a fire protection system, the smoke concentration, measured at the ceiling, shows a highly erratic and controlled pattern. From 10m to 100m from the fire source, all detectors registered a consistent 0% smoke concentration for the entire 250-second simulation period, demonstrating the effective performance of the combined systems in preventing smoke from spreading to this section of the tunnel. Beyond 100m, the smoke concentration began to fluctuate significantly. The detector at 110m showed intermittent spikes, reaching concentrations close to 100%, but with frequent drops back to 0%, suggesting that the system was effectively clearing smoke from the ceiling . At 120m, the concentration rose rapidly around 50 seconds and then fluctuated wildly between 0% and 100% for the rest of the simulation, indicating the system was struggling to maintain a constant low concentration but was still effective at a high level . This pattern of extreme fluctuation between low and high concentrations was also observed at 130m and 140m, where the detectors recorded large spikes to 100% but with frequent and significant drops, highlighting the system's active but inconsistent control . Finally, the detectors from 150m to 190m exhibited a similar volatile behavior, with continuous rapid fluctuations between high and low concentrations, reinforcing that while smoke was present at the ceiling in the downstream section, it was not allowed to stabilize or completely fill the tunnel

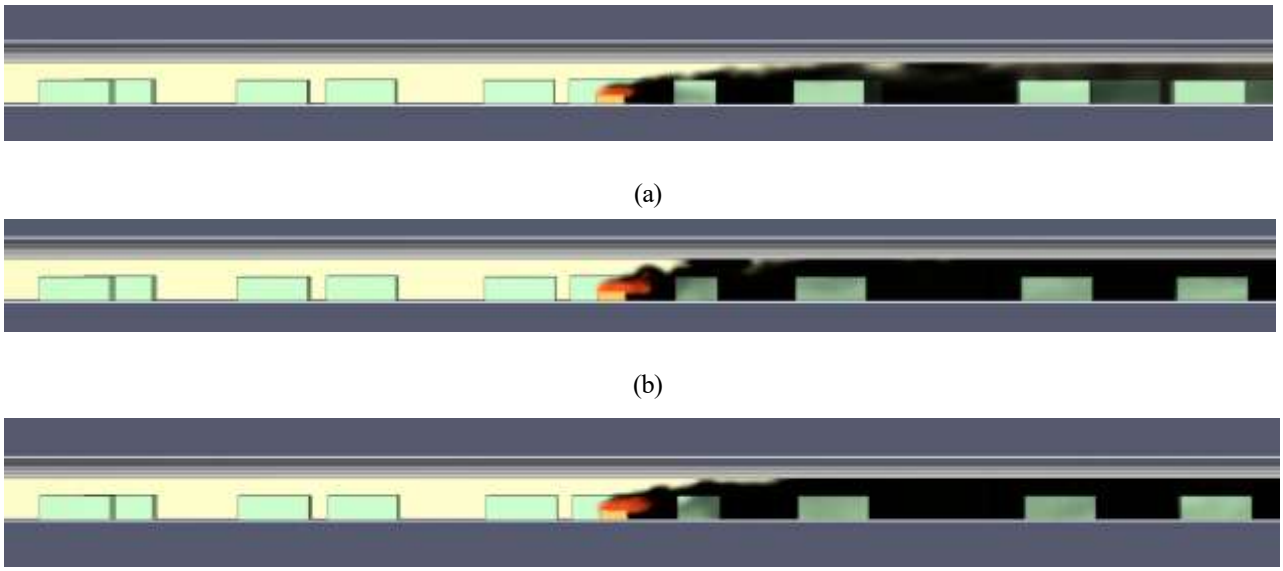

(a)

(b)

(c)

Fig. 60. Smoke distribution along tunnel length for 10 MW fire under integrated system at (a) 60s, (b) 15s, and (c) 240s.

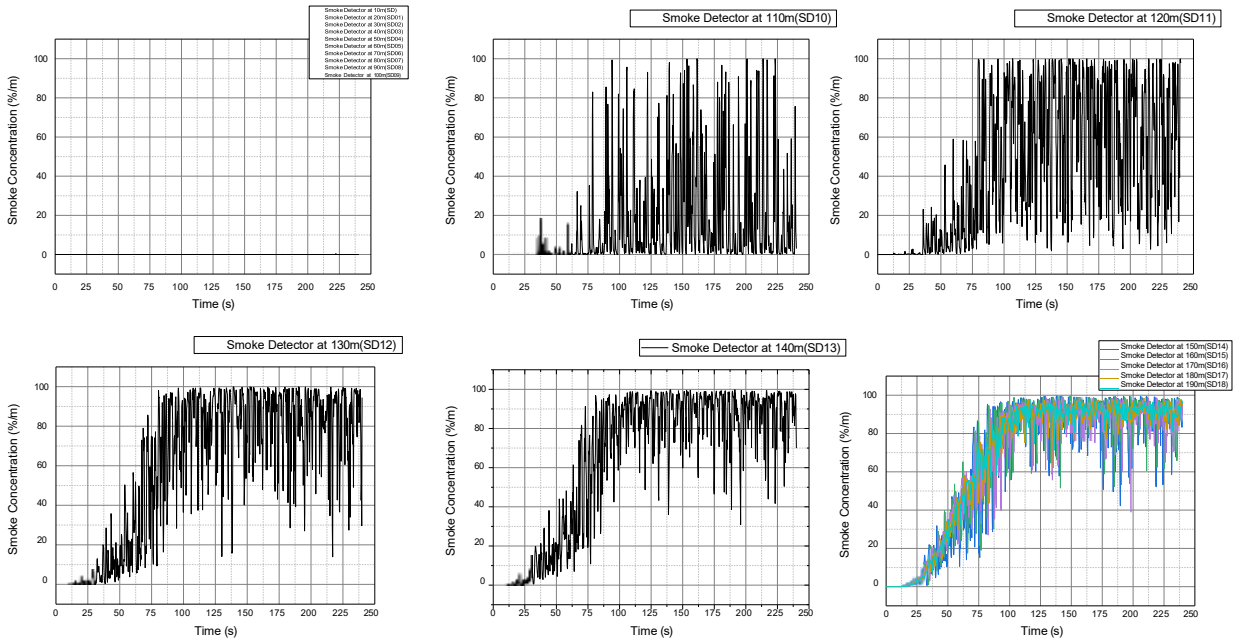

Fig. 61. Smoke concentration vs time from smoke detectors placed across tunnel length for 10 MW fire under integrated system

3.3.6. Visibility assessment

Case-1: With natural ventilation only

In the tunnel fire scenario without a mechanical ventilation system, the simulation results show a rapid and severe degradation of visibility, as indicated by the color scale where red signifies high visibility (30m+) and blue signifies low visibility (below 3m). At the start of the simulation (0 seconds), the tunnel's visibility is excellent, with a large section of the tunnel colored red. By 30 seconds, the visibility begins to degrade, with orange and yellow areas appearing in the tunnel, indicating visibility is decreasing. At 60 seconds, the visibility has significantly worsened, with large sections of the tunnel now green (15-18m visibility) and light green (12-15m visibility), and the initial appearance of some blue zones (below 3m visibility) in localized areas.

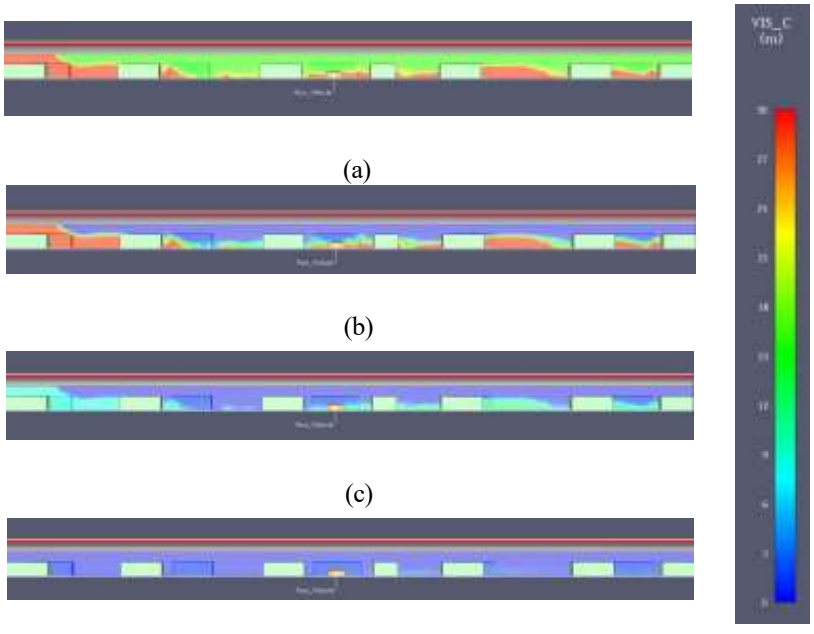

(a)

(b)

(c)

(d)

Fig. 62. Visibility distribution along tunnel length for natural ventilation in 10 MW fire at (a) 60s, (b) 120s, and (c) 210 sec and (d) 240s

By 90 seconds, the blue zones have become more widespread, indicating that visibility has dropped below 3m in significant portions of the tunnel, though some areas still have moderate visibility (green and yellow). The degradation continues, and by 120 seconds, the majority of the tunnel is colored blue, signifying extremely poor visibility, with only a few isolated patches of better visibility remaining. From 150 seconds to 240 seconds, the visibility remains critically low, with the tunnel being almost entirely filled with smoke and represented by large blue and light blue areas, indicating that visibility is consistently below 6 meters. This demonstrates that in the absence of a mechanical ventilation system, the tunnel quickly becomes unsafe due to severely compromised visibility.

Case-2: Integrated system

The time-lapsed visualizations of visibility at evacuation height demonstrate the high efficiency of the integrated safety systems in maintaining tenable conditions. At the start of the simulation, visibility is unobstructed throughout the tunnel, indicated by the red contour representing visibility greater than 30 meters. Following ignition, the generated smoke is immediately controlled by the longitudinal ventilation and transported exclusively in the downstream direction. As the simulation progresses, a zone of reduced visibility forms downstream of the fire, but its impact is limited. At 240 seconds, the area with visibility below the 10-meter critical threshold is present in the most of the downstream section of the tunnel.

This analysis provides a clear confirmation of the success of the safety systems. The most critical finding is the complete prevention of back-layering, which preserves the entire upstream section as a perfectly clear and safe escape route. Downstream, the combination of the sprinkler system reducing smoke production and the ventilation system diluting the smoke results in a well-managed environment. Unlike the hazardous smoke-logging seen in unmitigated scenarios, the visibility is maintained at a level that would allow for safe egress. This result shows that the integrated systems work effectively to not only control the direction of the smoke but also to limit its density, thereby ensuring a high level of life safety for occupants throughout the tunnel.

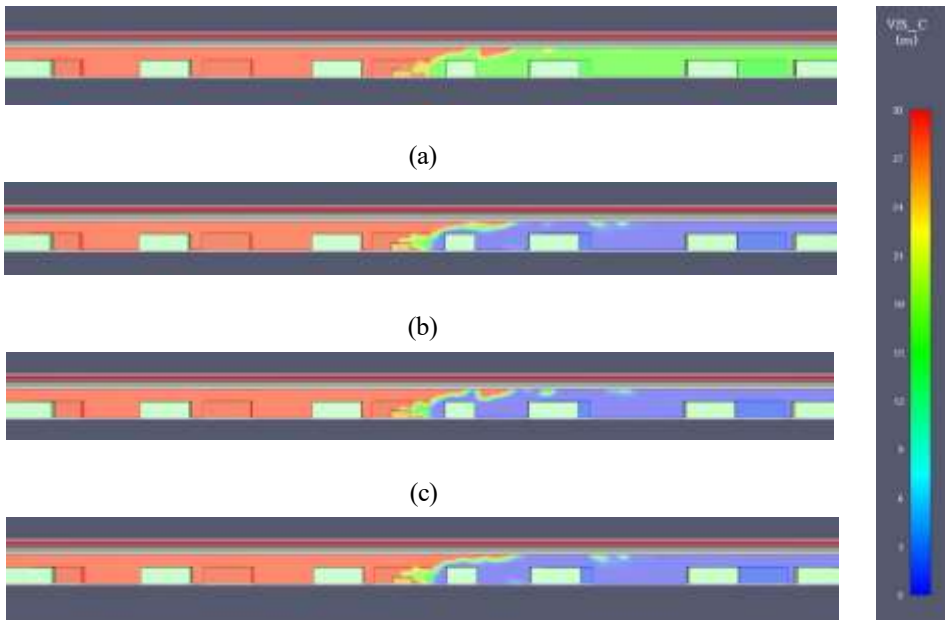

Fig. 63. Visibility distribution along tunnel length for integrated system in 10 MW fire at (a) 60s, (b) 120s, and (c) 210s and (d) 240s

3.3.7. Carbon monoxide distribution and evaluation

Case-1: With natural ventilation only

Under the 10 MW natural ventilation scenario, a hazardous bidirectional spread of carbon monoxide is observed. By 180 seconds, a CO mass flux reaching approximately 0.00004 kg/s/m² is established at the ceiling, propagating both upstream and downstream of the fire. By 240 seconds, this hazardous region has extended further, contaminating a significant portion of the tunnel ceiling in both directions. Although this CO layer is initially confined to the ceiling, the

significant back-layering and longitudinal spread indicate that subsequent mixing would cause CO concentrations at breathing height to surpass the ~1200 ppm tenability limit in both the upstream and downstream sections. This quantitative progression confirms the failure of natural ventilation to control toxic gas flow even for a smaller fire, compromising escape routes in both directions.

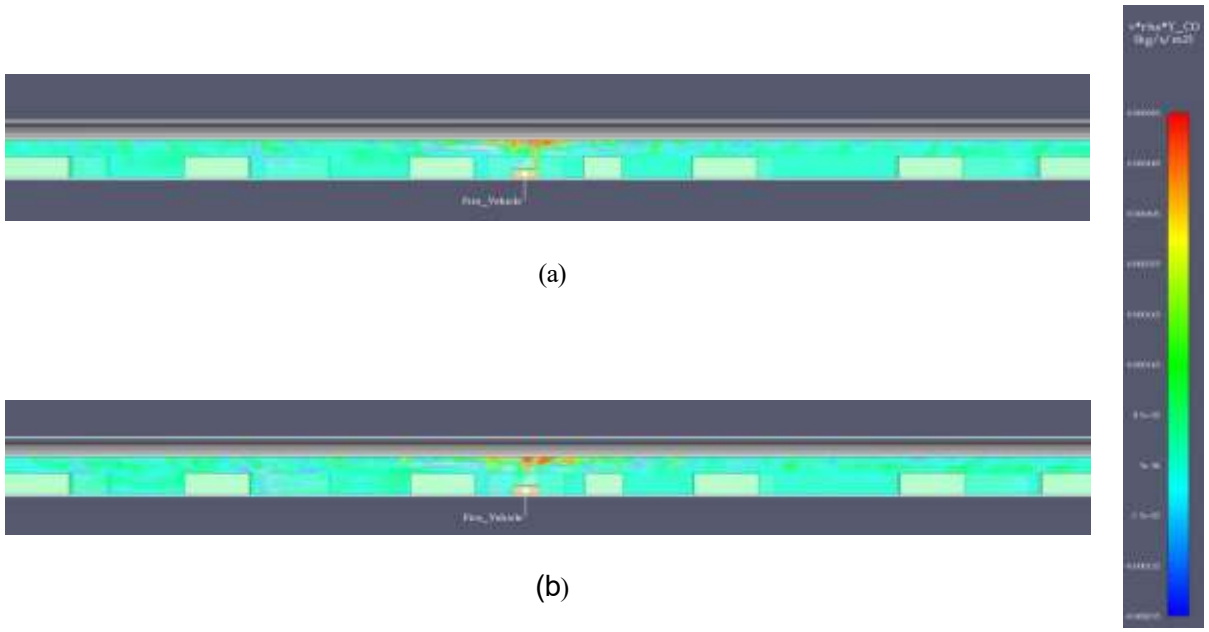

(a)

(b)

Fig. 64. CO concentration distribution along tunnel length for 10 MW fire (natural ventilation) at (a)180s and (b) 240s

Case-2: Integrated system

Under the 10 MW scenario with active fire protection and ventilation, the carbon monoxide distribution is effectively managed and contained. By 180 seconds, a controlled CO mass flux, peaking at approximately 0.00016 kg/s/m², is established in a stratified layer at the ceiling and is transported exclusively downstream of the fire. By 240 seconds, while the plume has extended further downstream, its peak flux remains stable and is confined to the ceiling jet, with no upstream spread observed. Because the entire CO layer is contained downstream and remains stratified, the upstream section of the tunnel is kept entirely free of CO, ensuring concentrations at breathing height remain well below the ~1200 ppm tenability limit for evacuees. This quantitative progression confirms the success of the integrated safety systems in controlling the toxic gas flow, thereby preserving the viability of the upstream escape route.

3.3.8. Sprinkler system response

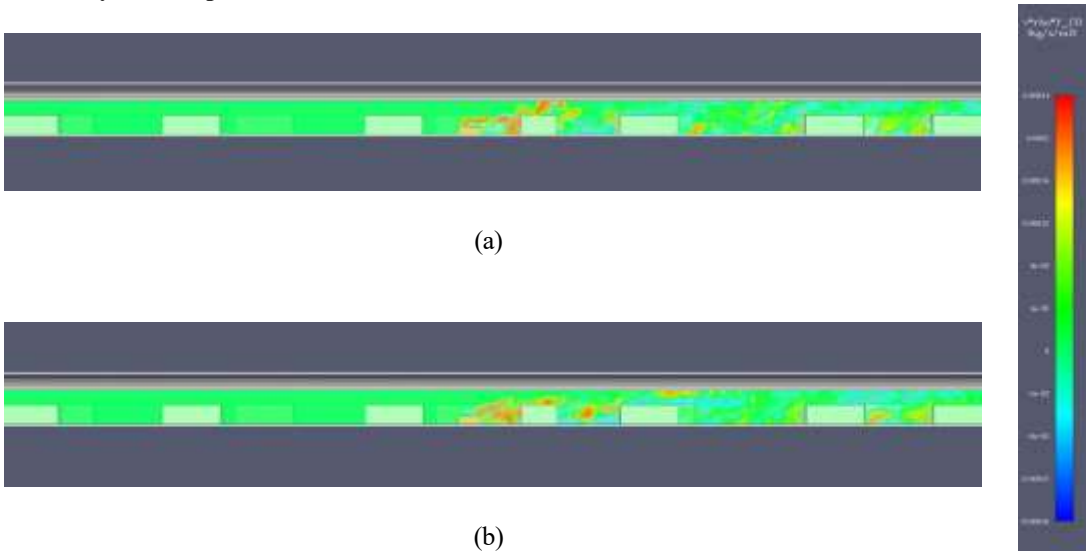

(a)

(b)

Fig. 65. CO concentration distribution along tunnel length for 10 MW fire (integrated system) at (a) 180s and (b) 240s

The temperature data from the sprinkler head locations reveals a critical interaction between the ventilation and suppression systems. The sprinklers located upstream of the fire (from 4.5 m to 99 m) recorded no change from the ambient temperature of approximately 35°C, confirming the absence of back-layering. Downstream of the fire, the hot gas layer caused a clear temperature rise at all sprinkler locations. However, a key finding is that the temperatures at all sprinkler heads remained below 55°C for the entire 250-second simulation, which is well below the activation temperature (e.g., 93°C) for a sprinkler system. Consequently, no sprinklers activated during this scenario.

This result demonstrates that for a 10 MW fire, the longitudinal ventilation system is so effective at controlling the thermal environment that it prevents the conditions from becoming severe enough to require sprinkler activation. The 2 m/s airflow dilutes the hot gases and increases convective cooling to such an extent that the ceiling temperatures are kept below the threshold for suppression. This highlights a key aspect of integrated system design: the primary life safety system (in this case, ventilation) successfully managed the hazard, rendering the secondary system (sprinklers) unnecessary for this specific fire size. This finding confirms that the tunnel environment remained highly tenable and the fire was effectively controlled by the ventilation alone.

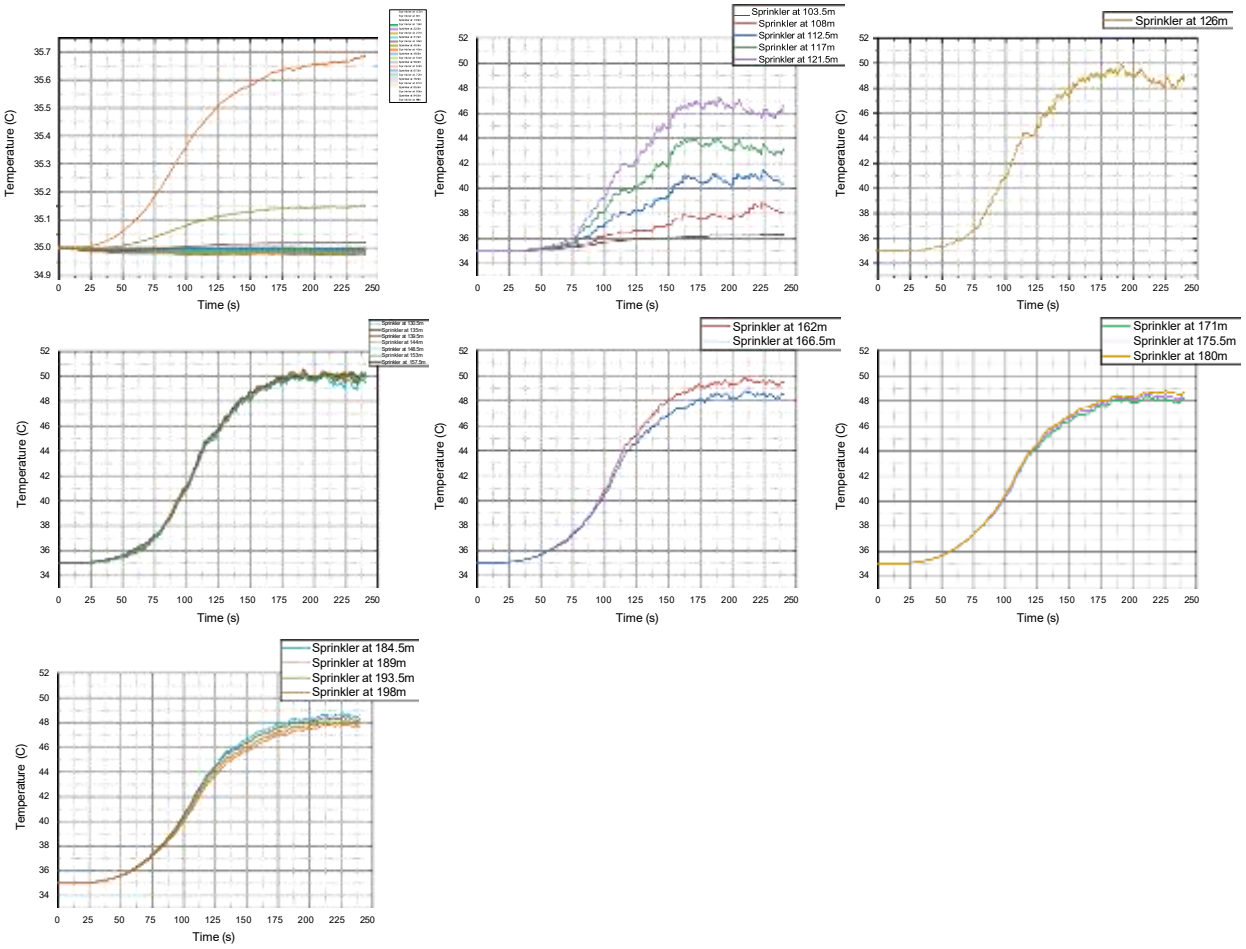

Fig. 66. Temperature–time profiles of sprinklers along tunnel length for 10 MW fire; activation not occurs.

4. Comparative discussion

4.1. Heavy goods vehicle (100 MW)

The most severe conditions were observed in the 100 MW HGV fire. Under natural ventilation, the HRR climbed steadily to 37.5 MW at 250 s, accompanied by catastrophic thermal and smoke conditions. Upstream thermocouples at 40 m exceeded 60 °C, while downstream reached 300–350 °C, far surpassing survivability limits. Vehicle thermocouples showed the fire vehicle exceeding 850 °C, adjacent vehicles rising above 700 °C, and even distant upstream vehicles surpassing 60 °C, confirming that no safe zones remained. Smoke spread bi-directionally, producing a uniform ceiling jet and tunnel-wide stratification. Visibility collapsed below 5 m throughout the tunnel by 240 s, while CO flux reached 0.001 kg/s/m², with concentrations surpassing 1200 ppm at breathing height everywhere.

With mechanical ventilation and sprinklers, improvements were evident though conditions remained critical. The HRR was moderated but still peaked at ~45 MW, higher than in the natural case, reflecting localized suppression balanced by fuel load intensity. Upstream zones remained tenable at 35 °C with no smoke accumulation, while downstream thermocouples recorded peaks exceeding 120 °C with turbulence near 100 120 m. Vehicle temperatures showed the fire vehicle above 800 °C, the first downstream vehicle at >550 °C, and further downstream vehicles below 100 °C. All upstream vehicles remained safe at 35–40 °C. Smoke was confined downstream, with detectors at 100–190 m reaching 100% concentration by 80–150 s, while upstream detectors stayed at 0%. Visibility followed the same pattern: upstream remained >30 m, but downstream dropped below 5 m after 120 s. CO flux remained confined downstream, but exceeded 1200 ppm, rendering the downstream section hazardous despite improvements. Within the 250 s simulation period, sprinklers activated sequentially between 108–157.5 m; sharp cooling drops at 135 m and 139.5 m were caused by upstream sprinkler activation, which reduced local temperatures and prevented their actuation. But the sprinkler present just above the fire vehicle at 103.5 m didn't actuate because the temperature didn't rise due to the ventilation system. The 144 m sprinkler actuated as the ceiling jet re-intensified, while those beyond 157.5 m did not actuate within 250 s. However, based on the temperature trend showing rising spikes, sprinklers closer to the fire seat and further downstream may have actuated beyond 250 s.

Table 4: Comparative analysis of 100 MW cases.

Parameter	Natural Ventilation (0.5 m/s)	Integrated System (Longitudinal Ventilation ≈2 m/s + Suppression System)
HRR (Heat Release Rate)	Climbed steadily to 37.5 MW at 250 s	Moderated but peaked at ~45 MW within 250 s (localized suppression balanced by fuel load)
Wall/Ceiling temperature	Ceiling temperatures peaked at ~700–785 °C near the fire; upstream thermocouples (40 m) >60 °C; downstream ~300–350 °C; severe structural heat load	Ceiling temperatures reduced to ~200–230 °C (≈70% lower); upstream thermocouples safe at 35–40 °C; downstream peaks >120 °C near 100–120 m
Vehicle temperature	Fire vehicle >850 °C; adjacent vehicles >700 °C; even distant upstream vehicles >60 °C — no safe zones	Fire vehicle >800 °C; first downstream vehicle >550 °C; further downstream vehicles <100 °C; upstream vehicles stable at 35–40 °C
Smoke concentration	Bi-directional spread; upstream and downstream detectors record rapid rise; near-fire detectors reach ~100%/m within 60–75 s; entire tunnel impacted by 240 s	Unidirectional downstream spread; upstream (10–90 m) remains at 0%/m; midstream (100–120 m) shows intermittent 80–100%/m spikes; downstream (130–190 m) reaches sustained 100%/m by 80–150 s
Visibility (tenability)	Initial stratification (~30 m visibility near floor until 60 s); <15 m by 120 s; <5 m across most of tunnel by 180–240 s (untenable both directions)	Upstream visibility >30 m throughout (safe egress route); downstream visibility <10 m after 120 s and <5 m by 180–240 s (untenable downstream)
CO concentration	CO flux spreads upstream and downstream; significant levels near fire and mid-tunnel; far downstream not heavily impacted at 240 s	CO transported only downstream; plume reaches tunnel end by 240 s; higher CO flux and larger red pockets downstream (greater toxicity risk)

Sprinkler response	No sprinklers; uncontrolled fire growth	Sprinklers activated sequentially between 108–157.5 m within 250 s; sharp cooling drops at 135 m and 139.5 m from upstream activations prevented their actuation; 144 m actuated as ceiling jet re-intensified; beyond 157.5 m inactive. Sprinklers reduced local heating and influenced HRR trend

4.2. Bus/Truck Fire (25 MW)

For the 25 MW bus/truck fire, natural ventilation allowed the HRR to peak at 25 MW by 150 s before decaying toward 10 MW by 250 s due to fuel and oxygen limitations. Wall thermocouples at the 100 m mark recorded severe conditions, with the left wall reaching peak about 250 °C and the right wall surpassing 300 °C. Both upstream and downstream locations recorded temperatures above 60 °C, confirming back-layering. Vehicle thermocouples showed the fire vehicle peaking at ~600 °C, adjacent vehicles reaching nearly 300 °C, and more distant vehicles staying below 125 °C, but all well above survivability thresholds. Smoke concentration data confirmed rapid and complete tunnel saturation, with detectors from 10–190 m reaching 100% smoke concentration within 25–140 s. Visibility dropped below 5m in both upstream and downstream within 180 s, while CO exceeded 1200 ppm throughout the tunnel, confirming untenability in both directions.

When mechanical ventilation and sprinklers were introduced, the HRR was capped at ~25 MW steady state, demonstrating suppression of growth beyond the design fire size. Wall thermal conditions improved significantly: upstream remained safe at <40 °C, while downstream peaked at 70–90 °C, breaching tenability but far less severe than in the natural case. Vehicle temperatures reflected this improvement, with the fire vehicle exceeding 500 °C, the immediate downstream vehicle exceeding 400°C, and upstream vehicles remaining at ambient levels. Smoke dynamics showed that upstream detectors remained clear at 0% smoke concentration, while downstream detectors between 110–150 m reached 80–100% concentrations at 60-100s. Visibility upstream was consistently above 30 m, but downstream fell below 5m after 150 s, limiting evacuation options for downstream occupants. CO remained largely confined downstream, though minor leakage was detected upstream, but concentrations stayed below critical thresholds. Sprinkler activation was recorded sequentially between 112.5–135 m, with characteristic sawtooth cooling patterns confirming effective water discharge. But the sprinkler present just above the fire vehicle at 103.5 m didn't actuate because the temperature didn't rise due to the ventilation system. However, based on the temperature trend showing rising spikes, sprinklers closer to the fire seat and further downstream may have actuated beyond 250 s.

Table 5: Comparative analysis of 25 MW cases.

Parameter	Natural Ventilation (0.5 m/s)	Integrated System (Longitudinal Ventilation ≈2 m/s + Suppression System)
HRR (Heat Release Rate)	Peaked at 25 MW by 150 s, then decayed to ~10 MW by 250 s (fuel/ oxygen limited)	Capped at ~25 MW steady state, suppression prevented further growth beyond design fire size
Wall/Ceiling temperature	Ceiling temperatures peaked at ~335 °C near the fire; Left wall peaked ~250 °C, right wall >300 °C at 100 m; upstream and downstream >60 °C, confirming back-layering	Ceiling temperatures reduced to ~185 °C (≈55% lower); Upstream walls safe at <40 °C; downstream walls peaked 70–90 °C (reduced but still above tenability)
Vehicle temperature	Fire vehicle ~600 °C; adjacent vehicles ~300 °C; distant vehicles <125 °C (all above survivability thresholds)	Fire vehicle >500 °C; first downstream vehicle >400 °C; upstream vehicles remained at ambien

Smoke concentration	Rapid, complete saturation; detectors 10–190 m reached 100% within 25–140	Upstream detectors remained at 0%; downstream detectors (110–150 m) reached 80–100% within 60–100 s
Visibility (tenability)	Fell below 5 m both upstream and downstream by 180 s (untenable in both directions)	Upstream visibility >30 m throughout; downstream fell below 5 m after 150 s (untenable downstream only)
CO concentration	Exceeded 1200 ppm throughout the tunnel (untenable both sides)	Largely confined downstream; minor upstream leakage detected but below critical thresholds
Sprinkler response	No sprinklers; uncontrolled fire spread	Sprinklers activated sequentially between 112.5–135 m; sawtooth cooling patterns confirmed effective discharge

4.3. Passanger vehicle fire (10 MW)

In the Passenger Vehicle Fire (10 MW) scenario, the HRR under natural ventilation followed an unchecked t^2 growth curve, peaking at 7.8MW , with thermocouple readings showing temperatures exceeding 106 °C at the fire location and surpassing the 60 °C tenability limit upstream at 60 m. Vehicles directly exposed to the plume recorded peak temperatures above 850 °C at the fire vehicle. Smoke spread bi-directionally along the ceiling, leading to uniform smoke stratification throughout the tunnel. By 240 s, visibility dropped to less than 5 m, while CO mass flux, spreading both upstream and downstream, with concentrations exceeding 1200 ppm, making evacuation in either direction impossible.

With the addition of mechanical ventilation and sprinklers, the scenario remained similar to the natural ventilation case because of the introduction of more oxygen due to addition of mechanical ventilation. Thermal conditions remained stable upstream, where temperatures were maintained at 35 °C, while downstream zones stabilized between 40–50 °C. The fire vehicle peaked at ~600 °C, and all upstream vehicles remained at ambient levels. Importantly, smoke propagation was confined downstream, as detectors from 10–100 m upstream recorded 0% smoke concentration, preserving visibility above 30m at downstream and ensuring a viable egress path. CO concentrations were confined to the downstream section, with no hazardous build-up in the upstream breathing zone. Notably, sprinklers did not activate in this scenario, as ceiling jet temperatures never reached the 93 °C activation threshold, indicating that ventilation alone was sufficient to preserve tenability in small fires.

Table 6: Comparative analysis of 10 MW cases.

Parameter	Natural Ventilation (0.5 m/s)	Integrated System (Longitudinal Ventilation ≈2 m/s + Suppression System)
HRR (Heat Release Rate)	Followed unchecked t^2 growth; peaked at **7.8 MW**	Capped at **~7.8 MW** in a steady state
Wall/Ceiling temperature	Ceiling temperatures peaked at ~235 °C near the fire; Local fire site >106 °C; upstream thermocouples (60 m) >60 °C (above tenability)	Ceiling temperatures reduced to ~95 °C (≈59% lower); Upstream stable at ~35 °C; downstream 40–50 °C (significantly safer than 25 MW and 100 MW cases)
Vehicle temperature	Fire vehicle >850 °C; adjacent plume-exposed vehicles overheated	Fire vehicle ~600 °C; upstream vehicles remained at ambient

Smoke concentration	Bi-directional spread; uniform stratification across tunnel by 240 s	Confined downstream; upstream detectors (10–100 m) stayed at 0% smoke concentration
Visibility (tenability)	Dropped <5 m throughout tunnel by 240 s (untenable both directions)	Upstream visibility >30 m preserved; downstream maintained >30 m until ~240 s (notable improvement over larger fires)
CO concentration	>1200 ppm both upstream and downstream (untenable)	Confined downstream only; no hazardous CO detected upstream
Sprinkler response	No sprinklers; uncontrolled fire growt	Sprinklers did not activate — ceiling jet never reached 93 °C activation threshold; ventilation alone maintained upstream tenability

5. Validation of Simulation Results Using Artificial Neural Network (ANN)

To further validate the accuracy of the numerical simulation results presented in this study, an Artificial Neural Network (ANN) approach was employed using the MATLAB Neural Network Fitting Tool (nftool). The objective was to assess the reliability of the predicted Heat Release Rate (HRR) values and their relationship to the resulting temperature distributions for all scenarios considered.

The HRR data obtained from the numerical simulations were used as the input parameters of the ANN model, while the corresponding temperature values were used as the output parameters. A feed-forward backpropagation neural network was trained, tested, and validated using the dataset. The performance of the ANN model was evaluated using the regression correlation coefficient (R-value), which indicates the degree of agreement between the predicted and target values.

The results of the ANN regression analysis showed that the R-values ranged between 0.97 and 0.99 for all scenarios, indicating an excellent correlation between the ANN-predicted temperatures and the simulation-derived values. Since an R-value close to 1 represents strong agreement, these results confirm the high accuracy and reliability of the simulation outcomes.

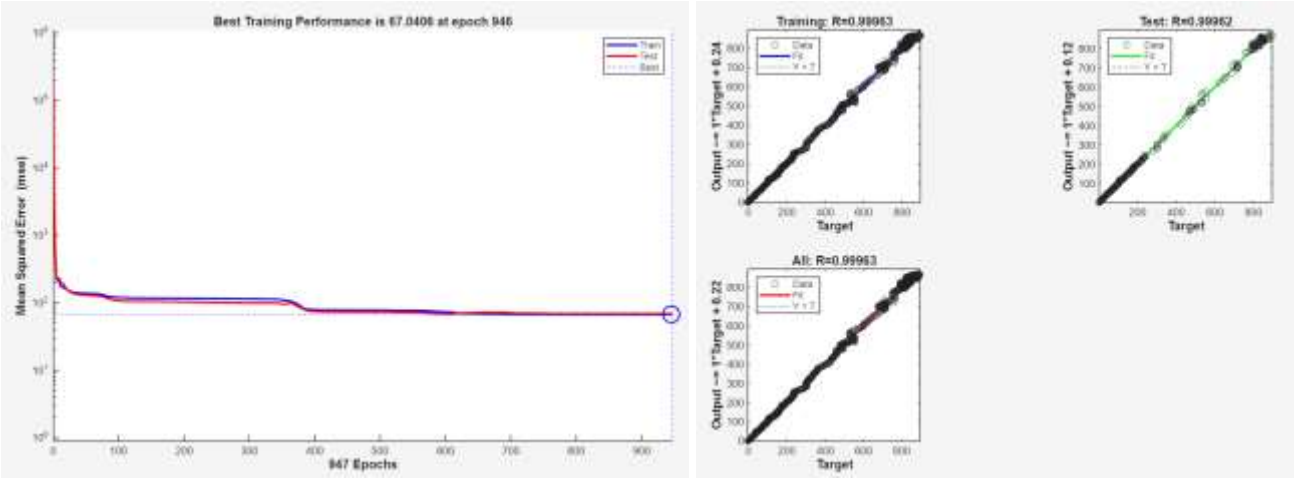

Fig. 67. Validation using ANN for 100 MW fire vehicle simulation under natural ventilation

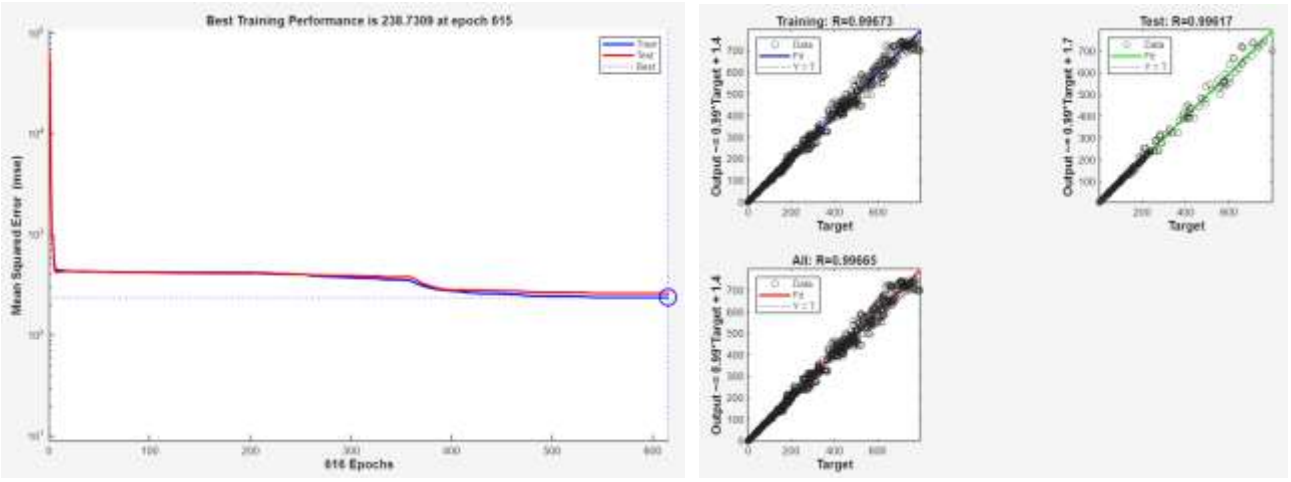

Fig. 68. Validation using ANN for 100 MW fire vehicle simulation under integrated system

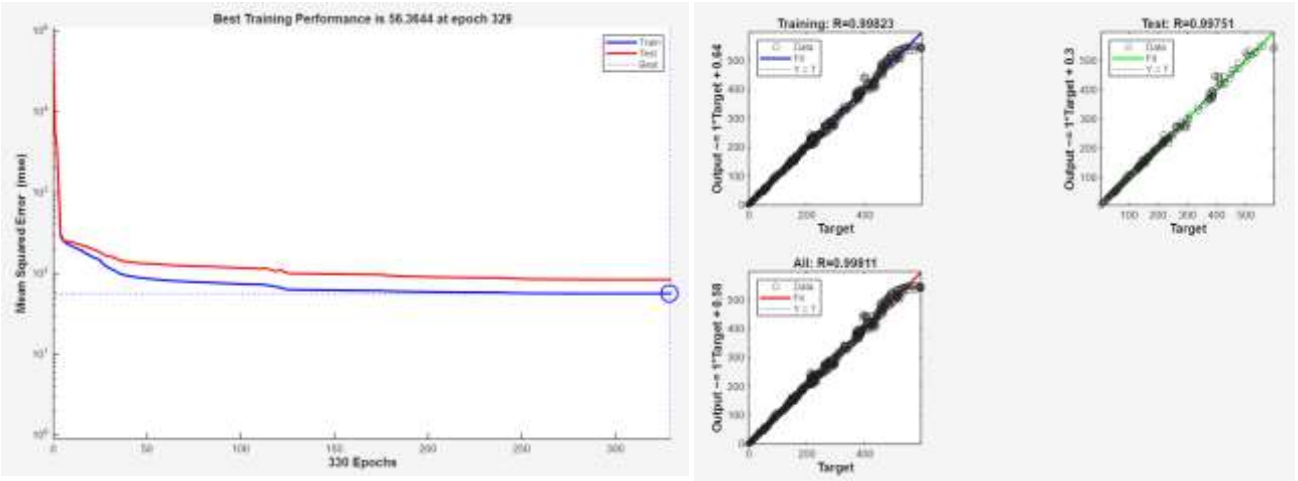

Fig. 69. Validation using ANN for 25 mw fire vehicle simulation under natural ventilation

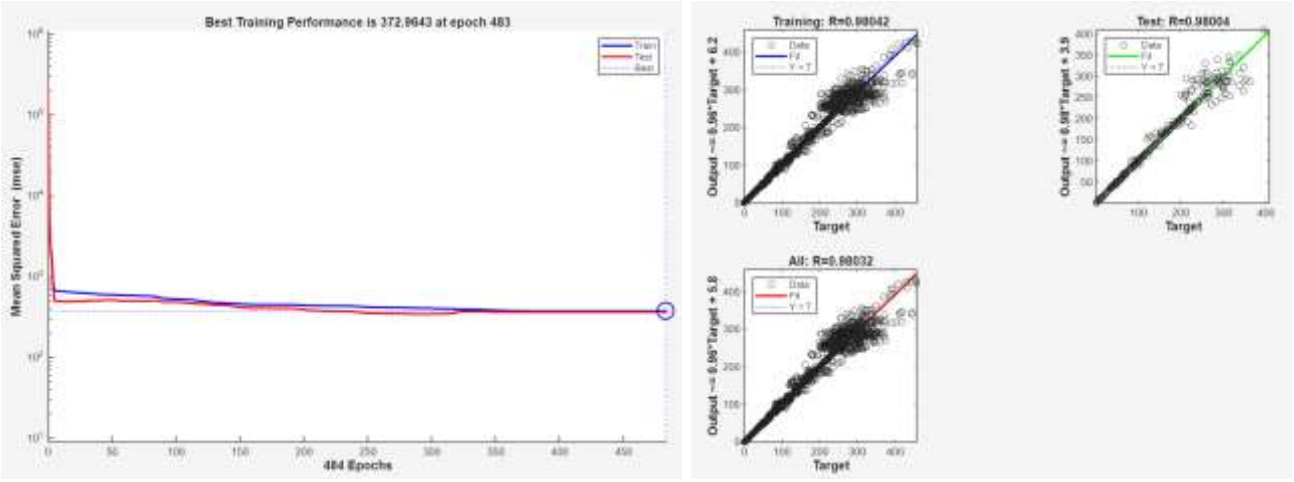

Fig. 70. Validation using ANN for 25 MW fire vehicle simulation under integrated system

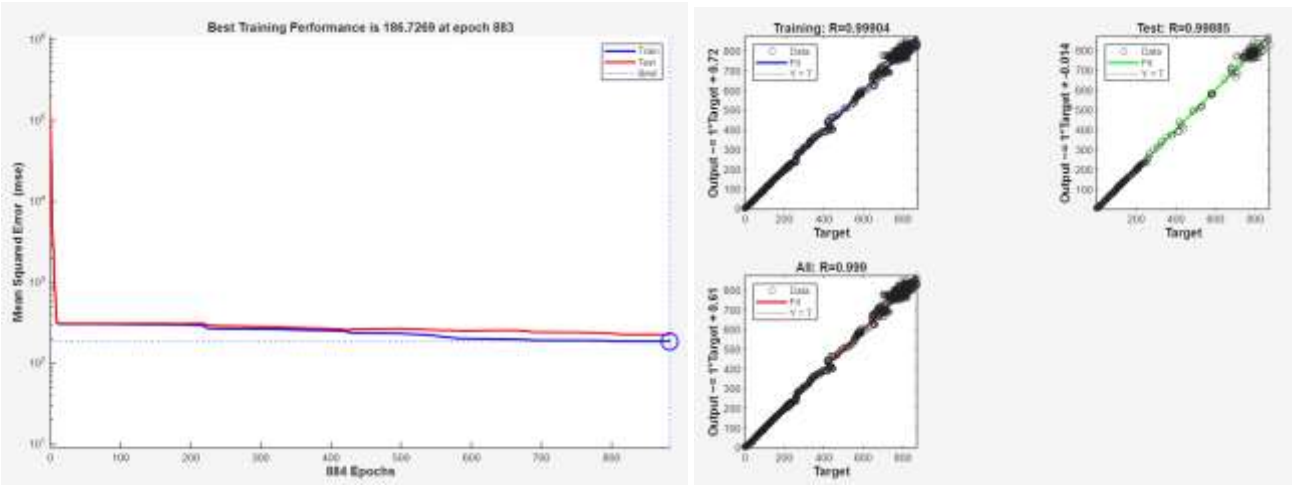

Fig. 71. Validation using ANN for 10 MW fire vehicle simulation under natural ventilation

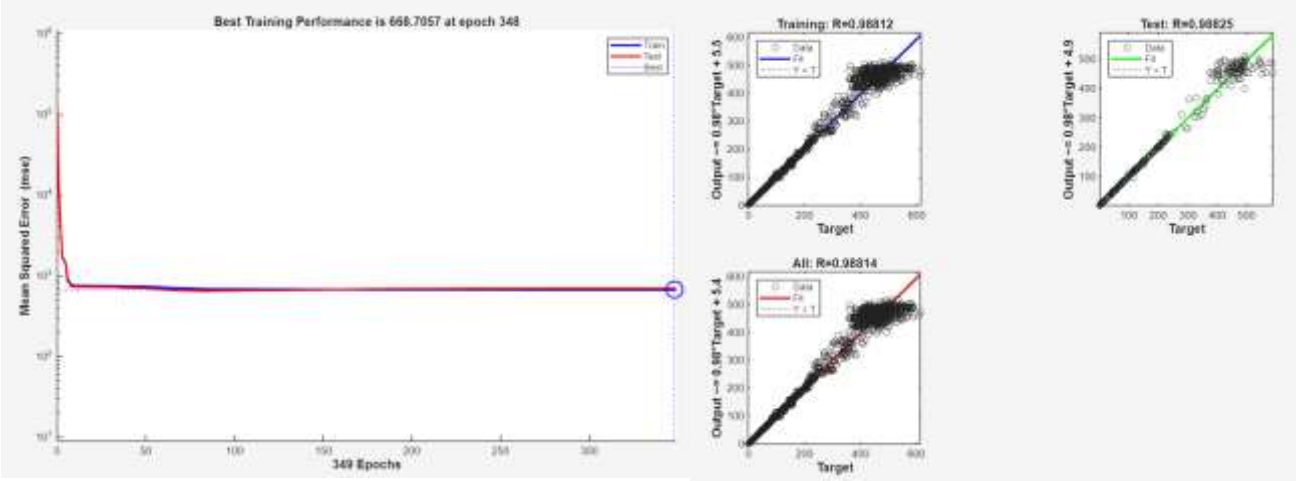

Fig. 72. Validation using ANN for 10 MW fire vehicle simulation under integrated system

Figures 67–72 present the ANN training performance, regression fits, and error histograms, which collectively demonstrate the robustness of the neural network model in replicating the simulation trends. These validation results provide strong evidence that the HRR–temperature relationship obtained from the simulations is consistent and trustworthy, thereby reinforcing the credibility of the presented numerical findings.

6. Conclusion

This study demonstrated, through CFD-based simulations, the critical role of integrated ventilation and suppression systems in mitigating road tunnel fire hazards. Across all three fire scenarios, natural ventilation alone was shown to be inadequate, as it led to rapid smoke back-layering, untenable thermal conditions, and high toxic gas concentrations within a short duration. In contrast, the combined application of longitudinal ventilation and sprinklers consistently preserved upstream tenability, directed smoke flow downstream, and improved evacuation visibility, even though severe localized heating persisted near the fire seat. Importantly, the fire growth in integrated cases was capped at levels comparable to natural-ventilation scenarios, preventing escalation to more hazardous conditions.

A key strength of this work lies in the comparative discussion presented for each case, where the fire scenarios were systematically examined under both natural and integrated configurations. Subsections dedicated to thermal response, smoke dynamics, CO distribution, visibility, and sprinkler activation allowed a structured comparison across cases, offering clarity on how system configuration and fire size influence tenability. This layered discussion not only highlights the mechanisms driving unsafe conditions under natural ventilation but also illustrates the improvements achieved with integrated systems. The validation of simulation outputs using ANN regression (R = 0.97–0.99) further reinforces the reliability of these findings.

Looking forward, future work should explore coupling detection systems with suppression and ventilation controls for dynamic, real-time response, as well as the application of artificial intelligence for predictive decision-making and

adaptive fan–sprinkler coordination. Additionally, extending this study to include transverse and semi-transverse ventilation strategies would provide a broader understanding of design options for next-generation tunnel fire safety systems.

7. Reference

[1]. Haukur Ingason, Ying Zhen Li, 2019. Large scale tunnel fire tests with different types of large droplet fixed firefighting systems. Fire Safety Journal, Vol 107, pp. 29–43.

[2]. Junli Luo, Zhisheng Xu, Fulin Li, Jiaming Zhao, 2019. Effect of vehicular blocking scene on smoke spread in the longitudinal ventilated tunnel fire. Case Studies in Thermal Engineering, Vol. 14, e100495.

[3]. Alan Beard, Richard Carvel, 2005. The Handbook of Tunnel Fire Safety. Thomas Telford. ISBN: 0727731688.

[4]. Jonatan Gehandler, 2015. Road tunnel fire safety and risk: a review. Fire Science Reviews, Vol. 4, Art. No. 2.

[5]. Jianying Bai, Haomiao Liao, Yangyuyu Xia, 2020. Study on Fire Accidents in Tunnels. IOP Conference Series: Materials Science and Engineering, Vol. 741, e012095.

[6]. Weiyue Liu, Minzhang Liu, Ru Chang, Bin Yang, Hao Cui, Chanyuan Li, Huan Zhang, 2023. Study on moving fire smoke characteristics and mechanical ventilation system of tunnel. Fire Safety Journal, Vol. 141, Article ID 103932.

[7]. Haukur Ingason, Ying Zhen Li, Anders Lonnermark, 2015. Tunnel Fire Dynamics. Springer.

[8]. M. Fera, Roberto Macchiaroli, 2010. Use of analytic hierarchy process and fire dynamics simulator to assess fire protection systems in a tunnel. Int. J. Risk Assessment and Management, Vol. 14 No. 6, pp. 504-529

[9]. Alireza Sarvari, Sayyed Majid Mazinani, 2019. A new tunnel fire detection and suppression system based on camera image processing and water mist jet fans. Heliyon, Vol. 5 Issue 6, e01879.

[10]. Lorenzo Barbato, Furio Cascetta, Marilena Musto, Giuseppe Rotondo, 2014. Fire safety investigation for road tunnel ventilation systems - An overview. Tunnelling and Underground Space Technology, Vol. 43, pp. 253-265

[11]. Jonatan Gehandler, 2015. Road tunnel fire safety and risk: a review. Fire Science Reviews, Vol. 4, Art. No. 2.

[12]. National Transportation Safety Board, Multivehicle Crash and Postcrash Tunnel Fire on Interstate 80, Green River, Wyoming, February 14, 2025, Report No. HWY25MH004, Mar. 2025.

[13]. The New Paper, “Car catches fire in KPE tunnel, flames put out by sprinklers,” Nov. 2, 2024.

[14]. Marian Hrubos, Dusan Nemec, Emilia Bubenikova, Peter Holecko, Juraj Spalek, Michal Mihalik, Marek Bujnak, Jan Andel, Tomas Tichy, 2021. Model-Based Predictive Detector of a Fire inside the Road Tunnel for Intelligent Vehicles. Journal of Advanced Transportation, Vol. 2021, Article ID 6634944, pp. 1-14.

[15]. Xiaoyun Wang, 2017. Fire Dynamics Simulator (FDS) Pyrolysis Model Analysis of Heavy Goods Vehicle Fires in Road Tunnels (Doctoral dissertation). University of Canterbury, Christchurch, New Zealand.

[16]. Ciro Caliendo, Gianluca Genovese, Isidoro Russo, 2020. Risk Analysis of Road Tunnels: A Computational Fluid Dynamic Model for Assessing the Effects of Natural Ventilation. Applied Sciences, Vol. 11, p. 32.

[17]. McGrattan and Kevin B, 2006. Fire dynamics simulator (version 4): technical reference guide. National Institute of Standards and Technology Special Publication 1018, p. 94.

[18]. K McGrattan, 2007. Verification and Validation of Selected Fire Models for Nuclear Power Plant Applications: Fire Dynamics Simulator (FDS), NUREG-1824, EPRI 1011999, Vol. 7.

[19]. McGrattan, Kevin B, Forney, and Glenn P, 2004. Fire dynamics simulator (version 4): user’s guide. National Institute of Standards and Technology Special Publication 1019, p. 90.

[20]. H. Y. Wang, 2009. Prediction of soot and carbon monoxide production in a ventilated tunnel fire by using a computer simulation. Fire Safety Journal, Vol. 44, pp. 394-406.

[21]. Sung C Kim, A Hamins, Matthew F Bundy, GH Ko, Erik L Johnsson, 2007. Analysis of Thermocouple Behavior in Compartment Fires. Fire Safety Science 7, p. 136.

[22]. Y. Wu, M.Z.A. Bakar, 2000. Control of smoke flow in tunnel fires using longitudinal ventilation systems a study of the critical velocity. Fire Safety Journal, Vol 35, pp. 363-390.

[23]. NFPA 13 Standard for the Installation of Sprinkler Systems. Accessed: Oct. 21, 2025

[24]. Daan Van den Broecke, Richard Emberley, Toni Sietz, Jose L Torero, Cristian Maluk, 2021. Study on the effectiveness of fire suppression deluge systems in tunnels. Tunnelling and Underground Space Technology, Vol. 108, Art. No. 103764.

[25]. NFPA 502 standard for raod tunnels. Accessed: Aug. 29, 2025.

[26]. Ciro Caliendo, Gianluca Genovese, Isidoro Russo, 2022. A 3D CFD modeling for assessing the effects of both longitudinal slope and traffic volume on user safety within a naturally ventilated road tunnel in the event of a fire accident. IATSS Research, Vol. 46, pp. 547-558.

[27]. Yu Jen Chen, Chi Min Shu, San Ping Ho, Hsiang Cheng Kung, Shen Wen Chien, Hsin Hsiu Ho, Wen Sheng Hsu, 2019. Analysis of smoke movement in the Hsuehshan tunnel fire. Tunnelling and Underground Space Technology, Vol 84, pp. 142-150.

[28]. Ciro Caliendo, Paolo Ciambelli, Maria Luisa De Guglielmo, Maria Grazia Meo, Paola Russo, 2018. Computational analysis of fire and people evacuation for different positions of burning vehicles in a road tunnel with emergency exits. Cogent Engineering, Vol. 5 (1), Art No. 1530834.

[29]. Ying Zhen Li, Haukur Ingason, 2013. Model-scale tunnel fire tests with automatic sprinkler. Fire Safety Journal, Vol. 61, pp. 298–313.

[30]. Haukur Ingason, Ying Zhen Li, Magnus Arvidson, Lei Jiang, 2022. Fire tests with automatic sprinklers in an intermediate scale tunnel. Fire Safety Journal, Vol. 129, Art No. 103567.